

LIBRARY Michigan State University

This is to certify that the

dissertation entitled

Testing and Simulation of Composite Laminates
Under Impact Loading

presented by

Xinglai Dang

has been accepted towards fulfillment of the requirements for

Ph.D. degree in Engineering Mechanics

Date 5/22/00

MSU is an Affirmative Action/Equal Opportunity Institution

0-12771

PLACE IN RETURN BOX to remove this checkout from your record.

TO AVOID FINES return on or before date due.

MAY BE RECALLED with earlier due date if requested.

DATE DUE	DATE DUE	DATE DUE
MAX 2 & 2009		

6/01 c:/CIRC/DateDue.p65-p.15

TESTING AND SIMULATION OF COMPOSITE LAMINATES UNDER IMPACT LOADING

By

Xinglai Dang

A DISSERTATION

Submitted to
Michigan State University
in partial fulfillment of the requirements
for the degree of

DOCTOR OF PHILOSOPHY

Department of Materials Science and Mechanics

ABSTRACT

TESTING AND SIMULATION OF COMPOSITE LAMINATES UNDER IMPACT LOADING

By

Xinglai Dang

Owing to their high stiffness-to-weight and high strength-to-weight ratios, fiberreinforced polymer-matrix composite laminates are excellent materials for highperformance structures. However, their properties in the thickness direction are very poor as they are weakly bonded by polymeric matrices through laminate interfaces. Accordingly, when a composite laminate is subjected to impact loading, high interlaminar stresses along with the low interlaminar strengths could easily result in interlaminar damage such as delamination. This thesis investigated the response of composite laminates under low-velocity impact and presented numerical techniques for impact simulation. To begin with, instrumented drop-weight impacts ranging from subperforation to perforation levels were introduced to composite laminates having various dimensions and thicknesses. Damaged composite laminates were then subjected to compression-after-impact tests for evaluations of residual properties. Experimental results revealed that perforation was an important damage milestone since impact parameters such as peak force, contact duration, maximum deflection and energy absorption, and residual properties such as compressive stiffness, strength and energy absorption all reached critical levels as perforation took place. It was also found that thickness played a more important role than in-plane dimensions in perforation process.

In order to understand more about the relationship between laminate thickness and perforation resistance and to present an economical method to improve perforation resistance, thick laminated composite plates and their assembled counterparts were investigated and compared. An energy profile correlating the impact energy and absorbed energy at all energy levels for each type of composite plates investigated was established and found to be able to address the relationship between energy and damage. Experimental results concluded that increasing thickness was more efficient than improving assembling stiffness in raising perforation resistance. As a first step to simulate composite response to impact loading, LS-DYNA3D was used for numerical analysis. However, due to its inability to describe interlaminar stresses, no delamination simulation could be achieved. As delamination played a very important role in damage process, a computational scheme capable of identifying interlaminar stresses and considering both numerical accuracy and computational efficiency was required for impact simulation. Accounting for interlaminar shear stress continuity and having degrees of freedom independent of layer number, a laminate theory named Generalized Zigzag Theory was formulated into a finite element subroutine and integrated into ABAQUS code. Due to the uses of Truesdell rate of Cauchy stress and rate of deformation tensors, the computational scheme was able to present reasonable interlaminar shear stresses via an updated Lagragian algorithm. Combining the calculated interlaminar stresses with a delamination failure criterion, the computer program was able to predict the response of composite laminates up to the onset of delamination. Further computational simulation involving all damage modes should be considered in future studies.

To My Family

ACKNOWLEDGMENTS

From my heart, deep gratitude and appreciation goes to my major advisor, Dr.

Dahsin Liu, for his constant encouragement and invaluable guidance. His contribution to the achievements of this work is significant.

Special thanks also extend to my dissertation committee members, Dr. T. Pence, Dr. Zhenfang Zhou, and Dr. H.Y. Tsai, for their academic support and encouragement through my Ph. D. program.

I am very grateful to my parents, Decang Dang and Junlan Fan, for their understanding, support and love. They worked very hard to support me all over past years.

Finally, I'd like to thank my wife, Xiaomei Xi, and my son, Edward Dang.

Without their help and love, the completion of this dissertation is impossible. For this reason, this dissertation is dedicated to them.

TABLE OF CONTENTS

List of Tablesvi	ii
List of Figures	X
Chapter 1	
INTRODUTION	. 1
1.1 Literature review	.1
1.2 Objectives	7
1.3 Organization of this thesis	7
1.4 References	8
Chapter 2	
SIZE EFFECTS ON IMPACT RESPONSE OF COMPOSITE LAMINATES	16
2.1 Introduction	17
2.2 Experimental methods	18
2.3 Experimental results	25
2.4 Discussions	48
2.5 Conclusions	54
2.6 References	55
Chapter 3	
IMPACT PERFORATION RESISTANCE OF LAMINATED AND ASSEMBLED	
COMPOSITE PLATES	59
3.1 Introduction	60
3.2 Experimental methods	62
3.3 Results and discussions	58
3.4 Conclusions	86
3.5 References	88
Chapter 4	
TESTING AND SIMULATION OF LAMINATED COMPOSITES SUBJECTED TO	
IMPACT LOADING	90
4.1.Introduction	
4.2 Instrumented Impact Testing	94
4.3 Computational Technique	94
4.4 Experimental Results	97
4.5 Computational Results	06
4.6 Conclusion1	07
4.7 References	11
Chapter 5	
SIMULATION OF COMPOSITE LAMINATES UNDER LOW-VELOCITY IMPAC	T
WITH CONTINUUM-BASED FINITE ELEMENT METHOD1	13
5.1 Introduction1	13

5.2 Experimental Technique	115
5.3 Computational Scheme	118
5.4 Results and Discussions	130
5.5 Conclusions	
5.6 References	143
Chapter 6	
CONCLUSIONS AND RECOMMENDATIONS	145
6.1 Conclusions	
6.2 Recommendations	150
Appendices	152
Appendix A	153
Appendix B	165
Appendix C	176

LIST OF TABLES

	Summary of peak forces and impact energy levels at penetration for composite laminates of various dimensions and thicknesses subjected	
	to impact and indentation loads	45
Table 2.2.	Ratios of specimen dimensions, thickness, and impactor diameter	50
	Impact bending stiffnesses, penetration thresholds and perforation thresholds of one-laminate and two-laminate composite plates	78
Table 4.1	Experimental results of impact parameters	96

LIST OF FIGURES

Figure 2.1 - Schematic diagram of impact testing machine
Figure 2.2 - Schematic diagram of NASA compression after impact testing fixture24
Figure 2.3 - Force histories at three impact velocities
Figure 2.4 - Relations between peak force and impact energy for composite laminates
with various dimensions and thicknesses
Figure 2.5 - Relations between contact duration and impact energy for composite
laminates with various dimensions and thicknesses29
Figure 2.6 - Relations between absorbed energy and impact energy for composite
laminates with various dimensions and thicknesses30
Figure 2.7 - Relations between residual compressive stiffness and impact energy for
composite laminates with various dimensions and thicknesses33
Figure 2.8 - Relations between residual compressive maximum force and impact energy
for composite laminates with various dimensions and thicknesses34
Figure 2.9 - Relations between residual compressive absorbed energy and impact energy
for composite laminates with various dimensions and thicknesses35
Figure 2.10 - Relations between impact characteristics and laminate thickness42
Figure 2.11 - Typical load-displacement relation from indentation testing
Figure 2.12 - Relations between mechanical properties degradation and hole size for
composite laminates with open holes46
Figure 3. 1 - Schematic diagram of impact testing machine
Figure 3. 2 - Schematic diagrams of some riveting and stitching patterns
Figure 3. 3 - Force-deflection curves of eighteen 1F composite plates70
Figure 3. 4 - The whole enegy profile of 1F case based on force-deflection curves given
in Figure 3.371
Figure 3. 5 - Relation between energy thresholds and impact bending stiffness of various
two-laminate composit plates80
Figure 3. 6 - The whole energy profiles of three laminated composite plates81
Figure 3. 7 - The whole energy profiles of four assembled composite plates82

Figure 3. 8 - The relation between perforation threshold and thickness for both laminated
and assembled composite plates85
Figure 4.1 - Schematic diagram of impact testing setup
Figure 4.2 - Force-displacement relations for laminates with various thicknesses98
Figure 4.3 - Force-displacement relations for laminates with various fiber angles99
Figure 4.4 - Force-displacement relations for laminates subjected to various impact Velocities
Figure 4.5 - Comparison of force history between ref. [4.7] and LS-DYNA3D101
Figure 4.6 - Comparison of displacement history between ref. [4.7] and LS-DYNA3D
Figure 4.7 - Force history of 15-layer laminate with fixed boundary condition and
subjected to 1m/s impact103
Figure 4.8 - Displacement history of 15-layer laminate with fixed boundary condition and
subjected to 1m/s impact104
Figure 4.9 - Velocity history of 15-layer laminate with fixed boundary condition and
subjected to 1m/s impact105
Figure 4.10 - Force histories of 9-layer laminate subjected to 1m/s impact and simulated
by various failure criteria108
Figure 4.11 - Force histories of 9-layer laminate subjected to 2.8m/s impact and
simulated by various failure criteria109
Figure 4.12 - Force histories of 9-layer laminate subjected to 3.5m/s impact and
simulated by various failure criteria110
Figure 5.1 - Schematic diagram of impact testing setup
Figure 5.2(a) - Force history of 15-layer laminate with fixed boundary
condition and subjected to 1m/s impact132
Figure 5.2(b) - Displacement history of 15-layer laminate with fixed boundary
condition and subjected to 1m/s impact133
Figure 5.3(a) - Force histories of 9-layer laminate subjected to 1m/s impact and simulated
by various failure criteria134

Figure 5.3(b) - Force histories of 9-layer laminate subjected to 2.8m/s impact and	
simulated by various failure criteria	135
Figure 5.4 - Force Vs. Displacement for [05/905/05] at V0=1.12 m/s	136
Figure 5.5 - Force vs. displacement for different impact velocities on [05/905/05]	137
Figure 5.6 - Force vs. displacement for different laminate thicknesses	138
Figure 5.7 - Force vs. displacement for different stacking sequences	139
Figure 5.8 - Force vs. displacement for different fiber angles	10

Chapter 1

INTRODUCTION

1.1 Literature review

Because of their well-known advantages compared to traditional materials, laminated composite materials are extensively used in industry. Superior strength-to-weight ratio, high specific modulus, tailored ability for a specific application, and environmental stability of laminated composites is very attractive to the aerospace industry and other industrial applications. However, under impact loading, which is induced by impacts during manufacture, normal operations, or maintenance in the life of the structure, laminated composites are very susceptible. Even at low velocity impact, the impact-induced damage such as matrix cracking, fiber breakage and delamination, can be very significant, and usually invisible to the naked eye. The impact-induced damage can cause serious structural degradation. Therefore, impact is an important subject in laminated composite analysis and very critical to industry application.

In order to develop improved composite materials and composite structural design method for the industry, it is essential to obtain a basic understanding of the impact phenomenon, damage mechanism, residual properties after impact, size effects, and assembly effects. Further development of computational simulation methods for laminated composite structures accounting for impact is a necessary step.

For this purpose, many experimental and analytical studies were performed and can be found in the review articles by Abrate [1.1-1.2]. In impact dynamics, the main concern is the characteristics of impact response, which include impact force history, impact displacement history, impact duration and impact energy absorption, etc. Determining the contact force history has been done experimentally (Delfosse [1.11], Yjihashi [1.24], and Chang and Sun [1.14]). Various mathematical models such as spring-mass models (Alderson [1.12], Teti [1.23], and Bucinell [1.13]), energy balance model (Moon [1.18], Poe [1.19-1.21], Chuancho [1.16]), and beam, plate and shell models (Christoforou and Swanson [1.15], and Gu and Legacy [1.17], and Prasad et al [1.22]) have been developed. Since impact induced damage was not accounted for in these models, generally, the practical effectiveness is limited. Tan and Sun [1.5] verified that an indentation law based on a quasi-static test could be used to investigate lowvelocity impact. This indentation law established a mathematical relationship between the contact force and the indentation for elastic contact. But, to determine the indentation parameters for a set of composite material and impactor, an indentation test was required. Although the indentation law could be integrated into computational scheme for various studies (Wang [1.58], Lin [1.59], Chen [1.6], Sun [1.7], and Lee [1.60]), a new characterization of indentation parameters was needed each time the material or geometry of composite or impactor was altered. As a consequence, for investigating impact response of laminated composites, a computational technique free of experimentdependent parameters might prove to be more efficient.

In some previous studies, Liu et al. [1.3-1.4] concluded that matrix cracking and delamination were the major damage modes in laminated composites subjected to low-

velocity impact. A correlation between bending stiffness mismatch and delamination size was established. This relation successfully used for phenomenological explanations of delamination size, location, and orientation in impacted composite laminates. But, to establish an accurate and efficient quantitative simulation, further understanding based on experimental testing and analysis is needed.

In practical application, in order to reduce the expense associated with impact testing of large prototype structures, small coupons are usually used in laboratories to characterize impact response. Then, the results are used for practical structure design. However, even made of identical materials, small coupons and practical large structures do not always behave the same way. This difference due to size change is referred to as size effects [1.30]. Some investigators [1.25-1.29] have concluded that size effects should be carefully examined in material characterizations and structural design.

Scaling laws are generally used to relate small coupon impact tests to practical large structural impacts. Based on dimensional analysis, Monrton [1.31] scaled both composite laminates and impact loading and verified the feasibility of using analytical scaling laws for predicting undamaged behavior for carbon-epoxy laminated beams. With a different approach, Qian et al. [1.32] also verified that analytical scaling laws could accurately describe the undamaged response to impact. Sankar [1.33] presented semi-empirical formulae for predicting impact characteristics such as peak contact force, contact duration, and peak strain on back surface. But no damage effects were considered in his studies. Therefore, in order to understand the size effects completely for laminated composites under impact loading, a whole-range investigation is needed ranging from elastic impact, subperforation impact, to perforation impact.

The size effects for laminated composites consist of in-plane dimensional effects and thickness effects. It is believed that, because of the population of the thin laminates, the in-plane dimensional effect gained more attention than thickness effect. As technologies of composite manufacturing advance, more and more thick-section laminated composites are used in non-aerospace industries. For example, thick-section laminated composites have been proved to be feasible designs for submarine hull and armored vehicle bodies. This implies that thickness effects may play an important role to size effects in laminated composites subjected to impact loading. Accordingly, a further study of thickness effects is necessary.

Impact analysis of laminated composite structures includes impact resistance analysis and impact tolerance analysis. Impact resistance is concerned with understanding how impact damage is initiated, developed and is helpful to finding methods to prevent or resist the impact damage, while damage tolerance is concerned with the effect of impact damage on the mechanical properties of laminated composite structures. Demuts [1.61] described Air Force draft requirements for damage tolerance under low-velocity impact. The minimum design strength after impact is specified. Many experimental studies [1.36-1.38] were performed to determine the residual strength of laminated composites under tension, compression, and bending.

Since under in-plane compression, most serious strength reductions are shown, the Compression After Impact (CAI) test [1.39] is mostly used to determine the residual strength of impact damaged composite laminates. Therefore, to characterize the residual properties of impacted composite laminates, CAI test always is the first choice.

As mentioned before, more and more thick-section composites are used for heavy-duty structures. Studies on thick laminates have gained much attention. These studies concluded that thick composite laminates behave quite differently from their thin counterparts, and thickness - as opposed to in-plane dimensions - has much greater influence on impact resistance of laminated composites under impact loading [1.45-1.47].

However as composite laminates become thicker, the manufacturing cost for high-quality composite laminates may become unaffordable. Because, in order to achieve uniform curing and thus uniform properties through the thickness of thick composite laminates, expensive microwave curing process is required (Wei [1.50]). Therefore, to meet the design requirement for high quality and reduce the manufacturing costs, assembled composite plates, which are organized by assembling multiple thin composite laminates together [1.51-1.52], may be considered as alternatives for thick laminated composite plates. A further study regarding the impact resistance and impact tolerance of assembled composite laminates is needed.

Experimental studies on composite laminates subjected to impact loading always come first rather than analytical or numerical simulations, because successful simulation must be based on the correct understanding and accumulated knowledge of experimental studies. In order to aid industrial applications with laminated composite structures that account for impact effects, computational simulation or prediction is a helpful tool for engineering design.

As indicated by Abrate [1.1, 1.2], the development of models for predicting damage and residual properties for composite laminates under impact loading is becoming imperative. Since delamination represents a major component of damage at

low-velocity impact, the prediction and simulation of delamination during impact should be the primary step. As many investigators concluded, the initiation of delamination always follows the matrix crack close to ply interfaces (Liu [1.57], Wang and Chang [1.66], and Choi Downs [1.67], etc.), and the transverse stress distribution at ply interfaces determines the onset and development of delamination.

But difficulties associated with prediction and simulation of delamination are due to the complexity of transverse stress distribution in the contact area. Therefore, an accurate stress distribution on the ply interface is essential for successful prediction of delamination.

Finite Element method is proved to be a valuable CAD tool for engineering application. A shell element for static analysis of laminated composites under large deformation was developed by Lee [1.65]. This element based on the Generalized Zigzag Theory [1.62] was demonstrated being an accurate and efficient element for static analysis of laminated composites. The interlaminar stress predicted from this element is verified to closely agree with exact solutions. Apparently, a further development on this element for dynamics analysis and impact analysis is logical for prediction and simulation of laminated composites under impact loading.

Linear Shear Slip Theory [1.63-1.64] was proved efficient for simulation of delamination. With the combination of Generalized Zigzag Theory and Linear Shear Slip Theory, a new shell element for prediction and simulation of delamination of laminated composites subjected impact loading may be proved as a valuable tool.

1.2 Objectives

Accordingly, the objectives of this dissertation are listed below:

- 1. The first objective is to perform a whole-range investigation ranging from elastic impact, subperforation impact, to perforation impact, to examine in-plane dimension effects and thickness effects, and to determine residual strength after impact with CAI test. This investigation will lead to further understanding of the response of composite laminates under low-velocity impact and to development of an accurate and efficient quantitative simulation.
- 2. The second objective is to investigate the impact resistance of assembled composite plates, as alternatives to thick laminated composites, and to examine various joining techniques. This investigation will benefit practical engineering applications with thick-section composite laminates.
- 3. The third objective is to evaluate available computational tools for analysis and simulation of composite laminates under low-velocity impact. By comparing computational results with test results, the computational tool can be examined.
- 4. Based on the knowledge from the experimental studies and the evaluation of computer simulation, to further improve the prediction and simulation of delamination of composite laminates under impact loading, the last objective is to develop a shell element for impact analysis of laminated composites.

1.3 Organization of this thesis

With the above objectives, this dissertation is divided into the following chapters.

Chapter 2 [1.49] starts with the first objective, experimental studies regarding the size effects are presented. Delamination effects on material property-degradation of impact

laminates are well recognized. A detailed discussion, and a simple explanation based on the bending rigidity is presented to experimental results. Thickness effects to impact resistance and tolerance is greatly significant to in-plane dimension effects. As an effort to meet design requirements and reduce manufacturing cost, Chapter 3 [1.69] describes various joining techniques including mechanical riveting, adhesive bonding, stitching and their combination for assembling multiple thin composite laminates. For evaluation of computational tools, a series of impact testing regarding thickness effect, fiber angle effect, and velocity effect is described in Chapter 4 [1.68], and comparison with computer simulation is made. LS-DYNA3D, a commonly used computer code for impact analysis, is evaluated. Based on Lee's static shell element, Chapter 5 presents a continuous effort for the development of a shell element for impact analysis, delamination prediction, and impact simulation of laminated composites. Also, some numerical studies against experimental results are given. Finally, in the last chapter, conclusions and recommendations are presented.

1.4 References

- 1.1. Abrate, S., "Impact on Laminated Composite Materials," Applied Mechanics Review, 44(4), 155-190, 1991.
- 1.2. Abrate, S., "Impact on Laminated Composites: Recent Advances," Applied Mechanics Review, 47(11), 517-544, 1994.
- 1.3. Liu, D. and Malvern, L.E., "Matrix Cracking in Impacted Glass/Epoxy Plates," Journal of Composite Materials, 21(7), 594-609, 1987.

- 1.4. Liu, Dahsin, "Impact-induced Delamination A View of Material Property Mismatching," J. Composite Materials, 22 (7), 674-691, 1988.
- 1.5. Tan, T.M. and Sun, C.T., "Use of Statical Indentation Laws in the Impact Analysis of Laminated Composite Plates," J. Applied Mechanics, 52, 6-12, 1985.
- 1.6. Chen, J.K. and Sun, C.T., "Dynamic Large Deflection Response of Composite Laminates Subjected to Impact," Composite Structures, 4, 59-73, 1985.
- 1.7. Sun, C.T. and Chen, J.K., "On the Impact of Initially Stressed Composite Laminates," J. Composite Materials, 19(6), 490-504, 1985.
- 1.8. Wu, E. and Yen, C., "The Contact Behavior Plates and Rigid Spheres," J. Applied Mechanics, 61, 60-66, 1994.
- 1.9. Tsai, S.W. and Wu, E.M., "A General Theory of Strength for Anisotropic Materials," Journal of Composite Materials, 5(1), 58-80, 1971.
- 1.10. Chang, F.-K. and Chang, K.-Y., "Post-Failure Analysis of Bolted Composite Joints in Tension or Shear-Out Mode Failure," Journal of Composite Materials, 21(5), 1987.
- 1.11. Delfosse D, Pageau G, Bennettt A, and Pousatrip A, "Instrumented impact testing at high velocities," J Composite Tech Res 15(1), 38-45, 1993
- 1.12. Alderson KL and Evans KE, "Dynamic Analysis of filament wound pipes undergoing low velocity transverse impact," Composites Sci and Tech 45, 17-22, 1992
- 1.13. Bucinell RB, Nuismer RJ, and Koury JL, "Response of composite plates to quasi-static impact events, ASTM STP 1110,TK o'Brien, ed, 528-549, 1991
- 1.14. Chang C and Sun CT, "Determining transverse impact force on a composite laminate by signal deconvolution," Exp Mech, 414-419, Dec., 1989

- 1.15. Christoforou AP and Swanson SR, "Analysis of impact response in composite plates," Int J Solids Struct 2792), 161-170, 1991
- 1.16. Chuanchao Z and Kaida Z, "the investigation of the behavior of laminates subject to low velocity impact," Proc 8th Int Conf on Composite Mater. (ICCM/8), Honlulu, 1991
 1.17. Guy TA and Lagace PA, "Compressive residual strength of graphite-epoxy
- laminates after impact," Proc of 9th DoD/NASA/FAA Conf on Fibrous Composites in Struct Des, DOT/FAA/CT-95-25, 253-274, 1992
- 1.18. Moon D and Shively JH, "Towards a unified method of causing impact damage in thick laminated composite," Proc 35th Int SAMPE Symp and Exhibition, Anaheim CA, April 2-5, 35, 1466-1478, 1990
- 1.19. Poe CC, "Summary of a study to determine low-velocity impact damage and residual tension strength for a thick graphite/epoxy motor case," Proc 17th Congress ICAS, Stockholm, Sweden, Sept 9-14, 1, 994-1004, 1990
- 1.20. Poe CC, "Relevance of impactor shape to nonvisible damage and residual tensile strength off a thick praphite/epoxy laminate," ASTM STP 1110, TK O'Brien, ed, 1991
- 1.21. Poe CC, "simulated impact damage in thick graphite/epoxy laminate using spherical indenters," J Reinf Plastics and Composites 10(3), 293-307, 1991
- 1.22. Prasad CB, Ambur DR, and Starnes JH, "Response of laminated composite plates to low-speed impact by airgun propelled and dropped weight impactors," 34th AIAA strut, Structural Dyn and Mat Conf, La Jolla CA, Pt2, 887-900, 1993
- 1.23. Teti R, Langella F, Crivelli Visconti I, and Caprino G, "Impact response of carbon cloth reinforced composites, Proc 5th Int Conf Composite Mat, ICCM-V, San Diego CA, July 19-Aug. 1, 373-381, 1985

- 1.24. Yjihashi S, "An intelligent method to determine the mechanical properties of composites under impact loading," Composite Struc 23, 149-163, 1993
- 1.25. Workshop on scaling effects in composite materials and structures, NASA Langley Research Center, Hampton, VA, November 15-16, 1993, Report No. 94-6, Institute for Mechanics and Materials, University of California, San Diego, CA.
- 1.26. Carpinteri, A., ed., Size-scale effects in the failure mechanisms of materials and structures, E & FN Spon, 1994.
- 1.27. S.B. Batdorf, Note on composite size effect, *J. Composite Technology and Research*, 45, 35-37, 1989.
- 1.28. I. Shahid, H.-T. Sun, and F.-K. Chang, Predicting scaling effect on the notched strength of prepreg and fiber tow-placed laminated composites, *J. Composite Materials*, 29(8), 1063-1095, 1995.
- 1.29. C.E. Harris and D.E. Morris, Effects of laminate thickness and specimen configuration on the fracture of laminated composites, *Composite Materials Testing and Design, ASTM STP 893*, 177-195, 1986.
- 1.30. Y. D. S. Rajapakse, ed., *Mechanics of Thick Composites*, AMD-Vol. 162, The American Society of Mechanical Engineers, 1993.
- 1.31. J. Morton, Scaling of impact-loaded carbon-fiber composites, *AIAA Journal*, 26(8), 989-994, 1988.
- 1.32. Y. Qian, S.R. Swanson, R.J. Nuismer, and R.B. Bucinell, An experimental study of scaling rules for impact damage in fiber composites, *J. Composite Materials*, 24(5), 1990.
- 1.33. B.V. Sankar, Scaling of low-velocity impact for symmetric composite laminates, *J. Reinforced Plastics and Composites*, 11, 297-305, 1992.

- 1.34. J.M. Whitney and R.J. Nuismer, Stress fracture criteria for laminated composites containing stress concentrations, *J. Composite Materials*, 8(3), 253-265, 1974.
- 1.35. J. Awerbuch and M. Madhukar, Notched strength of composite laminates predictions and experiments a review, *J. Reinforced Plastics and Composites*, 4, 1985.
- 1.36. W.J. Cantwell, P.T. Curtis, and J. Morton, Low velocity impact damage tolerance in CFRP laminates containing woven and non-woven layers, *Composites*, 14, 1983.
- 1.37. E.G. Guynn and T.K. O'Brien, The influence of lay-up and thickness on composite impact damage and compression strength, *proc. 26th AIAA SDM Conference*, Orlando, Florida, 187- 196, 1985.
- 1.38. A.A. Baker, R. Jones, and R.J. Callinan, Damage tolerance of graphite/epoxy composites, *Composite Structures*, 4, 15-44, 1985.
- 1.39. Standard Tests for Toughened Resin Composites, NASA RP 1092, 1983.
- 1.40. Liu, Dahsin, Impact-induced delamination a view of material property mismatching, *J. Composite Materials*, 22(7), 674-691, 1988.
- 1.41. E. Wu, E.-Z. Tsai, and Y.-C. Chen, Penetration into glass epoxy composite laminates," *J. Composite Materials*, 28, 1783-1802, 1994.
- 1.42. C.T. Sun and S.V. Potti, High velocity impact and penetration of composite laminates, proc. 9th Int. Conference on Composite Materials, 4, 157-165, 1993.
- 1.43. W. Goldsmity, C.K.H. Dharan and H. Chang, Quasi-static and ballistic perforation of carbon fiber laminates, *Int. J. Solid Structures*, 32, 89-103, 1995.
- 1.44. S.W.R. Lee and C.T. Sun, Dynamic penetration of graphite/epoxy laminates impacted by a blunt-ended projectile, *Composite Science and Technology*, 49, 1993.

- 1.45. Y. D. S. Rajapakse, ed., *Mechanics of Thick Composites*, AMD-Vol. 162, The American Society of Mechanical Engineers, 1993.
- 1.46. J. Morton, "Scaling of impact-loaded carbon-fiber composites," AIAA Journal, 26(8), 989-994, 1988.
- 1.47. Y. Qian, S.R. Swanson, R.J. Nuismer, and R.B. Bucinell, "An experimental study of scaling rules for impact damage in fiber composites," *J. Composite Mat*, 24(5), 1990.
- 1.48. B.V. Sankar, "Scaling of low-velocity impact for symmetric composite laminates,"

 J. Reinforced Plastics and Composites, 11, 297-305, 1992.
- 1.49. D. Liu, B. B. Raju, and X. Dang, "Size effects on impact response of composite laminates," *International Journal of Impact Engineering*, Vol. 21, No. 10, 1998
- 1.50. J. Wei, M.C. Hawley, J. DeLong, and M. DeMeuse, "Comparison of microwave and thermal cure of epoxy resins," *Polymer Engineering and Science*, 33(17), 1993.
- 1.51. C. Lee and D. Liu, "Tensile strength of stitching joint in woven glass fabrics," *J. Engineering Materials and Technology*, 112 (2), 125-130, 1990.
- 1.52. D. Liu, "Delamination resistance in stitched and unstitched composite plates subjected to impact loading," *Reinforced Plastics and Composites*, 9 (1), 59-69, 1990.
- 1.53. E. Wu, E.-Z. Tsai, and Y.-C. Chen, "Penetration into glass epoxy composite laminates," *J. Composite Materials*, 28, 1783-1802, 1994.
- 1.54. C.T. Sun and S.V. Potti, "High velocity impact and penetration of composite laminates," proc. 9th Int. Conference on Composite Materials, 4, 157-165, 1993.
- 1.55. W. Goldsmith, C.K.H. Dharan and H. Chang, "Quasi-static and ballistic perforation of carbon fiber laminates," *Int. J. Solid Structures*, 32, 89-103, 1995.

- 1.56. S.W.R. Lee and C.T. Sun, "Dynamic penetration of graphite/epoxy laminates impacted by a blunt-ended projectile", *Composite Science and Technology*, 49, 1993.
- 1.57. D. Liu, "Impact-induced delamination a view of material property mismatching,"

 J. Composite Materials, 22(7), 674-691, 1988.
- 1.58. Wang CY and yew CH, "Impact damage in composite laminates," Comput Struct 37(6), 967-982, 1990
- 1.59. Lin HJ and Lee YJ, "use of statical indentation laws in the impact analysis of composite laminated plates and shells," J Appl Mech 57(3), 787-789, 1990
- 1.60. Lee LJ, Pai CK, and Shiau LC, "Contact behaviours of laminated composite thin shells and a rigid ball," Proc 3rd European Conf on Composite Mat, Bordeaux, France, March 0-23, 315-320, 1989
- 1.61. Demuts E, "Damage tolerance of composites," Proc Am Soc for Composites, 4th Tech Conf, VPI, Blacksburg VA, Oct. 3-5, 425-433, 1990
- 1.62. Dahsin liu and Xiaoyu Li, "An overall view of laminate theories based on displacement hypothesis", Journal of Composite Materials, 30(14), 1996
- 1.63. Dahsin Liu, Lan Xu, and Xianqiang Lu, "Stress analysis of imperfect composite laminates with an interlaminar bonding theory," International Journal for Numerical Methods in Engineering, 37, 2819-2839, 1994
- 1.64. Xianqiang Lu and Dahsin liu, "Assessment of interlayer shear slip theory for delamination modeling," Composite Materials: Fatigue and Fracture, 4th Vol, ASTM STP 1156, 218-235, 1993
- 1.65. Chienhom Lee, "A continuum-based shell element for laminated composites under large deformation", Ph. D dissertation, Michigan State University, 1998

- 1.66. Wang HS and Chang FK, "Curvature effect on low-velocity impact damage in laminated composites," Proc 8th Int Conf on Composite Mat (ICCM/8), Honolulu, July 15-19, 28.K.1-11, 1991
- 1.67. Choi HY, Downs RJ, and Chang FK, "A new aproach toward understanding damage mechanisms and mechanics of laminated composites due to low-velocity impact: Part I Experiments," J Composite Mat 25, 992-1011, 1991
- 1.68. Liu,D. and Dang, X.,"Testing and simulation of laminated composites subjected to impact loading," Composite materials: fatigue and Fracture, 7th Vol., ASTM STP 1330, pp.273-284, 1998
- 1.69. Dahsin Liu, Basavaraju B. Raju, and Xinglai Dang, "Impact perforation resistance of laminated and assembled composite plates," Int J Impact Engng, to appear

Chapter 2

SIZE EFFECTS ON IMPACT RESPONSE OF COMPOSITE LAMINATES
SUMMARY

Delamination was known to be one of the most important damage modes in composite laminates subjected to impact loading. In an effort to further understand the impact response of composite laminates, various degrees of impact ranging from subperforation to perforation were introduced to glass/epoxy laminates through an instrumented dropweight impactor. In addition, composite laminates of various in-plane dimensions and thicknesses were examined for in-plane dimensional and thickness effects, respectively. Experimental results showed that in-plane dimensional effect was not as significant as thickness effect. The impacted composite laminates were then subjected to compression after impact (CAI) tests for characterizations of residual mechanical properties. Experimental results showed that perforation was the most important damage stage in composite laminates subjected to impact loading since impact characteristics (peak force, contact duration, and absorbed energy) and mechanical properties degradation (residual compressive maximum force and residual compressive absorbed energy) of composite laminates became stable once perforation took place. However, it was also found that delamination played a very important role in the characterizations of mechanical properties degradation. Since the impact response of composite laminates is due to plate bending to some extent, bending analysis was used to explain the greater influence of thickness effect to in-plane dimensional effect. It was also found that bending analysis was feasible for interpretation of delamination in mechanical properties degradation.

2.1 Introduction

Small coupons are usually used in laboratories for material characterizations. Results from small coupon tests are then used for large structural designs. However, small coupons do not always behave the same way as the large structures made of identical material. The difference of behaviors due to size change is usually called size effects. Some investigations regarding the performance of composite materials and structures at different sizes have been reported [2.1-2.5]. It has been concluded that size effects should be carefully examined in material characterizations and structural designs.

The study of size effects on impact-loaded composite laminates were focused on scaling laws and parameters. Morton [2.7] scaled both composite laminates and impact loading and verified the feasibility of using analytical scaling laws for predicting undamaged behavior. He also found that smaller specimens were always stronger than larger ones. In an effort to understand the scaling laws governing impact-loaded composite laminates, Qian, Swanson, Nuismer, and Bucinell [2.8] also verified that analytical scaling laws could accurately describe the undamaged response to impact. In addition, they concluded that the damage resulting from impact involved many complicated factors and the delamination size was consistent with the size effect. Aiming at simplifying the design procedures for scaling impact-loaded composite laminates, Sankar [2.9] presented semi-empirical formulae for predicting impact characteristics such as peak force, contact duration, and peak strain on back surface. No response beyond initial damage was investigated in his study.

In an effort to understand the size effects on the response of composite laminates subjected to impact loading, a whole-range investigation ranging from elastic impact, subperforation impact, to perforation impact, was performed. Both in-plane dimensional effect and thickness effect were included. In order to assess the degree of damage and to characterize the residual mechanical properties of impacted composite laminates, compression after impact (CAI) tests were also applied to damaged composite laminates.

2.2 Experimental Methods

1. Impact Testing

In this study, impact tests were performed on a DYNATUP GRC 8250 impact testing machine as shown in Figure 2.1. The impactor consists of three components: a dropping crosshead, an impactor rod, and an impactor nose. The steel impactor rod has a diameter of 12.5 mm (0.5 in) and is attached to the dropping crosshead. A force transducer having a force capacity of 22.24 kN (5000 lbs) was mounted at the tip of the impactor rod and encapsulated by a hemispherical nose. The total mass of the impactor was 11.9 kg (26.06 lbs). For an impact velocity up to 4 m/s (13 ft/s), the impactor was released from a chosen height up to 0.8 m (2.6 ft) and dropped freely along the loading frame. However, for an impact velocity higher than 4 m/s and up to 8 m/s, the impactor was raised to the highest point, i.e. 0.8 m, and a pneumatic unit located at the top of loading frame was used to provide an additional force to increase the impact velocity.

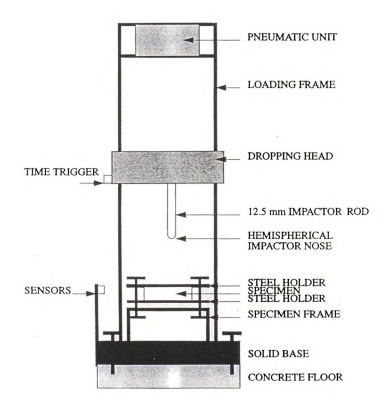


Figure 2.1. Schematic diagram of impact testing machine

Cross-ply laminates made of 3M glass-epoxy composite were investigated in this study. Two nominal thicknesses with averages of 2.24 mm and 6.69 mm were used for studying thickness effect. The former had a stacking sequence of $[0_2/90_2/0_2/...]_{18}$ while the latter $[0_3/90_3/0_3/...]_{51}$. These two types of stacking sequences could be viewed as thickness scaling of mixed mode since it combined a sublaminate mode which increased the laminar number from 9 to 17 and a layer- level mode which changed the layer thickness from 2-layer to 3-layer per each lamina. In this study, the 2.24 mm specimens were called *thin* laminates while the 6.69 mm specimens were considered *thick* laminates.

In impact tests, composite specimens with dimensions of 250 mm x 175 mm were placed between two steel plates. Each steel plate had a square opening in the center. There were three different sizes of square openings for studying in-plane dimensional effect, 125 mm, 84 mm, and 42 mm, resulting in three *effective impact zones* with dimensions of 125 mm x 125 mm, 84 mm x 84 mm, and 42 mm x 42 mm, respectively. Although all specimens had the same dimensions, i.e. 250 mm x 175 mm, they were named *large*, *intermediate*, and *small* laminates according to the three sizes of effective impact zone. In the impact tests, each set of specimen and steel holders was bolted at four corners to the specimen frame which was fixed to a concrete floor as shown in Figure 2.1.

As the impactor dropped and approached a composite specimen, it triggered two time sensors right before impact took place. The initial impact velocity could be calculated from the time interval required for the trigger to travel between the two sensors and the distance between them. Once impact began, the contact forces at many consecutive instants were detected by the force transducer. The force history was recorded in a computer. The maximum contact force was termed *peak force* while the

overall time duration of contact, *contact duration*. The corresponding velocity history of the impactor could then be calculated from integrating the force history (after being divided by the mass of impactor, i.e. 11.9 kg) and with the use of initial impact velocity. Similarly, the corresponding displacement history of the impactor could be calculated from integrating the velocity history.

Based on the force and displacement histories of the impactor, the energy history, which represented the history of energy transferred from the impactor to composite, could be calculated. In this study, the *absorbed energy* was termed as the amount of energy transferred from the impactor to composite at the end of an impact event while the *impact energy* was the kinetic energy of the impactor right before impact took place. The peak force, contact duration, and absorbed energy, along with the histories of force, displacement, and energy, were found to be the important characteristics of composite laminates subjected to impact loading.

2. Damage Inspections

The macroscopic damage modes of impacted composite laminates includes indentation, surface cracking, delamination, and perforation while the microscopic damage includes fiber breakage, matrix cracking, fiber-matrix debonding, etc. Among the macroscopic damage modes, perforation is the most apparent one when composite laminates experience perforation. However, delamination is also an important damage mode due to the fact that the residual mechanical properties of impacted composite laminates are strongly dependent on delamination areas and their locations at laminate interfaces. It is a time-consuming job, if not impossible, to identify delamination areas

and locations. Accordingly, in quantifying impact-induced damage, it is more realistic to use an "equivalent damage size" to account for total damage than to count all details of macroscopic and microscopic damage. The "equivalent damage size" is usually obtained from curve fitting and used as damage index for invisible damage. For example, Whitney and Nuismer [2.10] presented so-called characteristic lengths in their failure criteria for circular hole and line crack studies. Many other studies could be found in a review paper by Awerbuch and Madhukar [2.11].

In an effort to quantify the damage size of impacted composite laminates and its role in mechanical properties degradation, both ultrasonic C-scan and high-intensity light were used in this study. Besides perforation, delamination was identified as another apparent damage mode. However, because of difficulties involved in determining delamination area and location at each laminate interface, the determination of overall delamination area in this study was based on projecting delamination areas at all interfaces onto a single plane, i.e. enveloping the delamination areas at all interfaces. The projected delamination area and the size of perforation were then compared to determine their roles in mechanical properties degradation in composite laminates subjected to impact loading.

3. Compression After Impact (CAI) Testing

Since perforation and delamination were the dominant damage modes in impacted composite laminates and they strongly affected the compression performance of composite laminates, compression after impact (CAI) was commonly used in characterizing the residual mechanical properties of impacted composite laminates, e.g.

Ref. [2.12-2.14]. In this study, the NASA's compression after impact test [2.15] fixture shown in Fig. 2 was used for determining the residual compressive stiffness and residual compressive maximum force of impacted composite laminates. In addition, the residual compressive absorbed energy was also determined.

In performing CAI tests, impacted composite laminates were cut into 250 mm x 125 mm. The specimens were snug-fitted in the CAI fixture by knife edges along the two longitudinal sides as depicted in Figure 2.2. The specimens were further clamped at the top and bottom ends. Gaps of about 10 mm were left between the clamping ends and the top and bottom ends of knife edges, allowing the specimens to shorten during compression tests. A crosshead speed of 3.81 mm/min was chosen in compression tests. The CAI tests worked well for most thick composite laminates (6.69 mm) except for a couple of cases in which local damage due to crushing of laminate at clamping ends (top or bottom) took place when the composite laminates had either very small or no impactinduced damage. In order to avoid the local crushing damage, especially for those with small or no impact damage, end tabs were bonded to composite specimens. For thin specimens (2.24 mm), extra long end tabs which covered almost the entire length span of the composite specimens except for the area with impact-induced damage were used. However, the majority of thin specimens still experienced local crushing damage. It was determined that thin composite specimens of 2.24 mm were not suitable for use with the existing NASA's CAI test fixture.

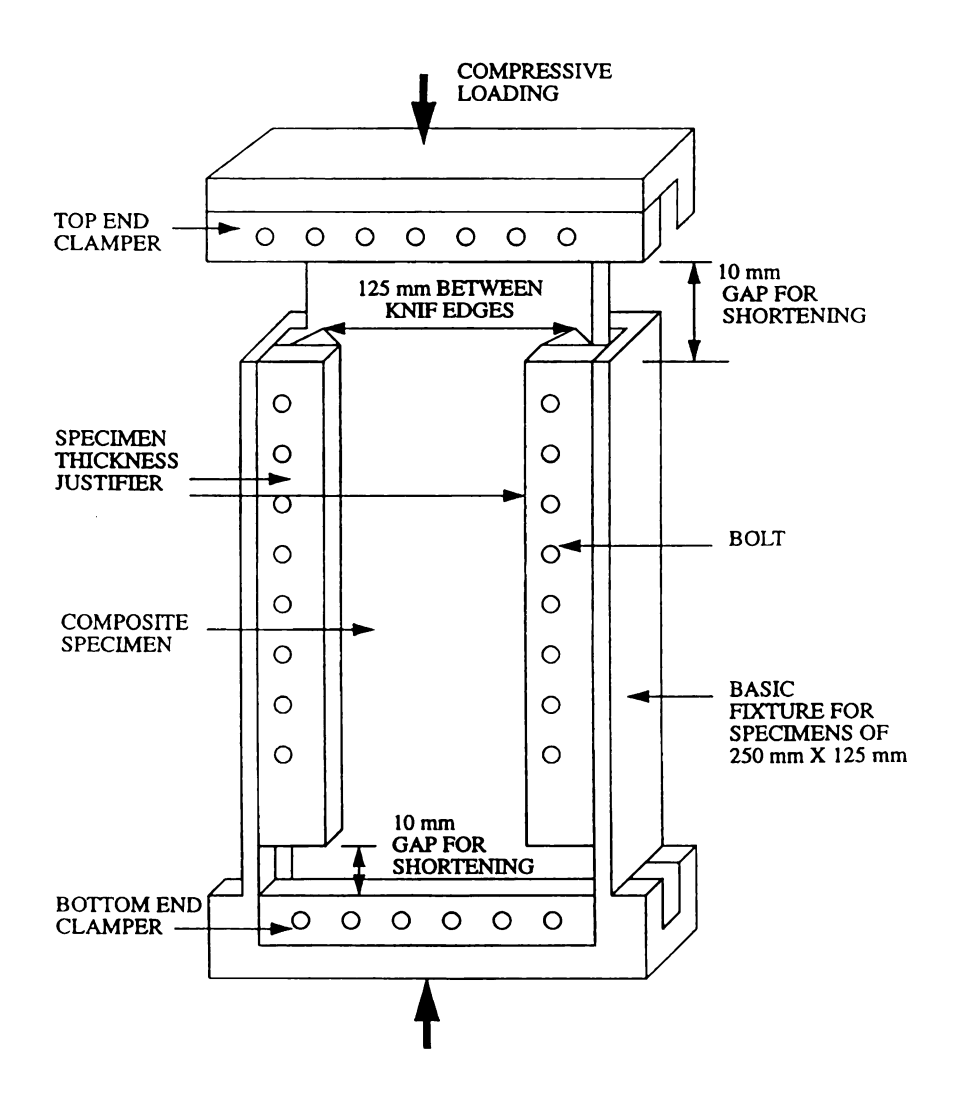


Figure 2.2. Schematic diagram of NASA compression after impact testing fixture

2.3 Experimental Results

1. Force History

Figure 2.3 shows the force histories of thick composite laminates (125 mm x 125 mm x 6.69 mm) at three different impact velocity levels. At low velocity (1.06 m/s), the impact damage in the composite laminate is insignificant and the composite laminate responds elastically since the loading and unloading curves are almost symmetric with respect to the peak force. As impact velocity increases (3.80 m/s), the unloading curve extends to the right, indicating that the composite laminate becomes softer as damage, such as delamination, becomes more significant. When the impact velocity is high (5.46 m/s), the primary section of contact duration is dramatically reduced, signifying the occurrence of perforation in composite laminate. The secondary section of contact duration is due to friction between the impactor and composite laminate after perforation.

2. Characteristics of Impact

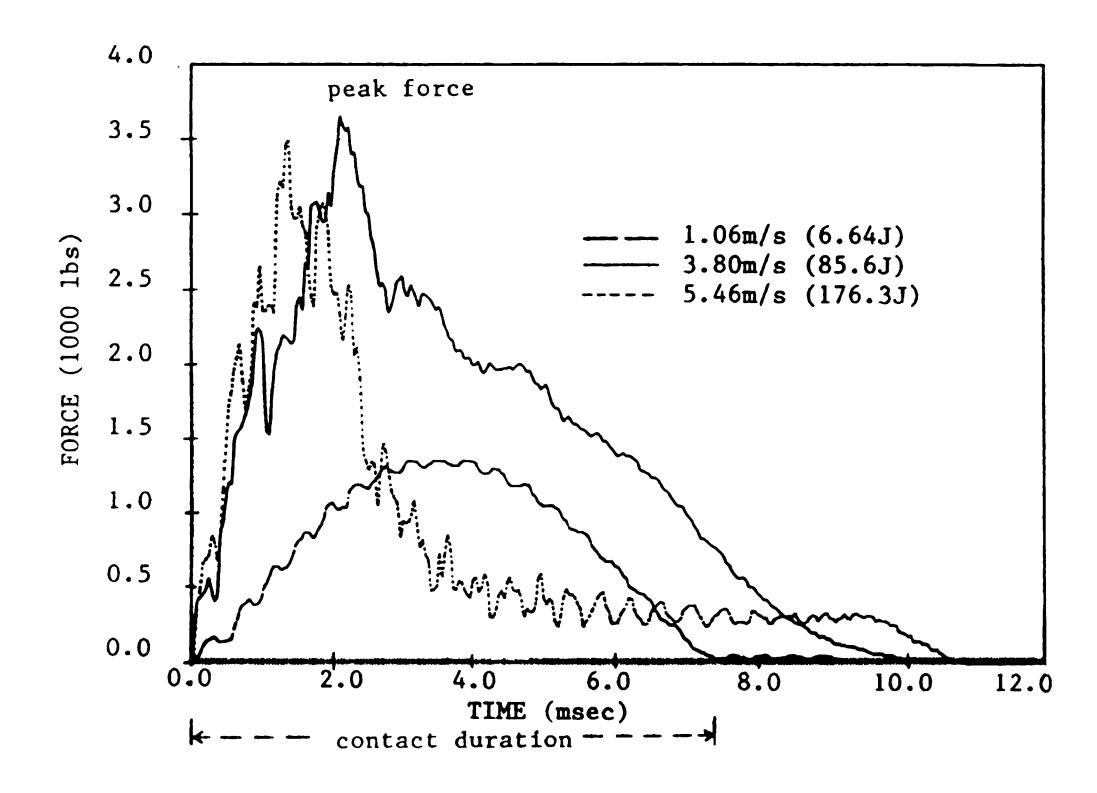
By examining the force and energy histories, it was concluded that peak force, contact duration, and absorbed energy were the most important characteristics of composite laminates subjected to impact loading. Figures 2.4-2.6 show the impact characteristics of both thick (6.69 mm) and thin (2.24 mm) laminates. The solid circles and open circles represent the characteristics for thick and thin composite laminates with effective impact zones of 125 mm x 125 mm, respectively. In addition, the dashed lines represent smooth curves of the solid circles while the solid lines represent smooth curves of the open circles in the diagrams. Figure 2.4 reveals that the peak forces increase as the impact energy increases. However, the value becomes relatively stable for thick

laminates and reaches a constant value for thin laminates. The turning points from nonlinear transition curves to stable or constant values are called critical points while the corresponding impact energy levels are called the *critical energy levels*. Similar results can also be seen from Fig. 6 for absorbed energy. In Figure 2.5, the contact duration is presented as a function of the impact energy.

For both thick and thin laminates, the contact duration increases rapidly as the impact energy increases. They reach individual peak points and sharply drop afterwards. The impact energy levels correspond to the peak points are also termed the critical energy levels.

3. Perforation Thresholds

As mentioned above that perforation is the most apparent damage mode in composite laminates subjected to impact loading. Hence, the perforation threshold is an important parameter in characterizing the response of composite laminates subjected to impact loading [2.17-2.20]. Since the peak force, contact duration, and absorbed energy all reach critical points when perforation takes place and the impact energy levels to cause perforation match with the corresponding critical energy levels, the perforation threshold of composite laminates can be identified through the following four methods: peak force, contact duration, absorbed energy and equal energy.



Fiure 2.3. Force histories at three impact velocity

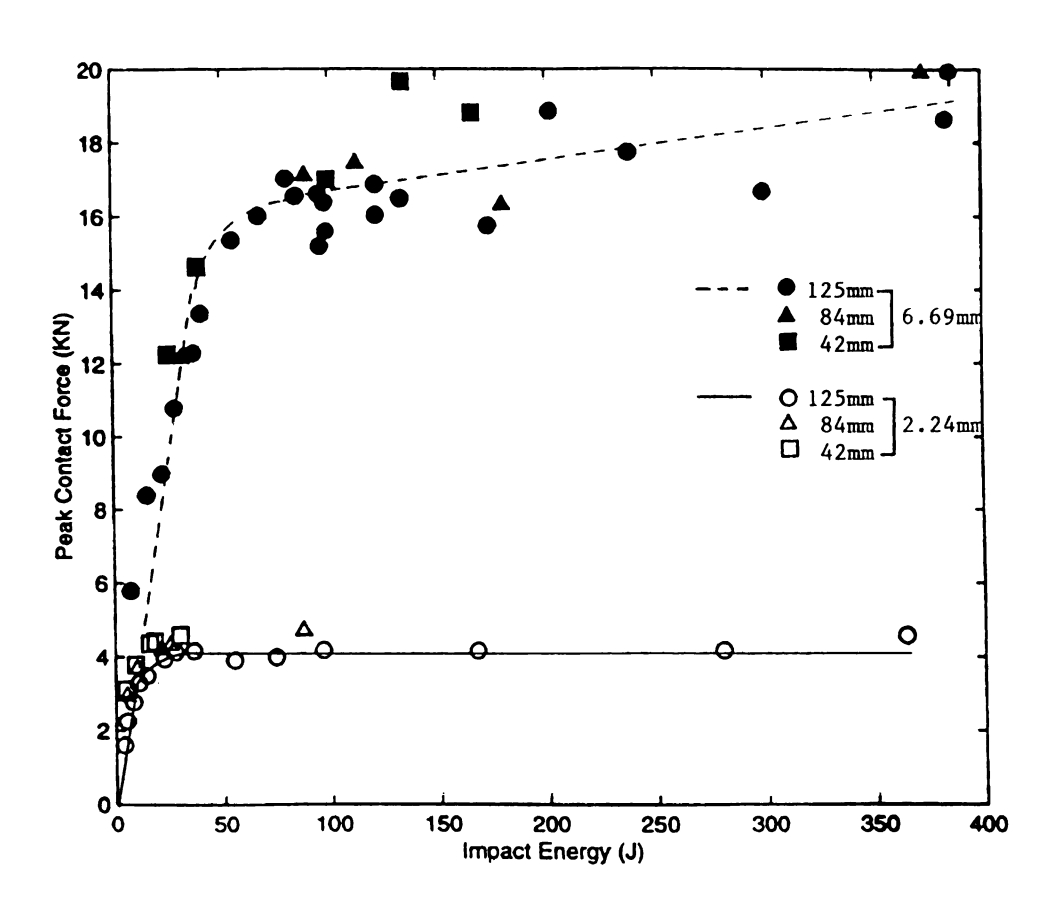


Figure 2.4. Relations between peak force and impact energy for composite laminates with various dimensions and thicknesses

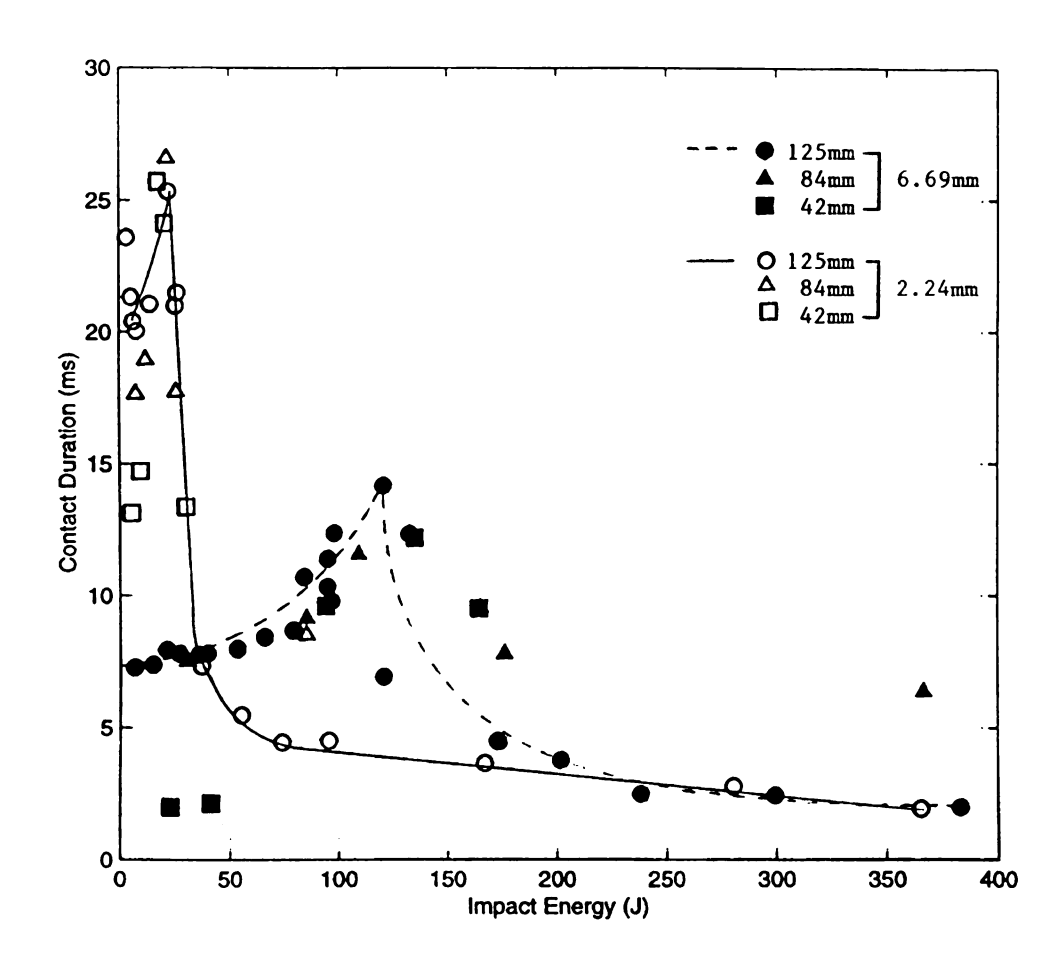


Figure 2.5. Relations between contact duration and impact energy for composite laminates with various dimensions and thicknesses



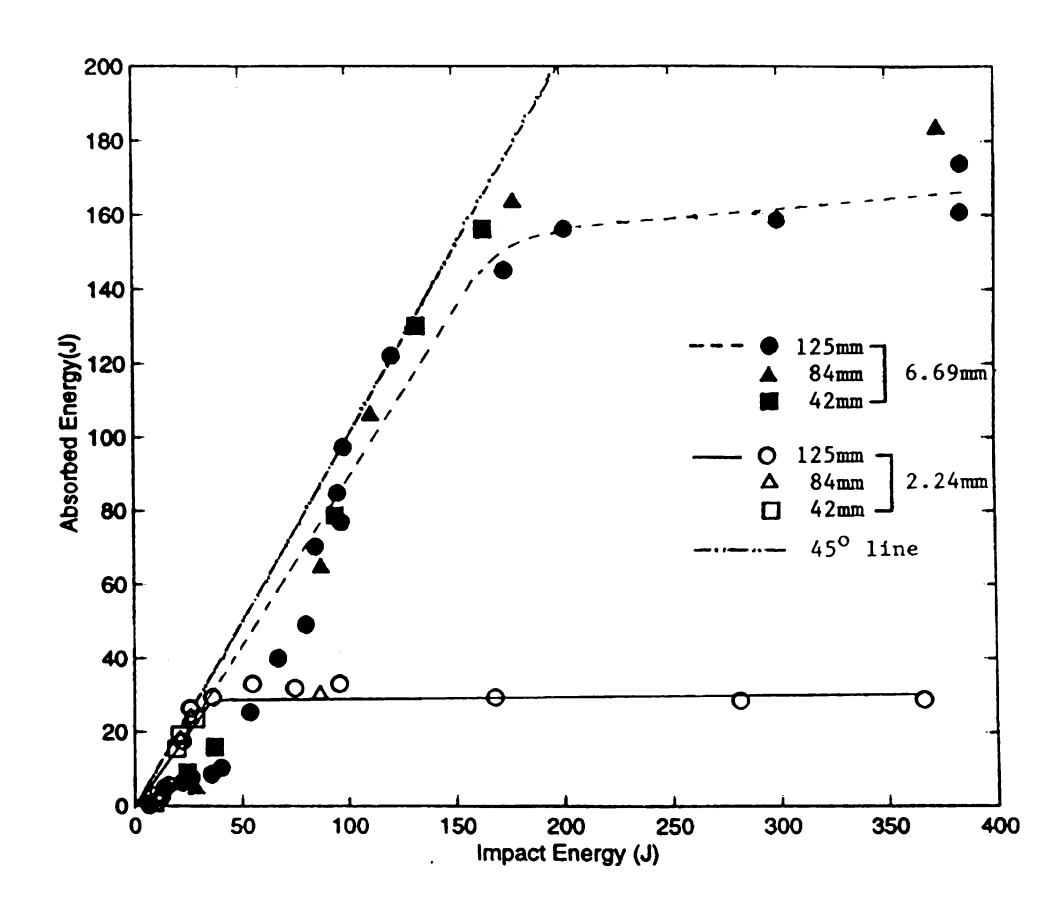


Figure 2.6. Relations between absorbed energy and impact energy for composite laminates with various dimensions and thicknesses

3.1 Peak Force Method

In Figure 2.4, the peak forces of thick composite laminates reach a relatively stable level, changing from a nonlinear transition curve to a straight line, around 16.2 kN when the impact energy is about 106 J (78 ft-lb), i.e. the critical energy level. This critical energy level was found to be slightly lower than the level to cause perforation by examining the impacted specimens. For thin composite laminates, the critical energy level is identified as 30 J (22 ft-lb) and is associated with a plateau of peak force of 4.2 kN. By examining the impacted specimens, it was found that this critical energy level was slightly higher than the energy level that caused perforation in thin composite laminates. The plateau seems to indicate that there was a maximum contact force that a thin composite laminate can sustain when it was subjected to impact loading and the maximum contact force was what required to perforate the thin composite laminate.

3.2 Contact Duration Method

The second method to identify the perforation threshold was based on the contact duration. Figure 2.5 shows the contact durations for thick and thin laminates at various impact energy levels. For thick composite laminates, the critical energy level is around 120 J (88.5 ft-lb) while it is around 21.5 J (16 ft-lb) for thin composite laminates. The former was very much the impact energy level to cause perforation since some thick specimens were perforated and some were not when subjected to this impact energy level. The latter was found to be slightly lower than that caused perforation since no thin specimens were perforated under this impact energy level.



3.3 Absorbed Energy Method

Shown in Figure 2.6, the absorbed energy approaches a relatively stable level around 150 J for thick laminates when impact energy level reaches 190 J (140 ft-lb), i.e. the critical energy level. This impact energy level was much higher than that obtained from the peak force analysis as given in section 3.1 and was confirmed to greatly exceed the impact energy level to cause perforation. It should be pointed out, however, that there were relatively few data points located between 100 J and 200 J. It was believed that insufficient data points within the range were responsible for errors in generating a smooth curve, and hence the inaccurate estimate. The estimate of perforation threshold for 2.24 mm laminates is around 35 J (25.8 ft-lb) when the absorbed energy reaches a constant level of 28.5 J. It was also higher than experimental observations.

3.4 Equal Energy Method

The fourth technique to identify the perforation threshold is based on comparison between impact energy and absorbed energy. It was found that composite laminates experienced perforation when these two energy levels became very close. In other words, perforation seemed to take place when the kinetic energy of the impactor was almost completely transferred to the composite laminate. Results based on this argument can be seen in Figure 2.6. The 45° line which represents equality between impact energy and absorbed energy goes through solid circles and an open circle, giving the perforation threshold of 120 J (88.5 ft-lb) for thick laminates and 26 J (19.2 ft-lb) for thin laminates. These two results were found to best match with experimental observations for perforation threshold among the four methods.

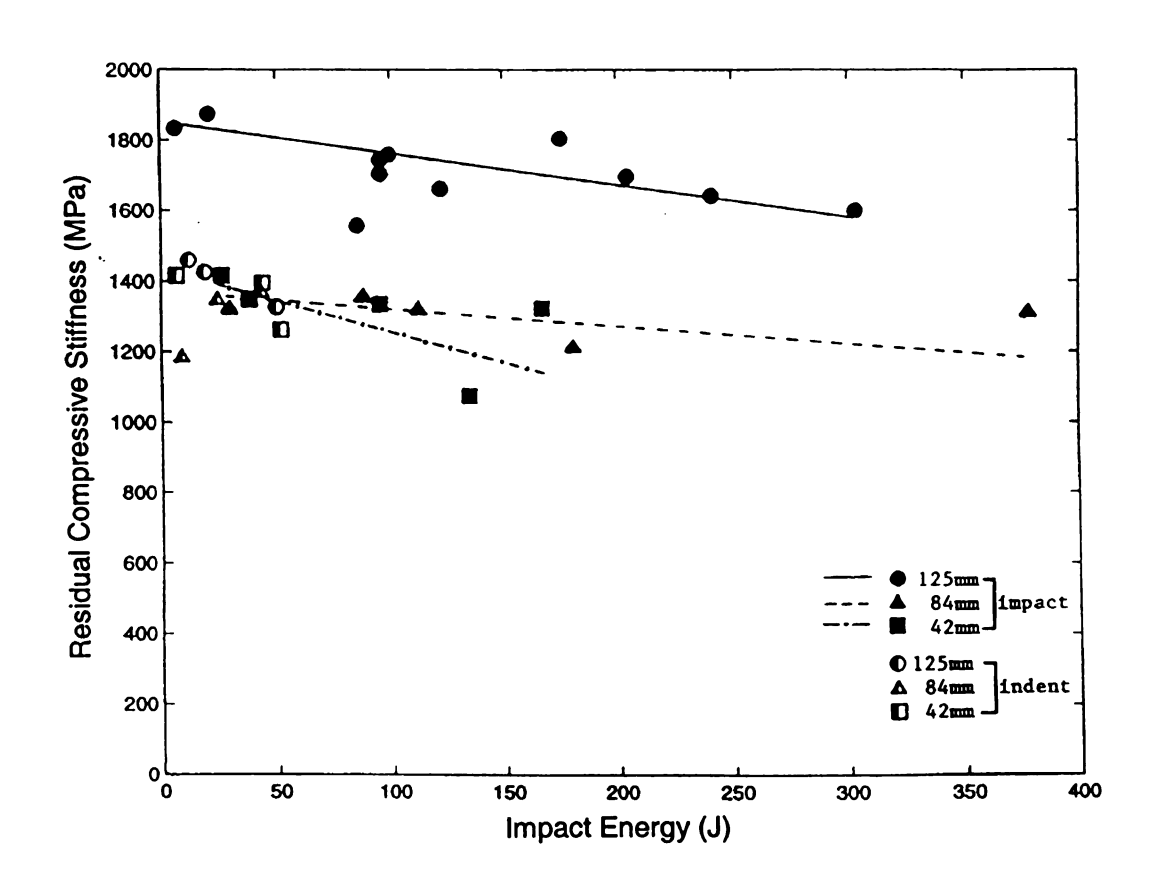


Figure 2.7. Relations between residual compressive stiffness and impact energy for composite laminates with various dimensions and thicknesses

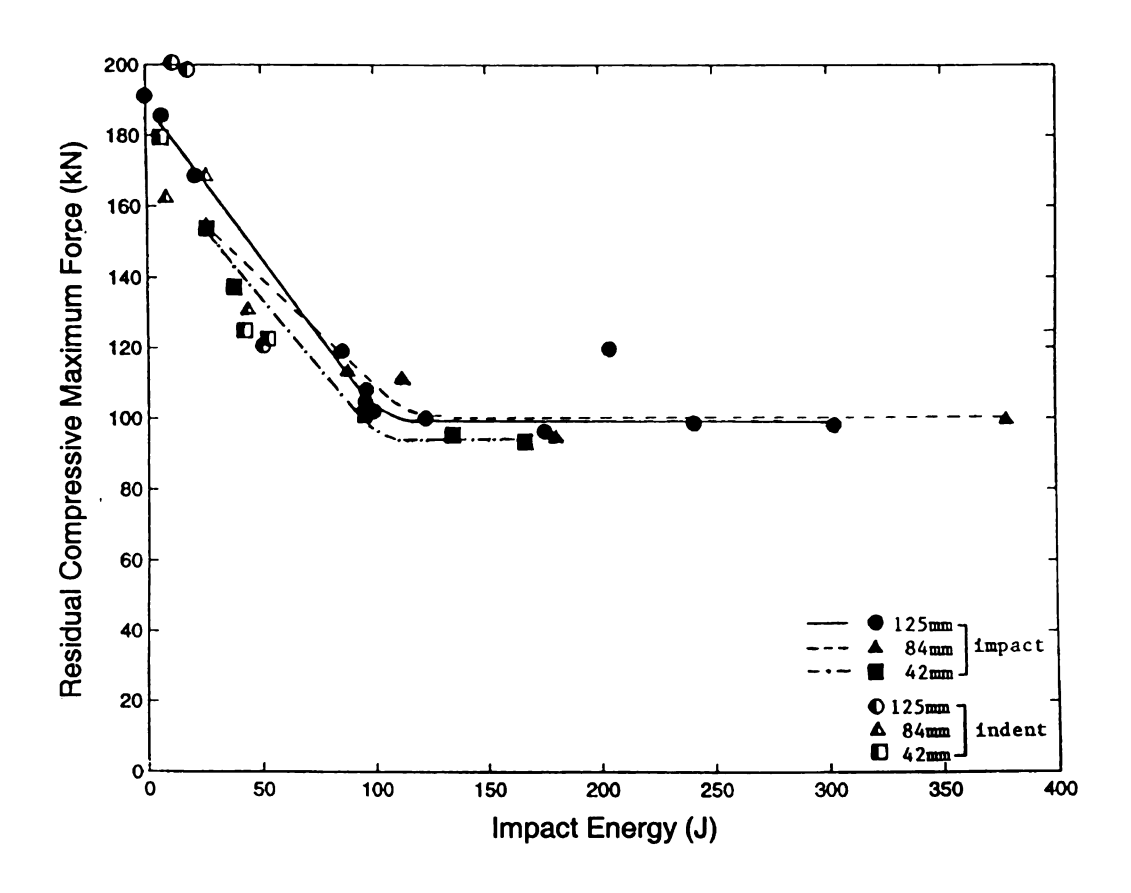


Figure 2.8. Relations between residual compressive maximum force and impact energy for composite laminates with various dimensions and thicknesses

ì				

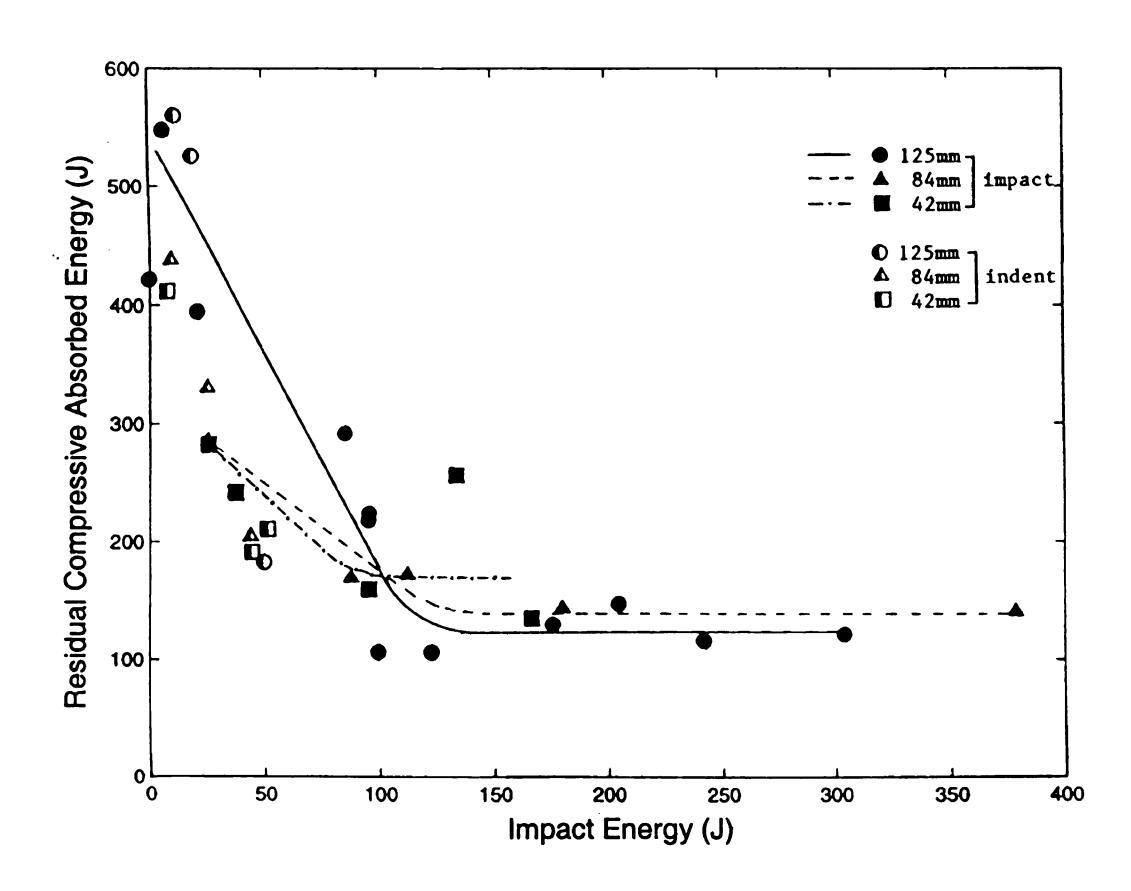


Figure 2.9. Relations between residual compressive absorbed energy and impact energy for composite laminates with various dimensions and thicknesses



4. Residual Compressive Properties

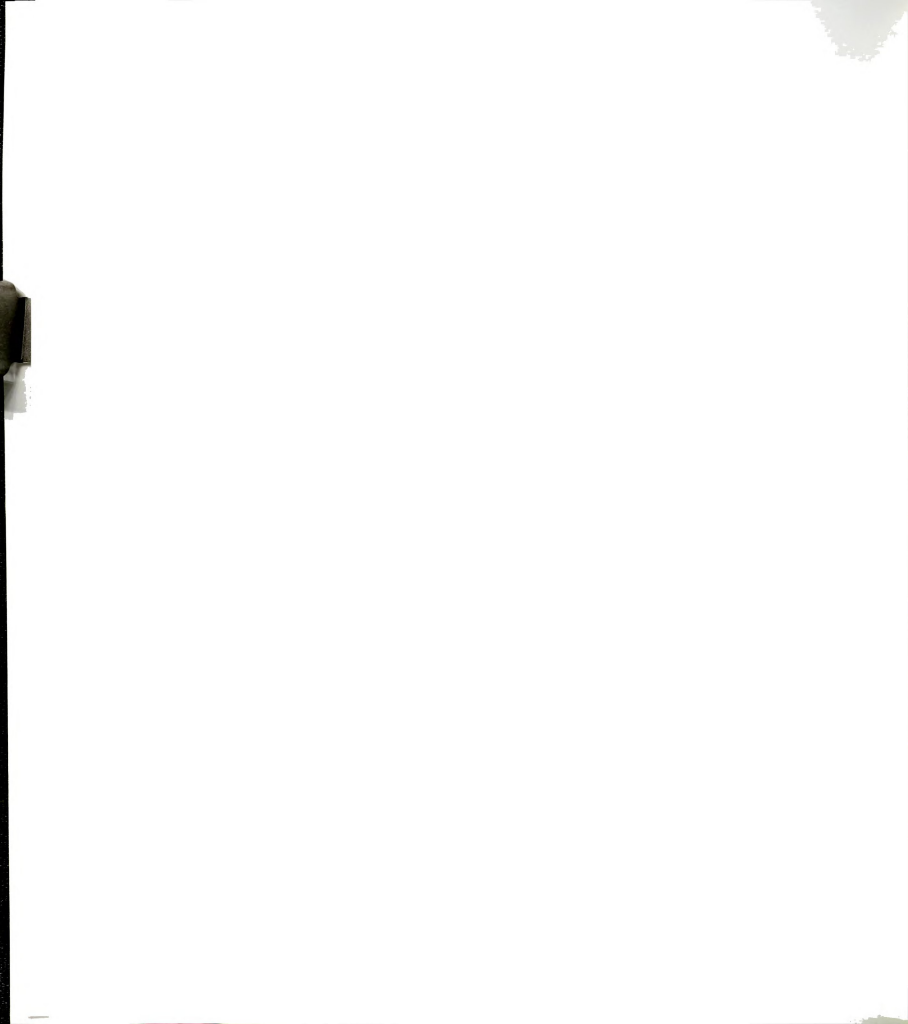
In addition to nondestructive investigations, an effective way to characterize the degree of impact-induced damage is to quantify the residual properties of composite laminates which have been subjected to impact. It has been reported by many researchers that compression after impact is an effective test for this purpose due to the fact that delamination is an important damage mode in impacted composite laminates and compressive properties of composite laminates are very sensitive to the size and location of delamination.

Figures 2.7-2.9 show the residual compressive stiffness, residual compressive maximum force, and residual compressive absorbed energy for thick composite laminates based on CAI tests. The residual compressive stiffness represents the slope of a forcedisplacement curve obtained from CAI test; the residual compressive maximum force represents the force to cause buckling, i.e. the peak force of the force-displacement relation; while the residual compressive absorbed energy can be calculated from the area under the force-displacement curve. The residual compressive stiffness decreases gradually as the impact energy increases. However, both the residual compressive maximum force and residual compressive absorbed energy drop rapidly from their initial values and become constants when the impact energy levels exceed individual critical levels. The critical energy levels were also identified to be closely related to the perforation threshold. This result indicates that a maximum mechanical properties degradation of composite laminates takes place at perforation. Once perforation takes place, some residual compressive properties of composite laminates cannot be further degraded. In other words, as far as the residual compressive maximum force and residual

compressive absorbed energy are concerned, perforation seems to be the most important damage stage in composite laminates subjected to impact loading.

As impact energy increases, the reduction of residual compressive stiffness is not as dramatic as those of residual compressive maximum force and residual compressive absorbed energy. This is believed to be related to the fact that there is no delamination-induced local buckling involved in the measurement of compressive stiffness. In other words, local buckling plays a very important role in the reductions of residual compressive maximum force and residual compressive absorbed energy. Consequently, the residual compressive maximum force and the residual compressive absorbed energy are better than the residual compressive stiffness in presenting mechanical properties degradation of composite laminates subjected to impact loading. For convenience of discussions, the mechanical properties degradation will be referred to degradations of residual compressive maximum force and residual compressive absorbed energy hereafter.

As mentioned above, perforation took place when the residual compressive maximum force and residual compressive absorbed energy became constants as the impact energy approached critical values, changing from nonlinear curves to constants. The impact energy levels corresponding to the constant values of residual compressive maximum force and residual compressive absorbed energy, i.e. critical energy levels, for thick-large (125 mm x 125 mm x 6.69 mm) composite laminates are 115 J and 135 J, respectively. These two values are close to the impact energy level for perforation threshold, i.e. 120 J, as given in section 3.4. Accordingly, besides the aforementioned four methods, the studies of residual compressive maximum force and residual



compressive absorbed energy present two additional options for estimating the perforation threshold.

The compression after impact testing was also performed for impacted thin composite laminates. Local crushing damage close to the top and bottom clamping ends occurred in many tests. Extra-long end tabs were used to reinforce the specimens' ends to prevent local crushing damage from happening. Unfortunately, among the very few specimens which had no local crushing damage, only a couple of them showed strong interaction between impact-induced damage and compression-induced damage. Hence, it was concluded that thin (2.24 mm) specimens are not suitable for CAI testing using NASA's test fixture.

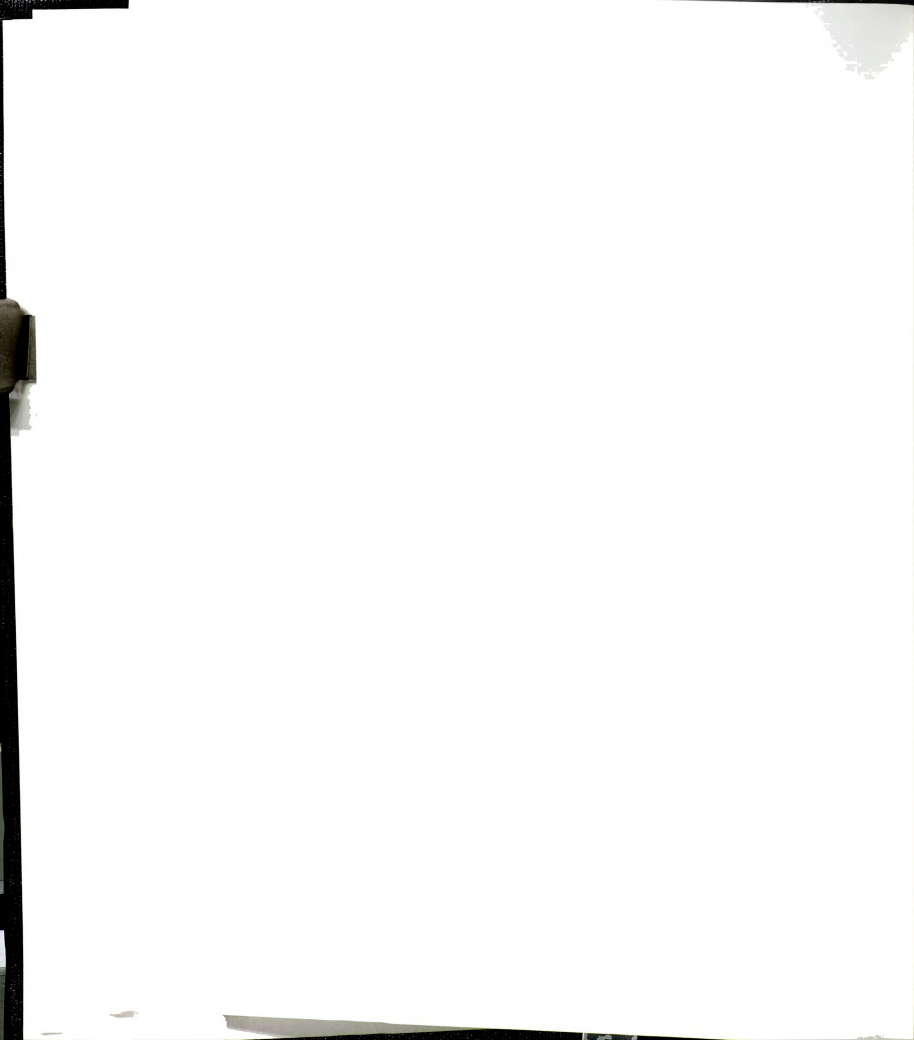
5. In-Plane Dimensional Effects

In addition to effective impact zone of 125 mm x 125 mm, other effective impact zones of 84 mm x 84 mm and 42 mm x 42 mm, i.e. intermediate and small specimens, were investigated for in-plane dimensional effects. Experimental results regarding the peak force are also shown in Figure 2.4. The solid triangles are for thick-intermediate (84 mm x 84 mm x 6.69 mm) laminates while the solid squares are for thick-small (42 mm x 42 mm x 6.69 mm) laminates. Although it can be concluded that the smaller the size of composite laminate the higher the peak force, the difference of peak force for the three effective impact zones is not as significant as that for thickness difference. In fact, the result that smaller specimens has higher peak forces coincides with the fact that the smaller the laminate dimensions the stiffer the composite laminate. Similar results are

also found for thin (2.24 mm) composite laminates, represented by open triangles and open squares.

The effects of dimensions on the contact duration is also shown in Figure 2.5. Although stiffer specimens are expected to have shorter contact durations than the softer counterparts, the difference shown in Figure 2.5 is not conclusive. Figure 2.6 gives the experimental results for the absorbed energy based on the three effective impact zones. It can be seen that the smaller the laminate size the higher the absorbed energy for thick composite laminates. Apparently, damage in smaller laminates is more serious than that in larger laminates because the former have higher stiffnesses than the latter. However, different results are found in the study for thin composite laminates.

In addition to the peak force, contact duration, and absorbed energy, the effects of dimensions on residual compressive properties can also be found in Figures 2.7-2.9. Although there are three effective impact zones, all the laminates have identical dimensions, i.e. 250 mm x 125 mm, for CAI tests. However, the residual compressive stiffness of thick-intermediate and thick-small composite laminates are smaller than that of thick-large composite laminates. The differences for the residual compressive maximum force and the residual compressive absorbed energy of the three effective impact zones are not as high as that of the residual compressive stiffness. In addition, the estimates of perforation thresholds for laminates with different effective impact zones seem to be close.



6. Thickness Effects

As mentioned above, the impact response of composite laminates changes significantly as the laminate thickness increases. The ratio of peak force between the thick-large and thin-large composite laminates is 4.01 (16.6 kN versus 4.14 kN). The ratio of absorbed energy is 4.62 (120 J versus 26 J). Apparently, these two numbers are higher than the thickness ratio, which is around 3 (6.69 mm versus 2.24 mm), exhibiting a nonlinear proportion with respect to thickness or the existence of size effect due to thickness.

In an effort to understand the thickness effect, two additional tests were performed. The first test examined two thin laminates (2.24 mm each). They were put together without an adhesive bonding between them. Together they were called a double-layer system and were subjected to an impact force. The second test was similar to the first one but had three thin laminates, namely a triple-layer system. Since 26 J was found to be the perforation threshold for a thin single-layer, double and triple energy levels were applied to the double- and triple-layer systems, respectively. The double-layer and triple-layer systems were found to be close to perforation. Experimental results for the three systems along with a thick (125 mm x 125 mm x 6.69 mm) laminate subjected to impact energy of 80 J are given in Figure 2.10.

Excellent linear relations were found among the single-, double-, and triple-layer systems. However, the results from the thick composite laminate are not near the linear regressions. Comparing to the triple-layer system, the peak force of the thick composite laminate is considerably higher while the contact duration is considerably lower. These results are believed to be attributed to higher stiffness of the thick composite laminate as

opposed to the triple-layer system. In fact, the bending stiffness of the thick composite laminate is about nine times higher than the triple-layer system.

The investigations for multiple-layer systems provides some fundamental insights into thickness effect. As shown in Figure 2.10, the impact energy levels for the triple-layer system and the thick composite laminate are about the same, i.e. around 78 J. This impact energy level is not too far away from perforating the triple-layer system, based on experimental observation, but is certainly much lower than the 120 J required to perforate the thick composite laminate. It is believed that the difference is attributed to the fact that the bending rigidity of the thick composite laminate is much higher than that of the triple-layer system, i.e. 9:1. This result concludes the superiority of impact resistance of a single-layer thick composite laminate to a multiple-layer system, which has the same thickness as the single-layer thick composite laminate.

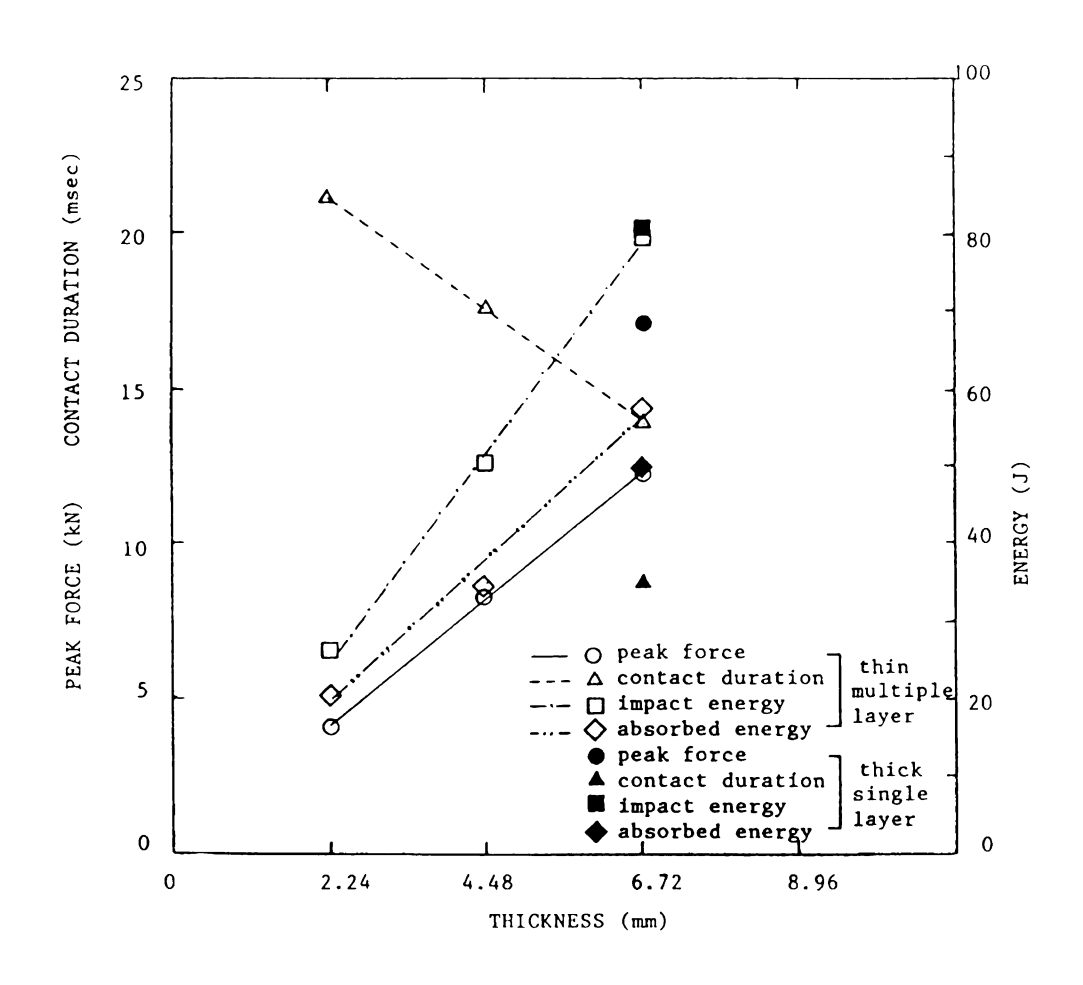
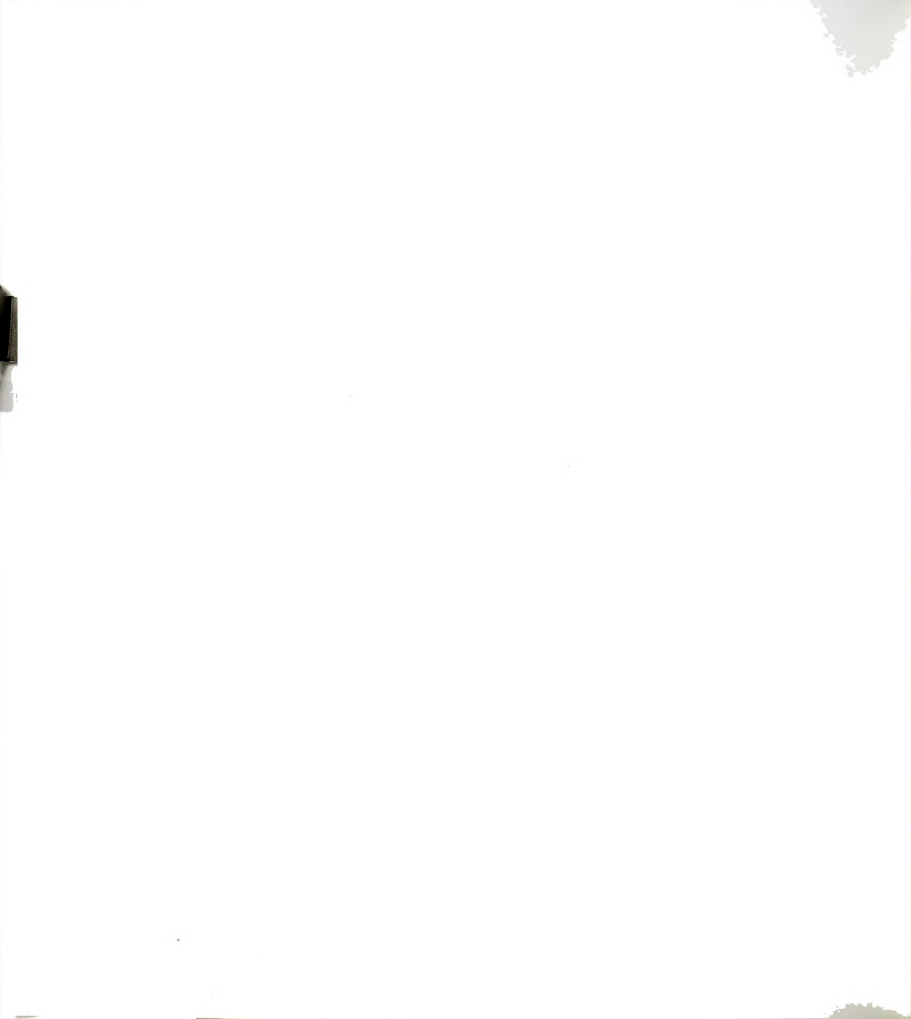


Figure 2.10. Relations between impact characteristics and laminate thicknesses



7. Strain Rate Effects

A commonly raised issue in investigating impact dynamics is regarding the difference and similarity of the roles of impact velocity and impact energy. More specifically, will composite laminates behave the same under constant impact energy but different impact velocities? Since the impactor mass and diameter are kept constants in the present investigation, impact energy is proportional to the second power of impact velocity. Accordingly, the aforementioned issue cannot be addressed. However, it should be recognized that, with the use of impact energy, both the peak force and absorbed energy increase linearly and reach stable values, and the residual compressive maximum force and the residual compressive absorbed energy decrease linearly and become constants when perforation takes place. Thus, the advantage of using impact energy to gain simple, linear relationships is clear.

In an effort to further understand the effect of impact velocity, or the strain rate effect, quasi-static indentation tests were performed. In this study, thick-large composite laminates were held by fixtures similar to those used in impact tests. The specimenholders were then fixed to the bottom grip of an Instron hydraulic testing machine and loaded by a steel indenter held by the top grip. The indenter had a diameter of 12.5 mm and a nose of hemispherical shape. The indentation was performed at a crosshead speed of 3.81 mm/min. The force history and displacement history were recorded by the load cell and the movement of hydraulic actuator, respectively.

Figure 2.11 gives a typical load-displacement relation of the quasi-static indentation. It starts with a linear relation until a local maximum was reached. It then drops to a local minimum due to delamination. The overall maximum load was



eventually achieved before perforation takes place. A descending curve follows due to the frictional force between the indenter and the composite laminate. Experimental results regarding the residual mechanical properties are also shown in Figs. 7-9 for comparisons with dynamic studies. The quasi-static results, which are represented by the half-open-and-half-solid symbols, are lower than dynamic impact results in many cases. This seems to explain the fact that composite laminates have higher stiffnesses and strengths at higher strain rates.

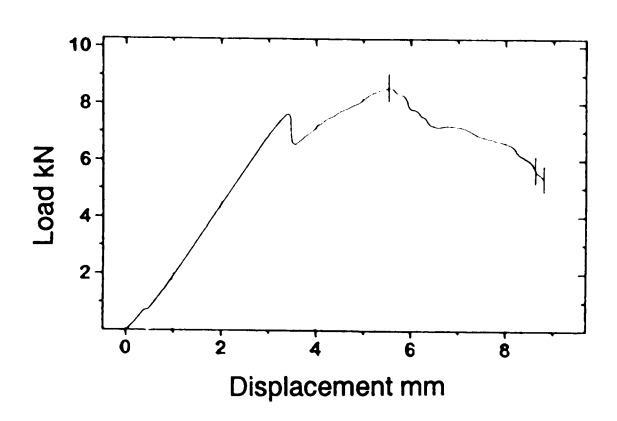


Figure 2.11. Typical load-displacement relation from indentation testing

Table 2.1. Summary of peak forces and impact energy levels at penetration for composite laminates of various dimensions and thicknesses subjected to impact and indentation loads

		Dimensions									
		Large 125 mm × 125 mm		Intermediate 84 mm × 84 mm		Small 42 mm × 42 mm					
Thicknesses		impact	indent	impact	indent	impact	indent				
Thick	Peak force (kN)	16.6	8.6	17.5	8.7	19.8	8.9				
6.69 mm	Impact energy (J)	120	51	112	44	130	52				
Thin	Peak force (kN)	4.14	1.56	4.21	1.44	4.22	1.85				
2.24 mm	Impact energy (J)	26.0	10.9	25.2	11.9	21.7	9.1				

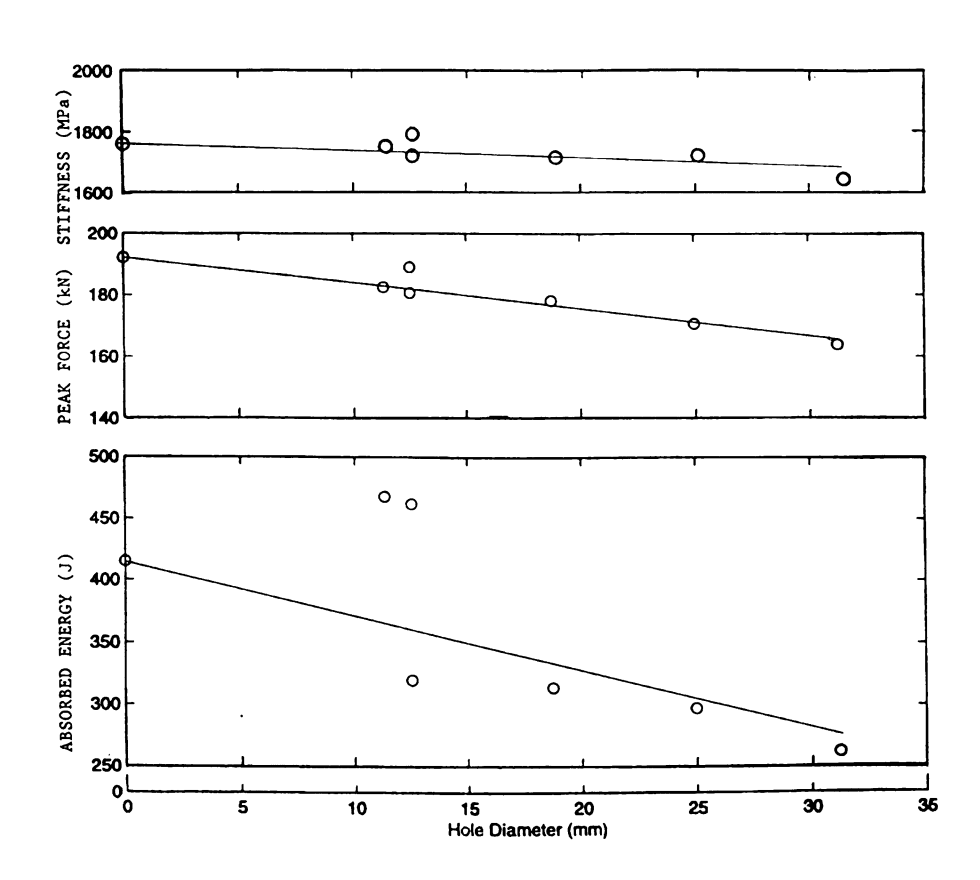


Figure 2.12. Relations between mechanical properties degradation and hole size for composite laminates with open hole

Although the indentation tests provide some fundamental knowledge on strain rate effect, the tests cannot be used to substitute impact tests. As shown in Figures 2.7-2.9, the level of indentation energy cannot be further raised once perforation takes place while the level of impact energy can always be increased by increasing impact velocity. Accordingly, the important feature that residual mechanical properties drop rapidly then approach constant levels as obtained from impact tests cannot be reproduced from indentation tests. Table 2.1 summarizes the peak forces and impact energy levels to cause perforation for composite laminates with various dimensions and thicknesses. It can be seen that there is a significant difference between impact and indentation responses, not to mention the difference in damage mode.

8. Open Hole Tests

Another study to understand the effects of damage mode on the compressive response of impacted composite laminates was based on open hole tests. In this study, tests were performed for thick-large composite laminates with holes of diameters ranging from 11.33 mm (29/64 in) to 31.25 mm (5/4 in). Figure 2.12 gives all three mechanical properties. When comparing Figure 2.12 with Figure 2.7, the difference of residual compressive stiffness between the ones with impact-induced damage and those with open holes is small. This is due to the fact that the residual compressive stiffness is only affected by the size of through-the-thickness opening, either impact-induced perforation or artificial open hole. However, both the residual compressive maximum force and residual compressive absorbed energy of composite laminates with a 12.5 mm hole, shown in Figure 2.12, are much higher than those with impact-induced perforation

(which has a perforation opening of approximately 12.5 mm and large delamination areas), given in Figurs 2.8 and 2.9. This result indicates that delamination also plays a very important role in the compressive response of impacted composite laminates.

Another result which can be obtained from Figure 2.12 is the so-called equivalent damage size. From Figures 2.8 and 2.9, the residual compressive maximum force and residual compressive absorbed energy reach 100 kN and 120 J, respectively, when perforation takes place. By extending the smooth lines in Figure 2.12, the hole sizes corresponding to 100 kN and 120 J, i.e. equivalent damage sizes, can be obtained. They are, however, much larger than the size of the impactor (12.5 mm) and even the specimen width (i.e. 125 mm) if linear regressions in Figure 2.12 are used. This result again indicates the very important role of delamination in mechanical properties degradation although it is not as apparent as perforation, sometimes even invisible to naked eyes.

2.4 Discussions

1. Size Effects

In this study, composite laminates of three effective impact zones and two thicknesses were investigated. However, the distinctions between the large and small, and the thick and thin laminates need to be further defined. According to the Classical Plate Theory, the definitions of thin and thick plates are tied to the ratio of in-plane dimension to thickness, l/h. Table 2.2 gives the ratios of l/h for all composite laminates investigated in this study. Since a ratio of 20 is usually considered as the minimum requirement for being qualified as a thin plate, 6.69 mm laminates are considered as thick

plates. Although the thick-large (125 mm x 125 mm x 6.69 mm) specimens and the thin-small (42 mm x 42 mm x 2.24 mm) specimens have almost identical l/h ratio, i.e. 18.7 and 18.8, respectively, experimental results between them were quite different. This indicates that the impactor diameter is also an important parameter in impact study.

The ratios of specimen in-plane dimension to impactor diameter, l/d, and specimen thickness to impactor diameter, h/d, are also shown in Table 2.2 along with the ratio of in-plane dimension to thickness l/h. It can be seen from the ratios given in Table 2.2 that l/h displays the equal important roles of in-plane dimensional and thickness effects, l/d shows the sole important role of in-plane dimensional effect, while h/d indicates the sole important role of thickness effect. Since experimental results show that thickness effect is much more significant than in-plane dimensional effect, h/d seems to be the most important ratio among the three ratios presented. Since the impactor diameter is kept constant in this study, the thickness of composite laminates is then the most important parameter in impact response.

Table 2.2. Ratios of specimen dimensions, thickness, and impactor diameter

		Dimensions I				
	l/h	125 mm	84 mm	42 mm	h/d	
TI: 1	6.69 mm	18.7	12.6	6.3	0.54	
Thickness h	2.24 mm	55.8	37.5	18.8	0.18	
l/d		10	6.7	3.4		

I is specimen dimension.h is specimen thickness.d is impactor diameter, 12.5 mm.

2. Comparison between In-Plane Dimensional and Thickness Effects

The response of composite laminates to impact loading, to some extent, resembles plate bending which is governed by bending rigidity. The bending rigidity is defined as where is Young's modulus and is the second moment of area which can be expressed as where is laminate dimensions and is thickness. In fact, the bending rigidity has been successfully used in interpreting the potential of delamination in composite laminates subjected to impact loading [2.16]. The definition of the second moment of area shows that it is proportional to the third power of thickness while it is only the first power of inplane dimension. Since the impact response of composite laminates as mentioned above is more strongly affected by thickness than by in-plane dimension, the bending rigidity, which is capable of discriminating between thickness and in-plane dimension, seems to qualify itself as an important element, if not the element, of an analytical model for perforation analysis.

The feasibility of utilizing bending rigidity in impact response analysis is also well supported by experimental results. As mentioned above, excellent linear relation of impact response exists when the impacted composite laminate is changed from single-layer to double-layer, and to triple-layer system. However, it is also found that the ratios of peak force and absorbed energy between thick and thin composite laminates are higher than the thickness ratio, exhibiting a nonlinear proportion with respect to thickness. Both of the results seem to provide a solid foundation of rationalizing the use of bending rigidity for perforation analysis.

3. Damage Modes

Both the peak force and absorbed energy of impacted composite laminates reach relatively stable levels once perforation takes place. In addition, the residual compressive maximum force and residual compressive absorbed energy drop to constant values when perforation takes place. All these seem to imply that the peak force and absorbed energy should also become constant instead of just stabilized when perforation is reached. Hence, more tests are required to further verify this hypothesis. However, whether the impact response and mechanical properties degradation become constant or stabilized, the most significant fact is that they both reach apparent turning points when perforation takes place. Accordingly, as far as material response is concerned, perforation is the most important damage stage in composite laminates subjected to impact loading.

As mentioned above, the damage modes in perforated composite laminates includes macroscopic damage, such as indentation, surface cracking, delamination, and perforation, and microscopic damage, such as fiber breakage, matrix cracking, fiber-matrix debonding, etc. All individual damage modes play important roles in impact response of composite laminates. However, based on open hole study, it can be concluded that perforation alone causes a small portion of mechanical properties degradation. It is delamination which is responsible for local buckling and hence significant mechanical properties degradation.

Perforation is easy to identify. It is about the size of impactor. However, delamination area and location are very difficult to measure, if not impossible. Since delamination plays a very important role in impact response and mechanical properties



degradation, many nondestructive techniques have been developed to identify delamination. In addition, it has been concluded that delamination cannot be represented by an equivalent hole size. It then is important to consider the true geometry of delamination, i.e. debonding between laminae, in delamination modeling.

4. Characteristics of Perforation and Delamination

The residual compressive stiffness is not strongly affected by delamination because local buckling does not occur in the early stage of a CAI test. In fact, it is dependent on a damage area combining the impactor and its surrounding area with through-the-thickness damage. Therefore, it is concluded that the modeling of compressive stiffness needs to be tied to the modeling of the through-the-thickness perforation zone. And a linear relation between the perforation opening and residual stiffness should be established.

The modeling of delamination can be approached from plate bending analysis. As a composite laminate bends, high interlaminar shear stresses are formed, resulting in delamination due to low interlaminar strengths. When the delaminated composite is subjected to uniaxial compression, local bending-buckling can take place in individual delaminated layers. Since bending rigidity decreases with the third power of thickness, as composites delaminates, both compressive maximum force and compressive absorbed energy degrade rapidly as delamination increases.

2.5 Conclusions

The following conclusions can be drawn from the investigations:

- 1. Once perforation takes place, both impact characteristics, such as peak force of impact, impact-contact duration and absorbed energy during impact, and mechanical properties degradation, such as residual compressive maximum force and residual compressive absorbed energy, reach turning points. Accordingly, these five parameters can be used to identify the perforation thresholds of composite laminates. Since these parameters are important elements of material response, perforation can be concluded as the most important damage stage, as far as material response is concerned, in composite laminates subjected to impact loading,
- 2. The study of size effects on impact response of composite laminates should be divided into two categories: in-plane dimensional effect and thickness effect. Among the ratios based on specimen in-plane dimensions, specimen thickness and impactor diameter, the ratio of specimen thickness to impactor diameter seems to best match with the experimental results. Since the impactor diameter is kept constant in this study, the thickness of composite laminates becomes the most important parameter in impact response. Hence, thickness effect is much more significant than in-plane dimensional effect.
- 3. In rationalize the superiority of thickness effect to in-plane dimensional effect on impact response, bending ri gidity should be considered as an important element for perforation analysis since it is proportional to the third power of thickness while only the first power of in- plane dimension. Its capability of discriminating between thickness and

in-plane dimension seems to be consistent with the experimental results that thickness effect is more significant than in-plane dimensional effect.

- 4. Although perforation is the most important damage stage, as far as material response is concerned, in composite laminates subjected to impact loading, perforation alone causes a small portion of mechanical properties degradation. It is delamination which also plays an important role in impact energy absorption and mechanical properties degradation since delamination has been identified as the other primary damage mode in impacted composite laminates.
- 5. The utilization of bending rigidity for perforation analysis can also be extended to delamination analysis. In fact bending rigidity has been successfully used in a previous study for predicting the potential of delamination of composite laminates subjected to impact loading. Its capability in interpreting the mechanical properties degradation is well supported by the experimental results that both compressive maximum force and compressive absorbed energy degrade rapidly when delamination exists while compressive stiffness does not.

ACKNOWLEDGEMENTS

This investigation was supported by the Independent Laboratory in-house Research (ILIR) program at the U.S. Army - Tank Automotive and Armaments Command's (TACOM) Research, Development & Engineering Center (TARDEC). The authors wish to express their sincere thanks for this financial support.

2.6 References

- 2.1. Workshop on scaling effects in composite materials and structures, NASA Langley Research Center, Hampton, VA, November 15-16, 1993, Report No. 94-6, Institute for Mechanics and Materials, University of California, San Diego, CA.
- 2.2. Carpinteri, A., ed., Size-scale effects in the failure mechanisms of materials and structures, E & FN Spon, 1994.
- 2.3. S.B. Batdorf, Note on composite size effect, *J. Composite Technology and Research*, 45, 35- 37, 1989.
- 2.4. I. Shahid, H.-T. Sun, and F.-K. Chang, Predicting scaling effect on the notched strength of prepreg and fiber tow-placed laminated composites, *J. Composite Materials*, 29(8), 1063-1095, 1995.
- 2.5. C.E. Harris and D.E. Morris, Effects of laminate thickness and specimen configuration on the fracture of laminated composites, *Composite Materials Testing and Design, ASTM STP 893*, 177-195, 1986.
- 2.6. Y. D. S. Rajapakse, ed., *Mechanics of Thick Composites*, AMD-Vol. 162, The American Society of Mechanical Engineers, 1993.
- 2.7. J. Morton, Scaling of impact-loaded carbon-fiber composites, *AIAA Journal*, 26(8), 989-994, 1988.
- 2.8. Y. Qian, S.R. Swanson, R.J. Nuismer, and R.B. Bucinell, An experimental study of scaling rules for impact damage in fiber composites, *J. Composite Materials*, 24(5), 559-570, 1990.

- 2.9. B.V. Sankar, Scaling of low-velocity impact for symmetric composite laminates, *J. Reinforced Plastics and Composites*, 11, 297-305, 1992.
- 2.10. J.M. Whitney and R.J. Nuismer, Stress fracture criteria for laminated composites containing stress concentrations, *J. Composite Materials*, 8(3), 253-265, 1974.
- 2.11. J. Awerbuch and M. Madhukar, Notched strength of composite laminates predictions and experiments a review, *J. Reinforced Plastics and Composites*, 4, 3-159, 1985.
- 2.12. W.J. Cantwell, P.T. Curtis, and J. Morton, Low velocity impact damage tolerance in CFRP laminates containing woven and non-woven layers, *Composites*, 14, 301-305, 1983.
- 2.13. E.G. Guynn and T.K. O'Brien, The influence of lay-up and thickness on composite impact damage and compression strength, *proc. 26th AIAA SDM Conference*, Orlando, Florida, 187-196, 1985.
- 2.14. A.A. Baker, R. Jones, and R.J. Callinan, Damage tolerance of graphite/epoxy composites, *Composite Structures*, 4, 15-44, 1985.
- 2.15. Standard Tests for Toughened Resin Composites, NASA RP 1092, 1983.
- 2.16. Liu, Dahsin, Impact-induced delamination a view of material property mismatching, *J. Composite Materials*, 22(7), 674-691, 1988.
- 2.17. E. Wu, E.-Z. Tsai, and Y.-C. Chen, Penetration into glass epoxy composite laminates," *J. Composite Materials*, 28, 1783-1802, 1994.
- 2.18. C.T. Sun and S.V. Potti, High velocity impact and penetration of composite laminates, proc. 9th Int. Conference on Composite Materials, 4, 157-165, 1993.

- 2.19. W. Goldsmity, C.K.H. Dharan and H. Chang, Quasi-static and ballistic perforation of carbon fiber laminates, *Int. J. Solid Structures*, 32, 89-103, 1995.
- 2.20. S.W.R. Lee and C.T. Sun, Dynamic penetration of graphite/epoxy laminates impacted by a blunt-ended projectile, *Composite Science and Technology*, 49, 369-380, 1993.

Chapter 3

IMPACT PERFORATION RESISTANCE OF LAMINATED AND ASSEMBLED COMPOSITE PLATES

ABSTRACT

A previous study on impact response of composite laminates concluded that impact perforation was the most important damage stage in composite laminates subjected to impact loading since impact characteristics and mechanical properties degradation of composite laminates reached critical levels once perforation took place. It was also found that thickness had greater influence on impact perforation resistance than in-plane dimensions. However, as the composite laminates became very thick, the manufacturing cost for obtaining high-quality composite laminates could become unaffordable. In an effort to meet designing requirements and to reduce manufacturing costs, assembled composite plates, which were organized by assembling multiple thin composite laminates together, were considered as alternatives for thick laminated composite plates. Various joining techniques including mechanical riveting, adhesive bonding, stitching joining and their combinations were used in assembling two- and four-laminate plates. Experimental results revealed that epoxy bonding outperformed other joining techniques. Although good bonding resulted in higher impact bending stiffness and subsequently higher perforation threshold, increasing the laminate thickness or the number of laminates was found to be more efficient in raising perforation threshold than improving the joining stiffness. As a major finding of the study, the assembled composite plates were found to

have perforation thresholds similar to the laminated counterpart. Hence, the former cobe used to replace the latter, at least, as far as perforation threshold was concerned.

Due to their high stiffness-to-weight and high strength-to-weight ratios, fil

3.1 Introduction

reinforced polymer-matrix composites are ideal materials for high-performal structures. They are usually used in thin-laminate form. As composite technological advance, more and more thick-section composites are used for heavy-duty structures. example, the applications of thick composite laminates for submarine hull and armount vehicle bodies have been proved to be feasible. The advancement from thin laminates thick laminates, however, is not trivial. It falls into a study categorized as scaling effectively as a scaling effective technologies such as laminate theory, contact algorithm, manufacture technique, etc. Since thick composite laminates behave quite differently from their technique, etc. Since thick composite laminates have gain very much attention [3.3].

Studies regarding the scaling effects on composite response to impact loading has been reported [3.4-3.6]. A similar study has been presented by the authors and the associate [3.7]. They have concluded in their study that perforation is the most imported damage stage in composite laminates subjected to impact loading. The reason is timpact characteristics (such as peak force, contact duration and absorbed energy) mechanical properties degradation (such as residual compressive maximum force are sidual compressive absorbed energy) of composite laminates reach critical values where

perforation takes place. They have also verified that thickness, as opposed to in-p dimensions, has much greater influence on perforation resistance.

However, as composite laminates become thick, the manufacturing cost for h

quality composite laminates may become unaffordable. For example, in order to ach uniform curing and thus uniform properties through the thickness of thick composite laminates, expensive microwave curing process is required [3.8]. In an effort to mee design requirements for high quality and to reduce the manufacturing costs, assem composite plates, which are organized by assembling multiple thin composite lamin together, are considered as alternatives for thick laminated composite plates in this students.

In assembling thin composite laminates together, three fundamental joi techniques including adhesive bonding, mechanical fastening, and stitching joining performed in this study. In addition, combined methods based on these three techni are also explored. Both adhesive bonding and mechanical fastening have been discussed in literature. Being virtually the combination of adhesive bonding mechanical fastening, stitching has also been found to be feasible for composite joi [3.9-3.10] and reinforcement [3.11]. Since it offers a relatively uniform load transfer in structural components involved, its application to assembling thin laminates is also interest in this study.

Accordingly, the objectives of this study are (1) to investigiate the joining stiff and perforation threshold of assembled composite plates based on various joi techniques, (2) to identify an efficient way of assembling thin composite laminates achieving high perforation threshold and (3) to explore the feasibility of replacing costly thick laminated composite plates by assembled composite plates.

3.2 Experimental Methods

1. Thin Composite Laminates

Composite laminates made of glass fibers and an epoxy matrix were investigated this study. The glass fibers were of E-glass type whereas the epoxy matrix was of 1002 resin. The composite laminates were of cross-ply type and had a stacking sequent of [0/90/0/...]₁₃. The nominal fiber volume fraction of the composite laminates was ab 53% and the averaged thickness was 3.2 mm. In this study, these composite laminates were assembled together to form two-laminate composite plates by using various join techniques.

2. Impact Testing

increase the impact velocity up to 8 m/s.

DYNATUP GRC 8200 machine was used for impact testing. A schematic diagram of impact testing machine was given in Figure 3.1. According to the diagram, the impact consisted of three components: a dropping crosshead, an impactor rod, and an impact nose. The steel impactor rod had a diameter of 12.5 mm and was attached to the dropping crosshead. A force transducer having a capacity of 22.24 kN was mounted on the freend of the impactor rod and encapsulated by a hemispherical nose. The impactor was at a dropping height of 0.91 m to give a constant impact velocity at 4.22 m/s for metests. The total mass of the impactor, however, ranged from 10.35 kg to 17.74 kg adding various deadweights to the crosshead), resulting in impact energy from 92 J 158 J. For impact energy higher than 158 J, another similar impact testing machine with pneumatic unit was used. The pneumatic unit was able to provide an additional force

In each impact test, a composite specimen with dimensions of 125 mm by 100 was placed between two steel plate holders, namely the top holder and the bottom has shown in Figure 1. Each holder had an opening of 100 mm by 75 mm in the control top holder was removable while the bottom one was attached to the frame of impact testing machine which was fixed on a solid foundation. The specimen and the steel holder were then C-clamped at four corners to the bottom steel holder. composite specimen thus had a fixed boundary condition. In impact testing, the impact contacted the center of composite specimens, resulting in so-called central impact.

In most impact tests, the crosshead was released from the preset height, and dro freely according to the gravitational force. However, for impact tests with energy he than 158 J, it was driven by both gravitational force and pneumatic force. As the impact dropped and approached the composite specimen, its time trigger passed through a sensor right before contact-impact occurred. The initial impact velocity was calculated from the distance between two edges on the time trigger and the time into they passes through the sensor. Once impact began, the contact forces at a consecutive instants were detected by the force transducer attached to the impactor. Force history was recorded in a computer. The corresponding velocity history of impactor could then be calculated from integrating the force history (after being divided by the mass of the impactor) and using the initial impact velocity. Subsequently corresponding displacement history of the impactor could be calculated from integrating the velocity history.

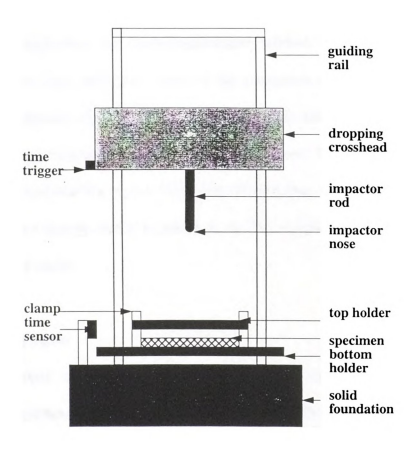


Figure 3. 1 - Schematic diagram of impact testing machine

Based on the force and displacement histories, the force-displacement relation and energy history of the impactor could be established. Assuming the impactor was perferigid and the energy loss on the contact-impact interface between the impactor and specimen was negligible, the force-displacement relation of the impactor could considered as the force-deflection curve of the composite specimen. And the kine energy of the impactor right before contact-impact took place, i.e. the *impact energy* would be the energy transferred to the composite specimen. However, depending on impact energy level and the type of specimen investigated, either a partial or the transcent amount of impact energy could be absorbed by the composite specimen in forms damage, heat and others.

3. Joining Techniques

In investigating assembled composite plates, the aforementioned 3.2mm-the glass/epoxy laminates were used as the building block. Many two-laminate composite plates were created. Each was formed by assembling two laminates together. Variationing techniques such as adhesive bonding, mechanical fastening, stitching joining, their combinations were investigated.

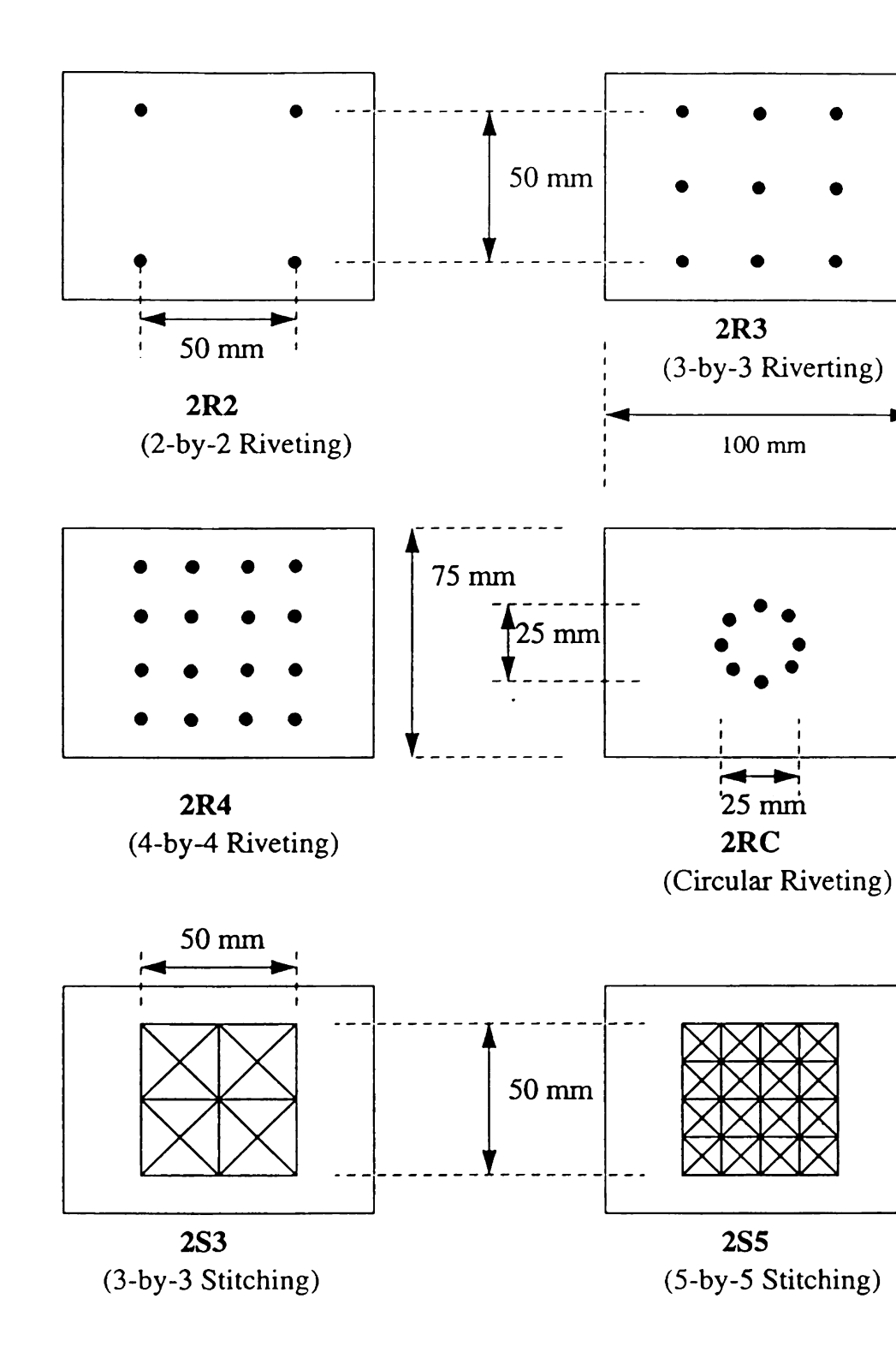


Figure 3. 2 - Schematic diagrams of some riveting and stitching patt

In adhesive bonding, the bonding surfaces of composite laminates were rouge with emery papers to promote later mechanical interlocking. They were then cleane acetone before being coated with either a Scotch double-sided tape or a two-part temperature curing epoxy. The former was manufactured by 3M while the latter brand name EnviroTex Lite. These two types of adhesive bonding represented didegrees of bonding rigidity and strength. For convenience of discussion, the taped laminate composite plates were called 2T (2 for two-laminate and T for taped) wheepoxy-bonded two-laminate plates 2B (B for bonded).

In mechanical fastening, square riveting patterns with various densities, such as 2, 3-by-3, and 4-by-4 per each 50mm-by-50mm area were created. Figure 2 show details of the riveting patterns. In performing riveting, holes were prepared by drilling bit before 4x580 steel rivets (1/8" in diameter and 1/4" in grip) were pushed using a riveting gun. In addition, a circular riveting pattern consisting of eight uniformly located on the circumference of a 25mm-diameter circle in the center composite laminates was also employed in the study. These four riveting patterns designated as 2R2, 2R3, 2R4 and 2RC. The first number of the designations, i.e. 2, represented for two-laminate plates. The second letter R stood for riveting while the number or letter gave riveting density or shape. That was, 2R2 was for 2-by-2, 2R for 3-by-3, 2R4 was for 4-by-4, and 2RC was for circular riveting. The circular ri

Similar to riveting, several stitching patterns were also used in assembling laminate composite plates. A 28 gauge steel wire was used as the stitching thread w stitching holes prepared by a drilling bit of 1/16" in diameter. For each four

forming a square unit, six stitching lines, two longitudinal, two hold diagonal as shown in Figure 3.2 were performed on each side of the of the stitching joints were prepared by pulling the stitching thread through holes as tightly as possible by hand. Stitching densities of 3-by-3, 5-by-each 50mm-by-50mm area were investigated. They were denoted as 2S respectively, where 2 was for two-laminate plates, S was for stitching number represented for stitching densities. Figure 3.2 also showed the of 2S3 and 2S5.

In addition to the individual joining techniques presented above composite plates were also assembled by using combined joining techniques was assembled by both epoxy bonding (B for bonded) and a 3-by-for riveting) and a 2BS3 assembled plate combined both epoxy bond stitching pattern (S for stitching). The investigations of these contechniques were part of the study in search of higher joining rigidity and

3.3 Results and Discussions

1. Force-Deflection Curves

as the building block and mentioned earlier were investigated. These designated as 1F in the study since they were of one-laminate and had condition during impact tests. The force-deflection curves of eighteen subjected to various levels of impact energy were shown in Figure 3.3.

ascending section of each force-deflection curve was termed the impact



due to its representation of the stiffness of composite laminates under impact-induced bending in the beginning of impact process. All the force-deflection curves seemed to ascend similarly, indicating similar impact bending stiffness. They then reached individual maximum levels. According to Figure 3.3, the maximum forces increased as the levels of impact energy increased. When the impact energy was high enough, the maximum forces seemed to have a similar value. This value was termed the *peak force* of the composite laminates under the specific central impact.

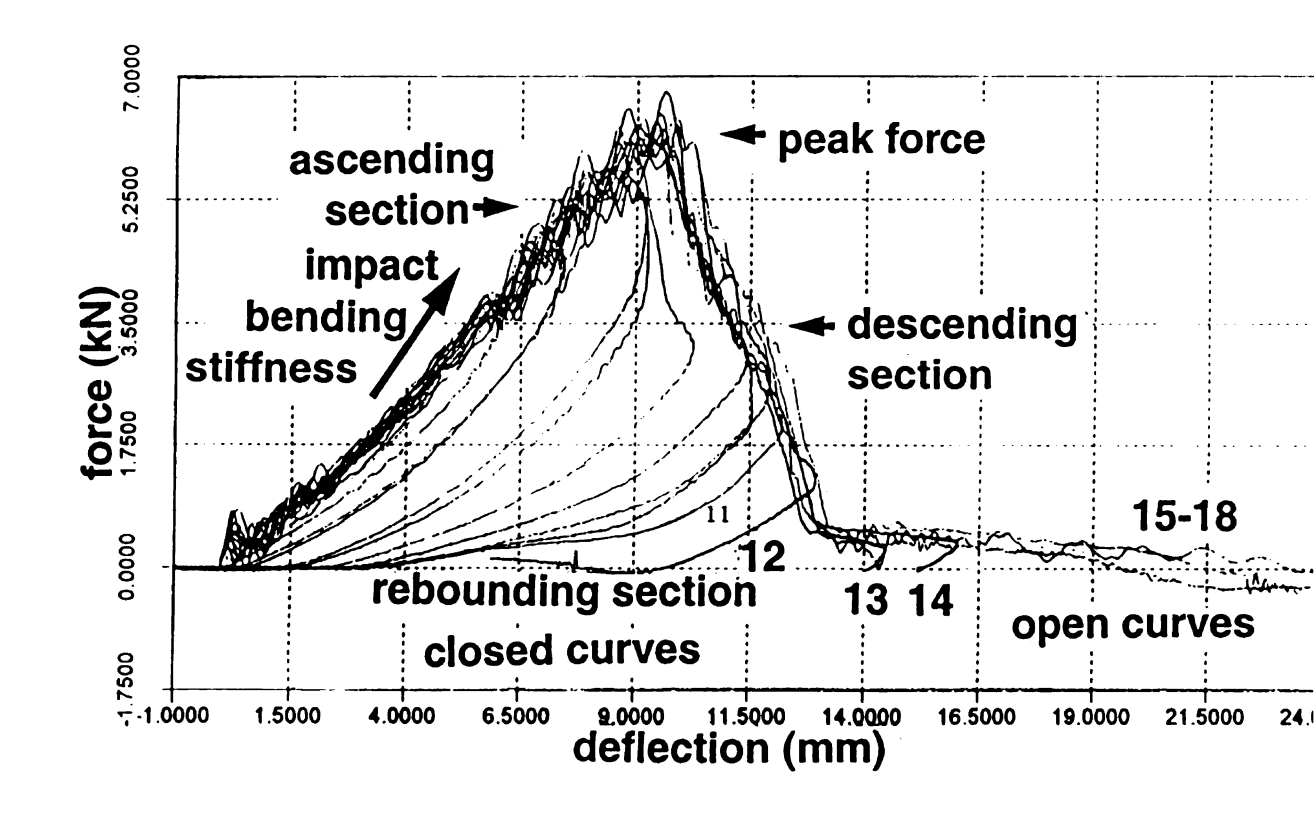


Figure 3. 3 - Force-deflection curves of eighteen 1F composite plates

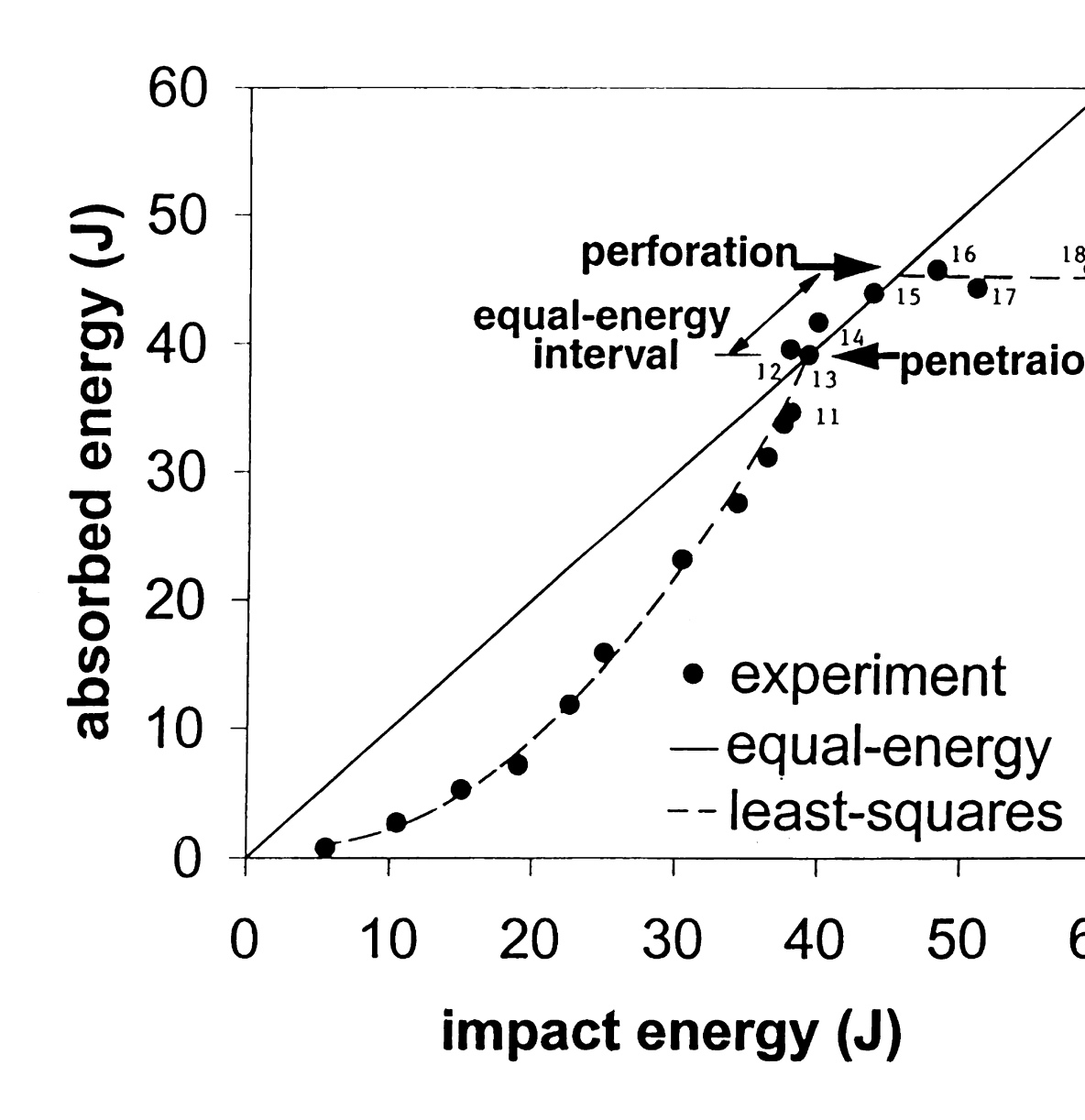


Figure 3. 4 - The whole enegy profile of 1F case based on force-deflection cui in Figure 3.3

In each subperforation impact, the force-deflection curve rised, reached a level and returned back to the origin. It formed a close curve representing the i impacting onto the composite laminate and rebounding from the composite laminate area enveloped by the closed curve was the *absorbed energy* of the composite under the specific impact. Apparently, as the impact energy increased, the enveloped increased, so did the absorbed energy. If the impact energy continued to perforation then took place. Once perforation occurred, the force-deflection curve longer be a closed curve. The area bounded by the open force-deflection curve deflection axis was then the energy absorbed by the perforated composite laminals interesting to point out that the impact events which had sufficiently higher energy to reach the peak force seemed to share partial descending sections together regardless of the rebounding sections, all the impact events seemed to master force-deflection curve.

2. Whole Energy Profile

As mentioned earlier, as far as residual properties were concerned, p seemed to cause the ultimate damage in composite laminates subjected to impact Once a composite laminate was perforated, any excess impact energy would be as kinetic energy in the impactor except that an insignificant amount would be into additional damage. Hence, perforation threshold was an important particular characterizing the impact response of composite laminates [3.12-3.15]. Since p contact duration and absorbed energy all reached critical levels when perforance [3.7], the perforation threshold of composite laminates could be identified

criteria based on the critical levels of peak force, contact duration, and absorbed energy. In addition, since impact energy should be completely absorbed by the composite laminates when perforation took place, the perforation threshold of composite laminates could be identified based on the equality between impact energy and absorbed energy [3.7].

Among the four criteria to identify the perforation threshold, the one based on equal energy between impacting and absorption was considered to be the most convenient and accurate technique [3.7]. Hence, a comparison between the impact energy and absorbed energy was required for judging the perforation threshold of composite plates. Results of eighteen 1F (one-laminate with fixed boundaries) specimens were given in Figure 3.4. In addition to the experimental data points, a least-squares fitting curve for the data points with impact energy up to the penetration threshold and a least-squares line for the data points with impact energy beyond the perforation threshold were also identified. Shown in Figure 3.4, the data points were represented by solid circles while the the least-squares fittings by dashed lines. Apparently, as the impact energy increased, the absorbed energy also increased.

In addition to the raw data points and least-squares lines, a line representing the equality between impact energy and absorbed energy was also added to Figure 4. It was called the *equal-energy line*. As could be seen from the diagram, the data points were quite lower than the equal-energy line when the impact energy was low. As the impact energy increased, the data points became closer to the equal-energy line. Eventually the data points and the equal-energy line merged together. They then remained roughly the same for an interval until the data points became smaller than the equal-energy line again.

The interval within that the data points overlapped with the equal-energy line was continuous the equal-energy interval. The discrepancy between the data points and the equal-energy line within the equal-energy interval as shown in Figure 3.4 was believed to be caused errors due to the numerical integrations mentioned earlier.

The equal-energy interval was bounded by two points. The point of lower bound named *penetration threshold*, indicating the onset of penetration. When penetration place, the impactor got stuck in the composite plate. Since very limited rebounding allowed in the impactor, the impact energy was almost completely absorbed by composite plate in forms of damage. As the penetration proceeded (the impactor m deeper into the composite plate), it required more energy for the impactor to be through the composite plate and to overcome the friction between the impactor and composite. Eventually perforation of the composite plate would be achieved. perforation occurred, any excess impact energy would be retained in the impactor in of kinetic energy. And the absorbed energy would be smaller than the impact en again. Thus, there was an upper bound for the equal-energy line. The point of u bound was called *perforation threshold*, indicating the completion of perforation pro Given in Figure 3.4, the penetration threshold was about 38 J and the perfora threshold was around 45.5 J for the 1F case. The difference between the penetra threshold and the perforation threshold, i.e. the equal-energy interval, was believed to dependent on the material type, the laminate thickness and the joining technique o composite plate.

Figure 3.4 was called the *whole energy profile* of the 1F (one-laminate with a boudnaries) case since it included the overall energy exchange between the impactor

the composite plates. The diagram was derived directly from the force-deflection cuves given in Figure 3.3. By closely comparing Figure 3.3 with Figure 3.4, it could be found that the force-deflection curves up to specimen No.11 were of closed type. Specimens No.12 to 14 were located in the transition zone between closed curves and open curves. They were close to the penetration threshold. Once perforation took place, approximately around specimen No. 15, the curves changed from closed type to open type.

3. Penetration Thresholds and Perforation Thresholds

The penetration and perforation thresholds of all assembled composite plates were identified from corresponding whole energy profiles and were given in Table 3.1. The 2R2 (2-by-2 riveting) case, however, had an indentical value for both penetration threshold and perforation threshold because there was no intesection between its least-squares curve and the equal-energy line. A similar result also occurred in the 2R4 (4-by-4 riveting) case. These results were possibly due to experiemental discrepancy. In addition, it should be pointed out that only one test was performed for 2S9 (9-by-9 stitiching) case due to the very much time required for the specimen preparation.

Based on Table 3.1, the 2R4 (4-by-4 riveting) case had the highest perforation threshold and penetration threshold. By examining the damage of impacted plates, it was found that the four rivets closest to the center of each plate, i.e. closest to the impactor, were always seriously distorted by the impactor during the impact process. It was believed that the distortions of steel rivets resulted in additional energy abosorption during impact. A special riveting pattern, namely 2RC (circular riveting), was then designed to avoid the problem and to verify the effects of high-density riveting on

specimens though the former was more locally concentrated and the latter global distributed. The penetration threshold and the perforation threshold for the 2RC we loss. J and 123.8 J, respectively, while they were both 138.9 J for the 2R4 can Accordingly, the 2R4 case was not used for comparison in the remaining studies.

Among the two-laminate assembled composite plates, 2B (two-laminate bonde 2RC (circular riveting), 2S5 (5-by-5 stitching), 2BR3 (bonded and 3-by-3 riveting) a 2BS3 (bonded and 3-by-3 stitching) had the perforation threshold close to 123 J while others were between 108 J and 115 J. It was believed that the adhesive bonding in the 2 2BR3 and 2BS3 cases contributed high rigidity and strength to the specimens, resulting high perforation thresholds. The high riveting density of 2RC and high stitching dens of 2S5 also made similar contribution to individual specimens. In fact, the perforation threshold increased as the riveting density increased from 2R2 (2-by-2 riveting) to 23 (3-by-3 riveting), and to 2RC. Similarly, the perforation threshold increased as the stitching density increased from 2S3 (3-by-3 stitching) to 2S5. Due to the single test is the 2S9 (9-by-9 stitching) case, the result was inconclusive and omitted from furth discussion.

Although high density of riveting and stitching seemed to make positive contribution to perforation threshold, it should be noted that their preparations also required execution threshold, it should be noted that their preparations also required execution to both time and labor. Besides, it was also possible that they introduced execution thresholds of 2B (two-laminate bonded), 2BR3 (bonded and 3-by-3 riveting) and 2BR3 (bonded and 3-by-3 riveting) and 2BR3 (bonding and 3-by-3 stitching) cases, the 2B case with penetration threshold of 120.8

outperformed the remaining two cases which had 105.2 J and 112.3 J, respectively. Accordingly, the experimental results seemed to indicate that pure epoxy bonding was sufficiently efficient for joining thin composite laminates. The additional riveting and stitching might cause more damage to composite laminates than effectively join them. The penetration threshods of all other cases were between 100.8 J and 108.9 J and were much lower than the 2B case. This result further confirmed the superiority of the joining efficiency of epoxy bonding in assembling thin (3.2 mm) composite laminates. In addition, it should be noted that the equal-energy intervals for all two-laminate composite plates seemed to be very similar.

Table 3.1: Impact bending stiffnesses, penetration tresholds and perforation thresholds of one-laminate and two-laminate composite plates

Specimen Type	Bending	Penetration	Perforation
	Stiffness	Threshold	Threshold
	(N/mm)	(J)	(J)
1F: one-laminate Fixed	933.0	38.0	45.5
2F: two-laminate Fixed	1831.7	100.8	114.7
2T: double-sided Taped	1740.4	104.7	111.1
2B: epoxy-Bonded	3370.9	120.8	123.0
2R2: 2x2 Riveting	1752.6	108.9	108.9
2R3: 3x3 Riveting	1762.3	105.1	115.8
2R4: 4x4 Riveting	1674.6	138.9	138.9
2RC: Circular Riveting	1694.5	105.9	123.8
2S3: 3x3 Stitching	1670.0	103.5	115.0
2S5: 5x5 Stitching	1663.0	108.2	120.0
2S9: 9x9 Stitching	1559.1*	108.5*	108.5*
2BR3: Bonded & Riveted	3538.5	105.2	121.2
2BS3: Bonded & Stitched	2977.8	112.3	120.8

^{*} based on only one test

4. Impact Bending Stiffness

Bending stiffness had been found to be an important parameter to delamination resistance [3.16] and perforation resistance [3.7]. In investigating the effects of joining technique on perforation resistance, the bending stiffnesses, which were the slopes of the force-deflection curves, of various assembled composite plates were identified and also listed in Table 3.1. Results of the two-laminate plates could be essentially divided into two groups. The bending stiffnesses of 2B (two-laminate bonded), 2BR3 (bonded and 3-by-3 riveting) and 2BS3 (bonded and 3-by-3 stitching) cases were from 3000 N/mm to 3500 N/mm. These values were about two times those of the remaining two-laminate cases. Since the impact bending stiffness changed with the type of assembled composite plates, it in fact was associated with the joining stiffness dut to the corresponding joining technique. Hence, the impact bending stiffness could be considered as an index of joining stiffness up to some extent.

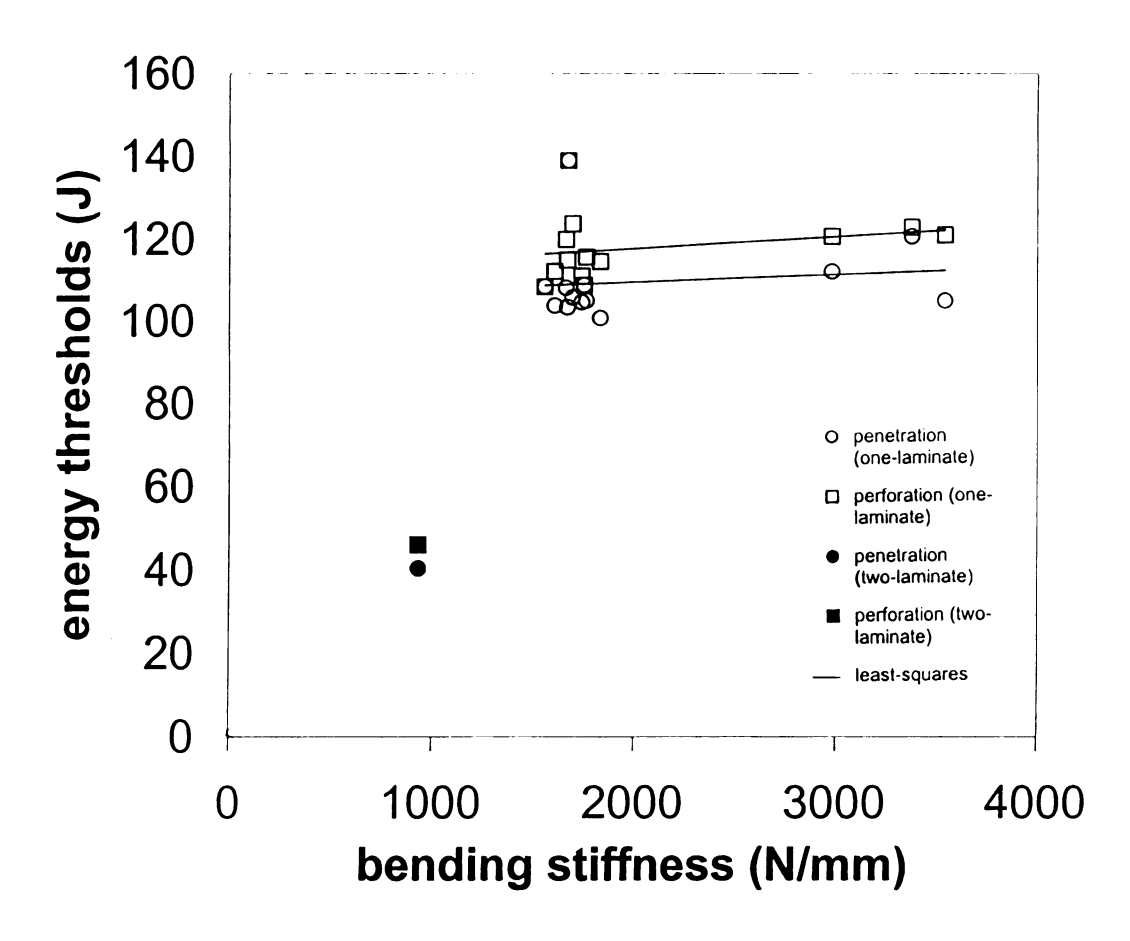


Figure 3. 5 - Relation between energy thresholds and impact bending stiffness of various two-laminate composit plates

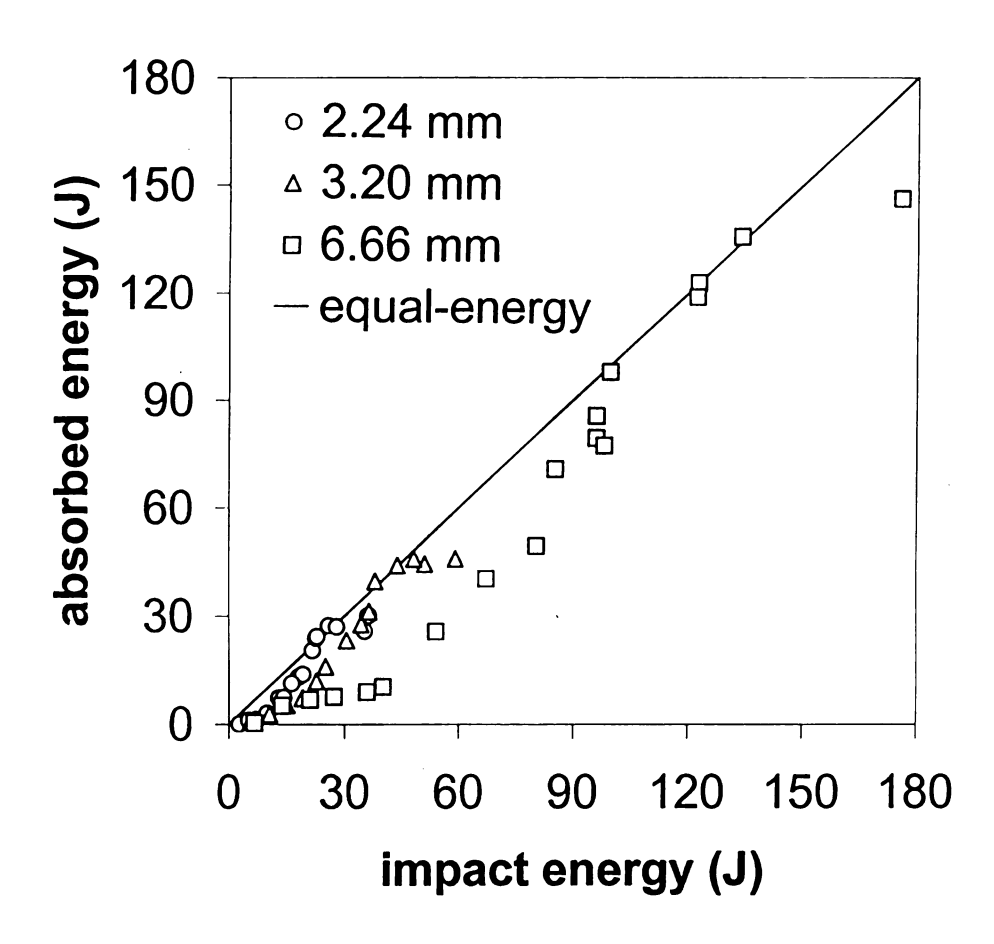


Figure 3. 6. The whole energy profiles of three laminated composite plates

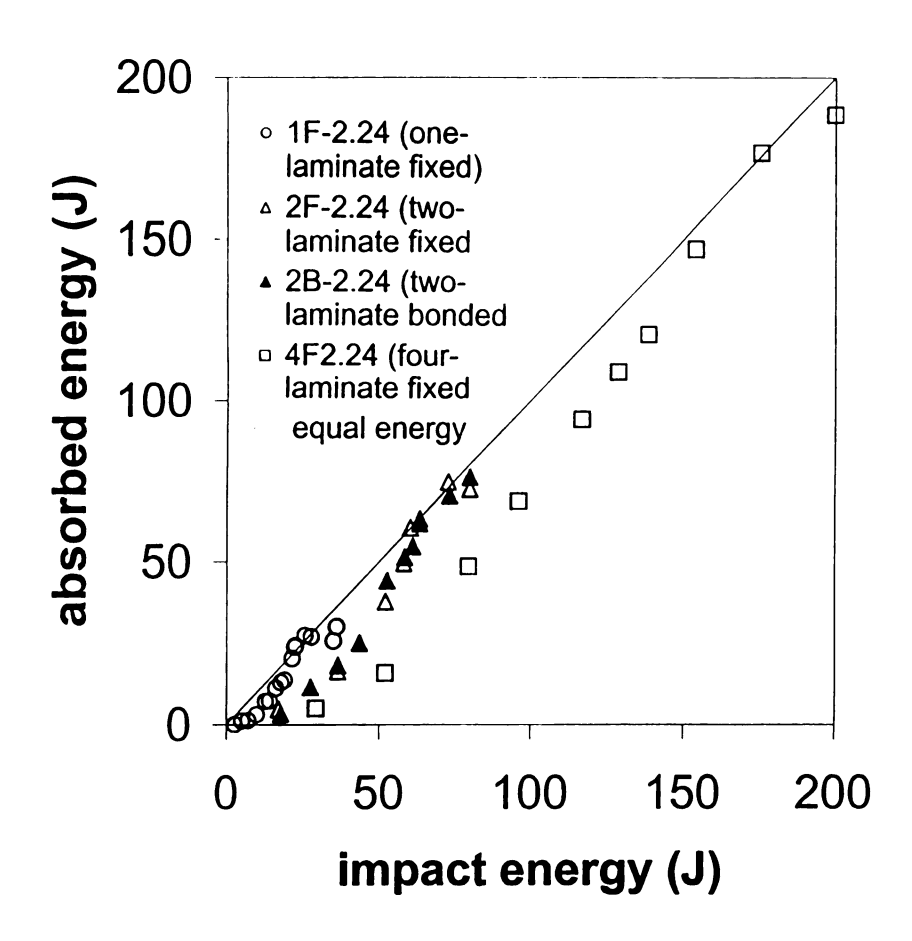


Figure 3. 7. The whole energy profiles of four assembled composite plates

The perforation thresholds and bending stiffnesses of two-laminate plates were put together in Figure 3.5. Apparently, there was a correlation between them. That was, the higher the bending stiffness of an assembled composite plate, the higher the penetration and perforation thresholds. However, when compared with those of the one-laminate case, i.e. 1F, the increase in penetration and perforation thresholds seemed to be more significant due to thickness increase than due to bending stiffness increase. In fact, by adding one more laminate to the one-laminate plates to become two-laminate plates, both energy thresholds and bending stiffenss were almost doubled. However, an increase in bending stiffness based on any joining technique did not seem to improve the penetration and perforation thresholds significantly.

5. Laminated Plates versus Assembled Plates

In verifying the feasibility of using assembled composite plates to replace laminated composite plates, a study comparing the impact bending stiffnesses and perforation thresholds of these two groups was necessary. In this study, besides the 1F (3.2 mm thick) case, two other types of composite laminate were investigated. These two types of composite laminate had cross-ply laminations and thicknesses of 2.24 mm and 6.66 mm. They were designated as 1F-2.24 and 1F-6.66. Their whole energy profiles were given in Figure 3.6 along with the 1F-3.2 case. Apparently, all of them had similar trends. And the equal-energy interval increased from 5 J for 1F-2.24 to 7.5 J for 1F-3.2, and to 40 J for 1F-6.66. This result confirmed that the equal-energy interval, or the penetration process, was dependent on the thickness of composite plates.

In order to further confirm that thickness, instead of bending stiffness, played a efficient role in improving perforation resistance, an investigation on thickness ef was performed. The composite laminates used in this study were of 1F-2.24. They material properties identical to those of 1F-3.2 specimens. However, their stace sequence was [0/90/0/...]₉ and nominal thickness was 2.24 mm. In addition to the 2.24 case, assembled composite plates such as 2F-2.24 (two-laminate with boundaries), 2B-2.24 (two-laminate bonded) and 4F-2.24 (four-laminate with boundaries) cases were created. Their whole energy profiles were presented in Figure for comparison. Although the difference of impact bending stiffensses between 2Fand 2B-2.24 was as much as that between 2F and 2B (both based on 3.2-mm lamin cases, their whole energy profiles were very similar. However, the whole energy proof 1F-2.24, 2F-2.24 and 4F-2.24 were quite different. Apparently, the thicker assembled composite plate, the higher the capability of energy absorption. According Figure 3.7, the penetration thresholds for 1F-2.24, 2F-2.24, 2B-2.24 and 4F-2.24 about 22 J, 63 J, 62 J and 157 J, respectively, and the perforation thresholds for t were about 27 J, 73 J, 73 J and 182 J, respectively. The equal-energy intervals, i.e difference between the penetration thresholds and the perforation thresholds, for the cases were thus 5 J, 10 J, 11 J and 25 J. This result combined with those of earlier stu provided evidences that the equal-energy interval was dependent on the thickness composite plates.

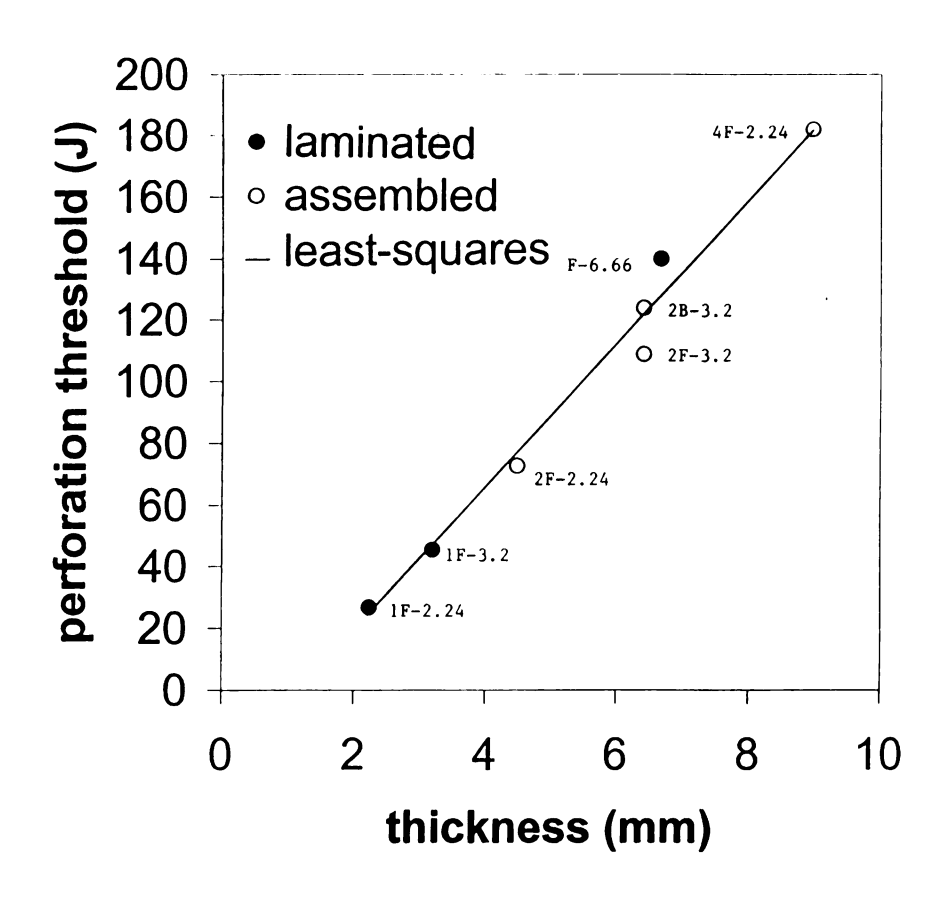


Figure 3. 8 - The relation between perforation threshold and thickness for both laminated and assembled composite plates

The perforation thresholds of both assembled cases, including 1F-2.24, 2F-2.24, 2B-2.24, 2F-3.2, 2B-3.2, 4F-2.24, and laminated cases, including 1F-2.24, 1F-3.2 and 1F-6.66, were also summarized in Figure 3.8 for comparison. Apparently, the assembled cases were very similar to the laminated cases because they were all closely located along a least-squares line. It then could be concluded that the perforation threshold of a composite plate was dependent on thickness only, regardless of being laminated or assembled. In other words, the assembled composite plates could be used as alternatives for thick laminated composite plates, at least, as far as the perforation threshold was concerned.

3.4 Conclusions

The following conclusions can be drawn from above investigations:

- 1. Various joining techniques such as mechanical riveting, adhesive bonding, stiching joining and their combinations were used in assembling two-laminate and four-laminate composite plates. Pure epoxy bonding was found to be the most efficient joining technique in assembling the composite laminates together since it gave the highest bending stiffness and perforation threshold.
- 2. Among the assembled two-laminate composite plates, the perforation threshold increased as the bending stiffness increased. However, the increase of perforation threshold based on the improvement of bending (joining) stiffness was limited. A more efficient way to significantly increase the perforation threshold was to



increase the thickness of composite laminates or to use assembled multi-laminate composite plates.

- 3. A technique named whole energy profile was presented for characterizing impact-perforation resistance. When penetration took place, the absorbed energy was approximately equal to the impact energy. When perforation occurred, the absorbed energy was again smaller than the impact energy. Experimental results revealed that the equal-energy interval, which was the difference between the penetration threshold and perforation threshold, increased as the thickness of composite plates increased.
- 4. Based on the studies, it was found that assembled composite plates were very comparative with laminated composite plates in both bending stiffenss and perforation threshold. This result verified the advantage of using assembled composite plates over thick laminated composite plates since the cost of making thick laminated composite plates with high quality increased significantly as the thickness increased.

ACKNOWLEDGEMENTS

This investigation was supported by both Michigan Research Excellence Fund and the U.S. Army TACOM-TARDEC ILIR program. The authors wish to express their sincere thanks for the financial supports.

3.5 References

- 3.1. Workshop on scaling effects in composite materials and structures, NASA Langley Research Center, Hampton, VA, November 15-16, 1993, Report No. 94-6, Institute for Mechanics and Materials, University of California, San Diego, CA.
- 3.2. A. Carpinteri, ed., Size-scale effects in the failure mechanisms of materials and structures, E & FN Spon, 1994.
- 3.3. Y. D. S. Rajapakse, ed., *Mechanics of Thick Composites*, AMD-Vol. 162, The American Society of Mechanical Engineers, 1993.
- 3.4. J. Morton, "Scaling of impact-loaded carbon-fiber composites," *AIAA Journal*, 26(8), 989-994, 1988.
- 3.5. Y. Qian, S.R. Swanson, R.J. Nuismer, and R.B. Bucinell, "An experimental study of scaling rules for impact damage in fiber composites," *J. Composite Materials*, 24(5), 559-570, 1990.
- 3.6. B.V. Sankar, "Scaling of low-velocity impact for symmetric composite laminates," *J. Reinforced Plastics and Composites*, 11, 297-305, 1992.
- 3.7. D. Liu, B. B. Raju, and X. Dang, "Size effects on impact response of compositelaminates," *International Journal of Impact Engineering*, Vol. 21, No. 10 pp837-854,1998
- 3.8. J. Wei, M.C. Hawley, J. DeLong, and M. DeMeuse, "Comparison of microwave and thermal cure of epoxy resins," *Polymer Engineering and Science*, 33(17), 1132-1140, 1993.

- 3.9. C. Lee and D. Liu, "Tensile strength of stitching joint in woven glass fabrics," J. Engineering Materials and Technology, 112 (2), 125-130, 1990.
- 3.10. D. Liu, "Photoelastic study on composite stitching," Experimental Techniques, 14 (1), 25-27, 1990.
- 3.11. D. Liu, "Delamination resistance in stitched and unstitched composite plates subjected to impact loading," *Reinforced Plastics and Composites*, 9 (1), 59-69, 1990.
- 3.12. E. Wu, E.-Z. Tsai, and Y.-C. Chen, "Penetration into glass epoxy composite laminates," *J. Composite Materials*, 28, 1783-1802, 1994.
- 3.13. C.T. Sun and S.V. Potti, "High velocity impact and penetration of composite laminates," proc. 9th Int. Conference on Composite Materials, 4, 157-165, 1993.
- 3.14. W. Goldsmith, C.K.H. Dharan and H. Chang, "Quasi-static and ballistic perforation of carbon fiber laminates," *Int. J. Solid Structures*, 32, 89-103, 1995.
- 3.15. S.W.R. Lee and C.T. Sun, "Dynamic penetration of graphite/epoxy laminates impacted by a blunt-ended projectile", *Composite Science and Technology*, 49, 369-380, 1993.
- 3.16. D. Liu, "Impact-induced delamination a view of material property mismatching,"

 J. Composite Materials, 22(7), 674-691, 1988.

Chapter 4

TESTING AND SIMULATION OF LAMINATED COMPOSITES SUBJECTED TO IMPACT LOADING

ABSTRACT

Because composite laminates are very susceptible to impact loading even at low velocity, low-velocity impact is an important subject in laminated composite analysis. The impact-induced damage is usually invisible to naked eyes and can cause serious structural degradation. Many low-velocity impact tests were performed in some previous studies; however, most of them were phenomenological analysis. In an effort to further understand the responses of composite laminates under low-velocity impact and to develop an accurate and efficient quantitative simulation in the future, this study was aimed at performing some instrumented impact tests and computer simulations. A commonly used computer code - LS-DYNA3D - was evaluated in this study and the results were valuable for future development of a new computer code. In the study, a low-velocity impact event investigated by Sun and Chen with an indentation law and verified by experiments was used to justify the finite element model and contact parameters. Once the computational scheme was established, it was used for a broader investigation consisting of composite laminates with various thicknesses, fiber angles, and impact velocities. Computational results revealed that the peak contact force and maximum deflection were strongly affected by the thickness of composite laminates while the fiber angles investigated seemed to play a less significant role. In addition, it was concluded that because delamination modeling was not included in the LS-

DYNA3D, the computer code needed to be modified if it was to be used for accurate impact simulations.

4.1 Introduction

Laminated composites are very susceptible to impact loading. Composite damage such as fiber breakage, matrix cracking, fiber-matrix debonding, and delamination can take place in composite laminates even when they are subjected to impact forces at low velocity. These damage modes usually cannot be detected by naked eyes. However, their effects on composite structural degradation are always very significant.

Many impact tests were performed and can be found in the review articles by Abrate [4.1,4.2]. In some previous studies [4.3,4.4], Liu et al also concluded that matrix cracking and delamination were the major damage modes in composite laminates subjected to low-velocity impact. A correlation between bending stiffness mismatch and delamination size was established. The relation was successfully used for phenomenological explanations of delamination size, location, and orientation in impacted composite laminates. In an effort to further understand the response of composite laminates under low-velocity impact and to establish an accurate and efficient quantitative simulation, the objectives of the present study are to perform some instrumented impact tests and to simulate the impact responses with a commonly used computer code - LS- DYNA3D. The results from this study are believed to be very valuable for future improvement and/or development of computer modeling and simulation for impact analysis.

In modeling the composite response under low-velocity impact, Tan and Sun [4.5] verified that an indentation law based on a quasi-static test could be used to investigate

low-velocity impact. For a set of composite material and impactor, an indentation test was required to identify the corresponding indentation parameters. Once the indentation law was established, it could be integrated into a computational scheme for various studies [4.6, 4.7]. In their study [4.8], Wu and Yen also investigated the relationship between impact force and laminate indention. The numerical method they used was derived from three-dimensional anisotropic elasticity. Effects of material and geometrical parameters on force-indentation relation were also examined in their study. Their results seemed to agree well with Sun and Chen [4.7].

Because of its strong dependence on parameters obtained from experiments, the approach based on the indentation law usually gave good prediction of composite responses under low- velocity impact. However, it should be pointed out that a new characterization for indentation parameters was needed each time the material or geometry of the composite or impactor was altered. As a consequence, for investigating the effects of material type, lamination, fiber orientation, and thickness on impact response of composite laminates, a computational technique free of experiment-dependent parameters might prove to be more efficient. In search of a more efficient technique for studying impact responses of various composite laminates and impactors, the present study examined an existing computational scheme, namely LS-DYNA3D. The effects of laminate thickness, fiber angle, and impact velocity on composite response were of primary concerns along with the feasibility of using LS-DYNA3D for impact analysis.

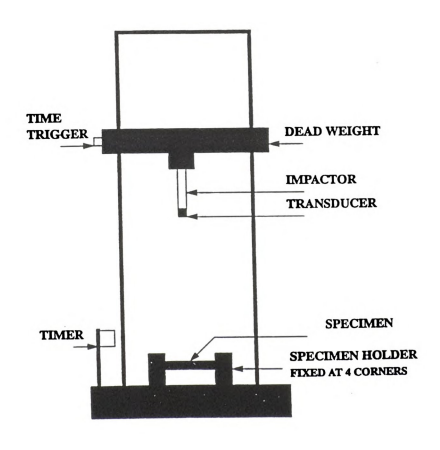


Figure 4.1 Schematic diagram of impact testing setup

4.2 Instrumented Impact Testing

The impact tests in this study were performed on a DYNATUP impact testing machine. The impactor was a steel rod which had a diameter of 12.5mm and was attached to the dropping head as shown in Figure 4.1. A force transducer having a maximum force limit of 13,350N was mounted at the tip of the rod and encapsulated by a spherical head. Specimens with dimensions of 125mm x 100mm were clamped by two steel holders from both sides with a rectangular opening of 100mm x 75mm in the center. The specimens and the specimen holders were then C-clamped to the bottom of the impact testing frame which was nearly fixed to the ground with many dead weights.

As the impactor dropped and approached a specimen, it triggered the timer and started the recording clock. The force history detected by the force transducer was then recorded in a computer. The corresponding displacement of the transducer or the deformation of the specimen could be calculated through double integrations. The force history, the deformation history, and the energy history were found to be the important characteristics of individual composite laminates under impact. In addition, the maximum peak force, the maximum deflection, the contact duration, and the energy absorption capability were also found to be important parameters for impact analysis.

4.3 Computational Technique

A dynamic finite element code named LS-DYNA3D was used in this study for impact simulations. In performing the finite element analysis, finite element models for

both composite laminates and a semi-spherical impactor were built. The composite material was AS4/3501-6 and had the following elastic constants:

$$E_{11}$$
= 120 GPa, E_{22} = E_{33} = 7.9 GPa, G_{12} = G_{23} = G_{31} = 5.5 GPa, V_{12} = V_{13} = V_{23} = 0.3

The composite laminates had dimensions of 100mm x 75mm. The thickness of individual ply was considered to be 0.25mm. The solid element was used in the finite element models because it gave better results than the shell elements. Full models were built for all specimens, resulting in a mesh of 40 x 40 x 15 for a 15-ply laminate. The laminate models were then fixed around four edges and subjected to a spherical impactor with a diameter of 12.5mm and a mass of 24g at the center of the laminates. The impact velocity ranged from 1 m/s to 5m/s. These finite element models were used throughout the investigations of this study unless otherwise mentioned.

Instead of an indentation law to identify the contact force and indentation, the LS-DYNA3D used a contact algorithm to calculate the contact-impact response. Accordingly, besides an initial impact velocity, a contact parameter named penalty coefficient needed to be determined through comparisons with experimental results and then assigned in the finite element simulations. The LS-DYNA3D gave results of force history and deformation history. Other information such as peak force, contact duration, maximum deflection, and energy absorption engaged in the impact events could be drawn from the histories. Since this study was focused on the comparison between the composite performance and computer simulation under low-velocity impact, the failure process available in the LS-DYNA3D was also imposed in the feasibility studies.

Table 4.1 Experimental results of impact parameters

Types of Effect Stacking Sequences	Impact Velocity m/s	Contact Duration, ms	Peak Force, kN	Maximum Deflection, mm	Energy Absorption, J
Thickness:	0.00		2.24		2.00
$[0_3/90_3/0_3/90_3/0_3]$ $[0_3/90_3/0_3/90_3/0_3/90_3/0_3]$	0.98 0.98	4.65 4.00	3.34 4.41	1.47 1.19	0.89 0.84
Fiber Angle:	0.70	4.00	7.71	1.17	0.04
[0 ₃ /90 ₃ /0 ₃ /90 ₃ /0 ₃]	0.98	4.65	3.34	1.47	0.89
[30 ₃ /-30 ₃ /30 ₃ /-30 ₃ /30 ₃]	0.97	4.55	3.33	1.52	0.81
[45,1-45,145,1-45,145,]	0.97	4.30	3.50	1.27	0.81
$[60_3/-60_3/60_3/-60_3/60_3]$	0.97	4.35	3.46	1.52	0.81
Velocity:					
$[0_3/90_3/0_3]$	0.99	8.15	1.78	2.79	1.04
$[0_3/90_3/0_3]$	1.59	8.43	2.95	4.32	2.59
$[0_3/90_3/0_3]$	2.77	10.05	3.61	8.38	14.25
$[0_3/90_3/0_3]$	3.40	6.25	3.70	13.46	25.76
$[0_3/90_3/0_3]$	3.95	4.70	3.34	12.70	23.15
$[0_3/90_3/0_3]$	4.49	3.20	3.32	11.94	24.81

4.4 Experimental Results

The following three types of studies were performed: thickness effect, fiber angle effect, and velocity effect. Table 4.1 shows the details of the stacking sequence and the impact parameters of primary concerns while Figures 4.2, 4.3, and 4.4 are the force-displacement relations for the thickness effect, fiber angle effect, and velocity effect, respectively. The following statements can be summarized from these results:

A. (Thickness Effect) The laminate stiffness and strength increase as the laminate thickness increases, resulting in the increase of peak contact force and decreases of contact duration, maximum deflection, and energy absorption.

B. (Fiber Angle Effect) Due to the alternative lay-up and near-square geometry, fiber angle does not play a significant role in impact response for composite laminates with the same thickness.

C. (Velocity Effect) For thin composite laminates under subperforation impact, contact duration, peak contact force, maximum deflection, and energy absorption all increase as the impact velocity increases.

D. (Velocity Effect) Once penetration takes place, both contact duration and peak contact force decrease while maximum deflection remains about the same level as the impact velocity increases.

E. (Velocity Effect) There is a significant jump in energy absorption due to penetration. The energy absorption remains about the same level even when the impact velocity increases.

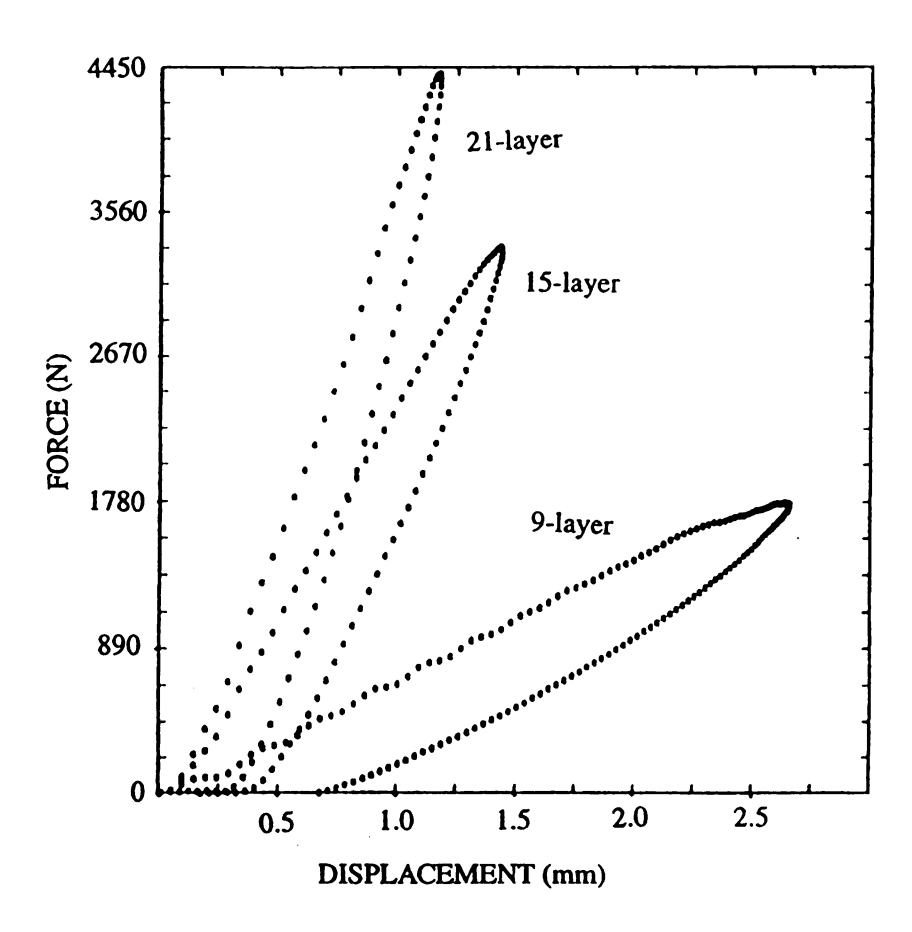


Figure 4.2. Force-displacement relations for laminates with various thicknesses

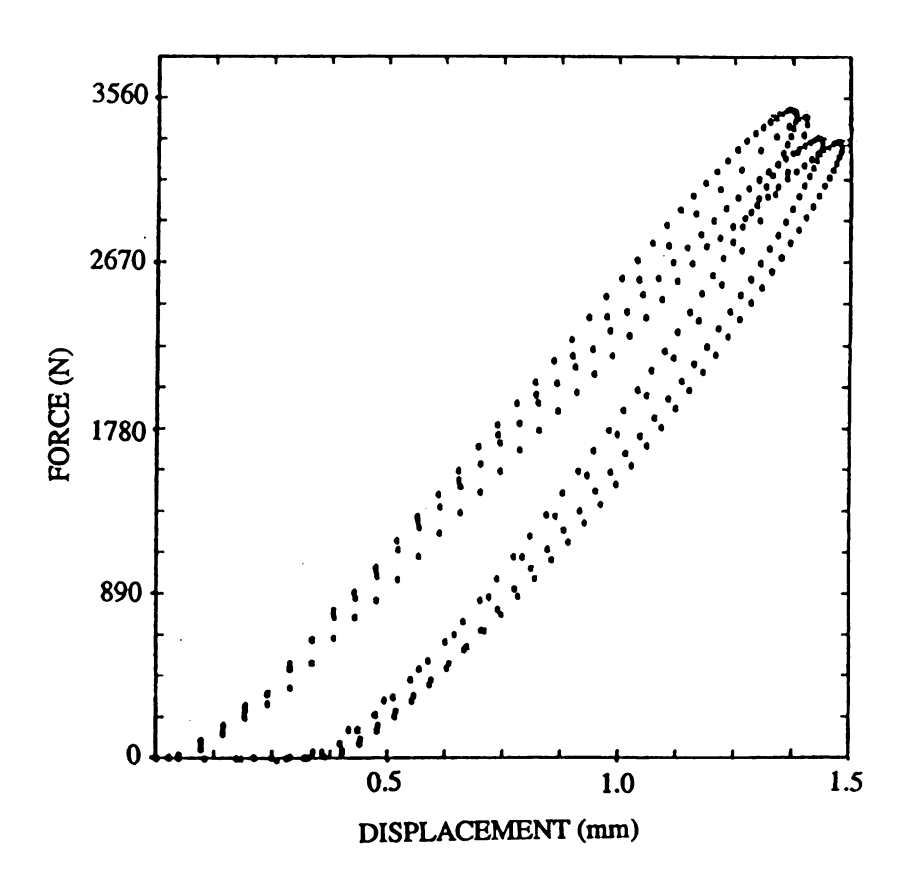


Figure 4.3. Force-displacement relations for laminates with various fiber angles

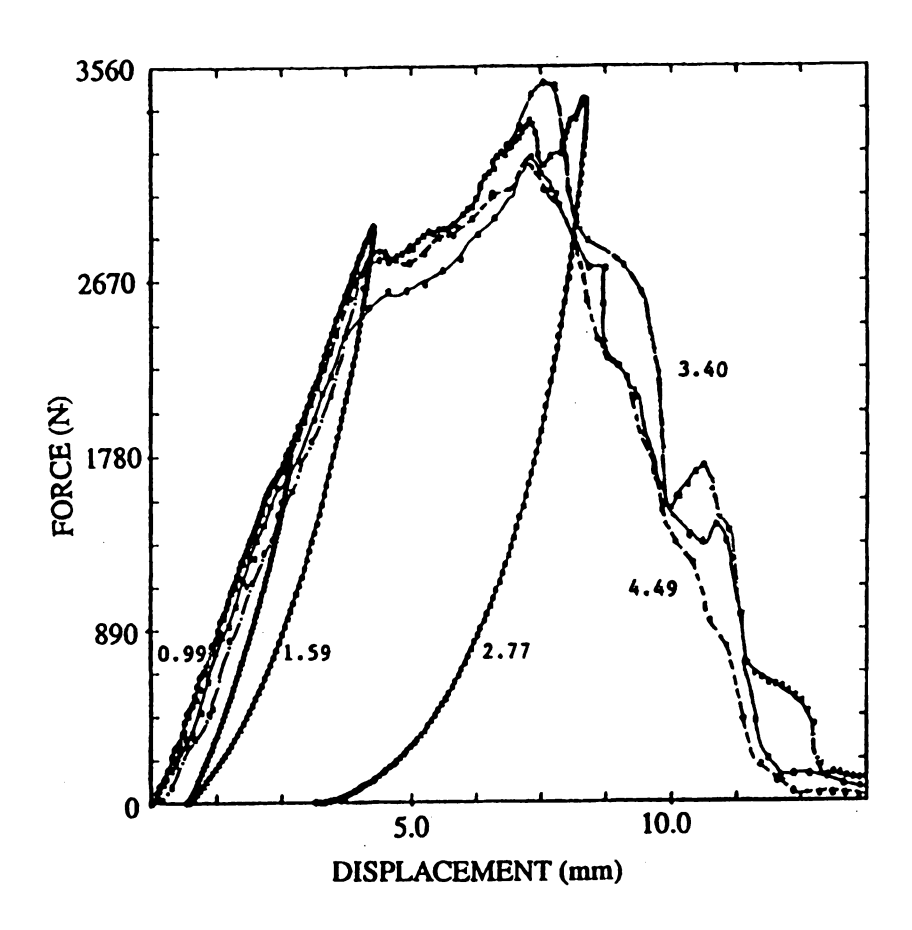


Figure 4.4 - Force-displacement relations for laminates subjected to various impact velocities

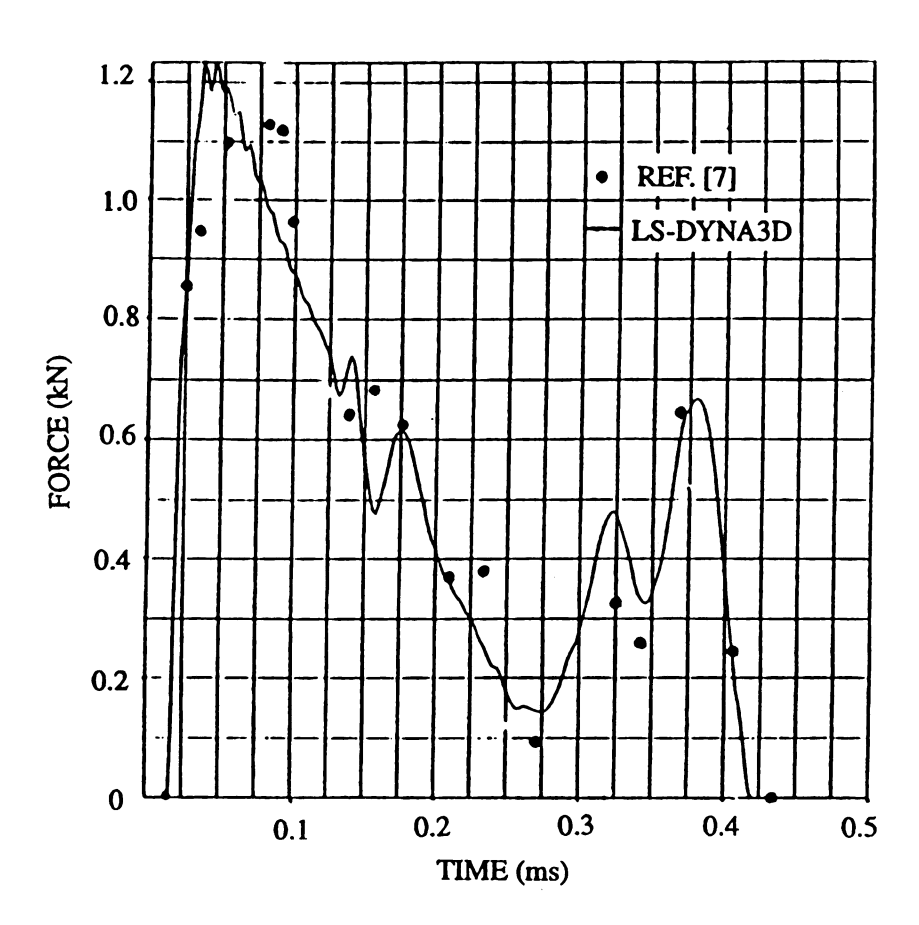


Figure 4.5 - Comparison of force history between ref. [4.7] and LS-DYNA3D

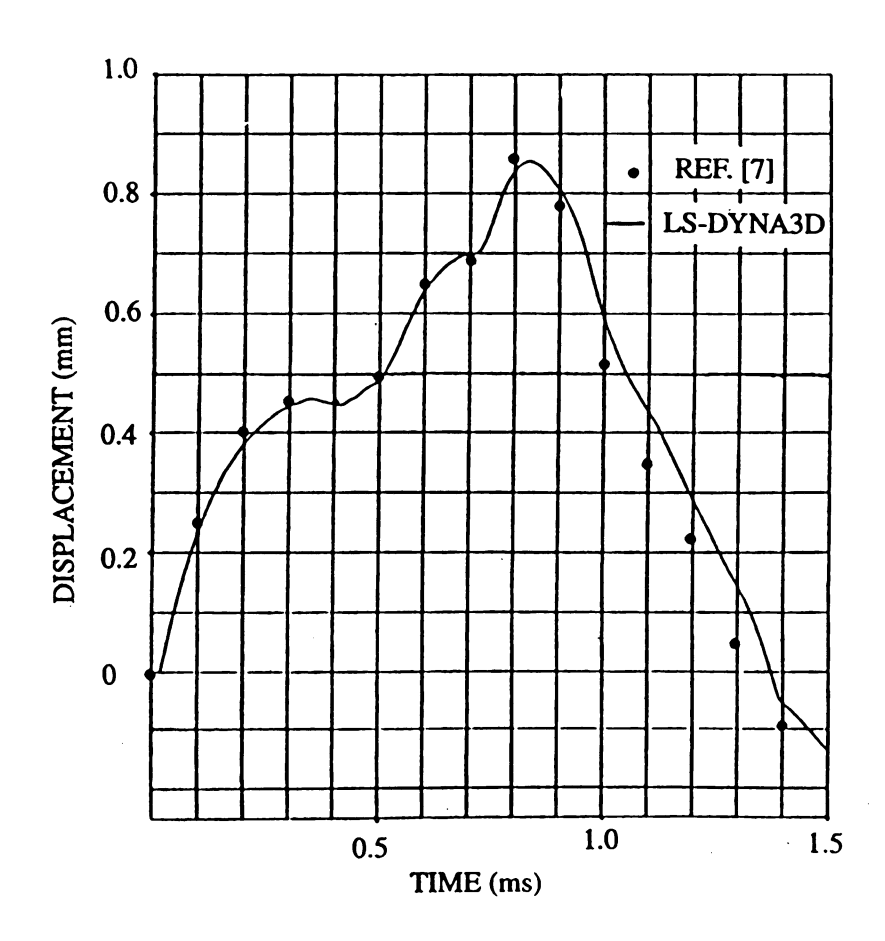


Figure 4.6 - Comparison of displacement history between ref. [4.7] and LS-DYNA3D

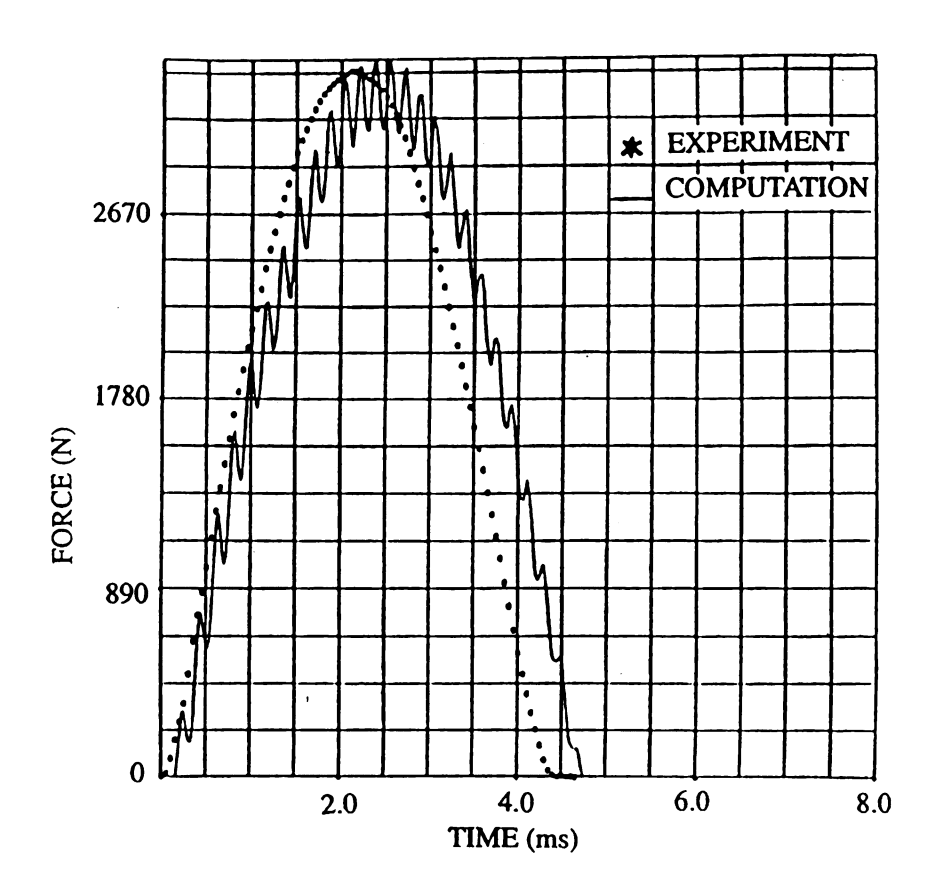


Figure 4.7 - Force history of 15-layer laminate with fixed boundary condition and subjected to 1m/s impact

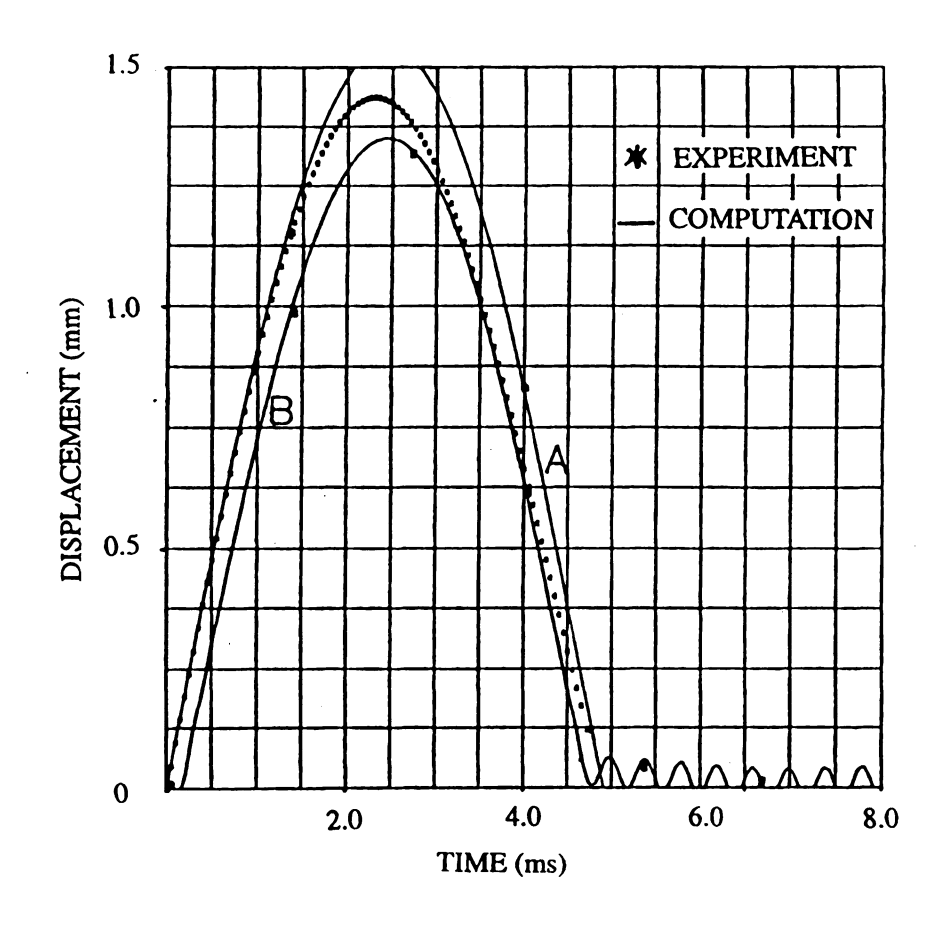


Figure 4.8 - Displacement history of 15-layer laminate with fixed boundary condition and subjected to 1m/s impact

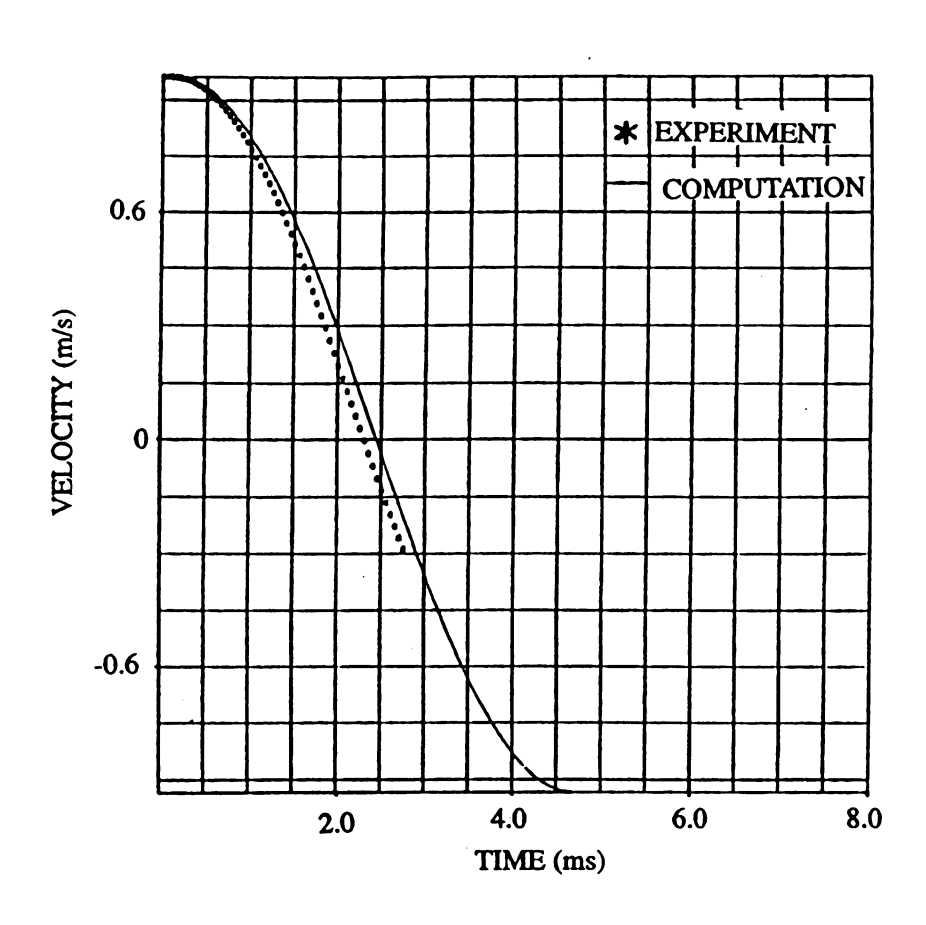


Figure 4.9 - Velocity history of 15-layer laminate with fixed boundary condition and subjected to 1m/s impact

4.5 Computational Results

1. Justification

Before investigating the effects of material properties and geometrical parameters on impact response of composite laminates, the finite element models and the associated contact parameters were justified by comparing the LS-DYNA3D results with those obtained from the approach based on indentation law by Sun and Chen [4.7]. In the justification, the stacking sequence and the impactor of the finite element simulations were identical to those defined in Reference [4.7] but different from those used in later investigations. It was found that a 40 x 40 mesh was able to give good agreement with Sun and Chen's. Figures 4.5 and 4.6 show the force history and deflection history, respectively. The solid line represents the results from LS-DYNA3D while the enhanced dots are those from Reference [4.1].

2. Summary

Similar studies regarding the thickness effect, fiber angle effect, and velocity effect were also performed by the LS-DYNA3D simulation. Figures 4.7, 4.8, and 4.9 show the comparisons between the experimental results and the finite element simulations for the 15-layer laminate, i.e. $[0_3/90_3/0_3/90_3/0_3]$, under 1m/s impact. The experimental results are designated by asterisk symbol while the finite element simulations the solid lines. The notations A and B for the solid lines represent for the results for the impactor and the specimen, respectively. In addition to the impact velocity of 1m/s, impact velocities of 2.8m/s and 3.5 m/s were also performed and the results based on various failure criteria and associated progressive damage models, such as Tsai- Wu failure criterion [4.9],

Chang-Chang failure criterion [4.10], MTL54 (partially Chang-Chang failure criterion) [4.11], and pure elastic assumption are given in Figures 4.10, 4.11, and 4.12.

Based on the computational results, the following statements can be summarized:

A. (Thickness Effect) Based on comparisons of force history, deflection history, and velocity history, the computational results for 9-layer laminates agree well with the experimental counterparts if fixed boundary conditions is imposed in the simulations. However, simply- supported boundary conditions seems to give better results for 15-layer and 21-layer simulations.

- B. (Fiber Angle Effect) Simply-supported boundary condition also give good results for angle-ply laminates which consist of 15-layers.
- C. (Velocity Effect) At subperforation impact, the lower the velocity, the better the simulation.
- D. (Velocity Effect) Both Tsai-Wu and MTL54 (partially Chang-Chang failure criterion) seem to give reasonable simulation before penetration takes place.

4.6 Conclusion

The LS-DYNA3D gives accurate predictions for the response of impacted composites before delamination takes place. In order to closely simulate the progress of impact-induced damage, a new type of finite element and a new failure criterion which account for interlaminar stresses are required.

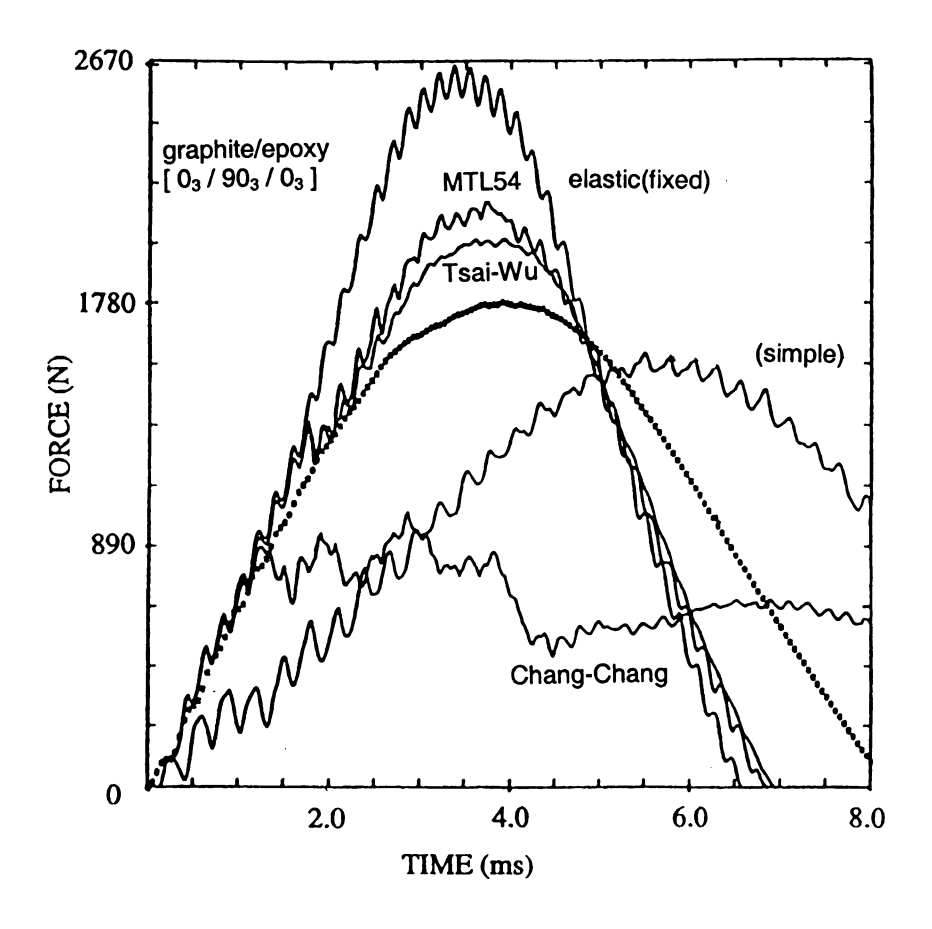


Figure 4.10 - Force histories of 9-layer laminate subjected to 1m/s impact and simulated by various failure criteria

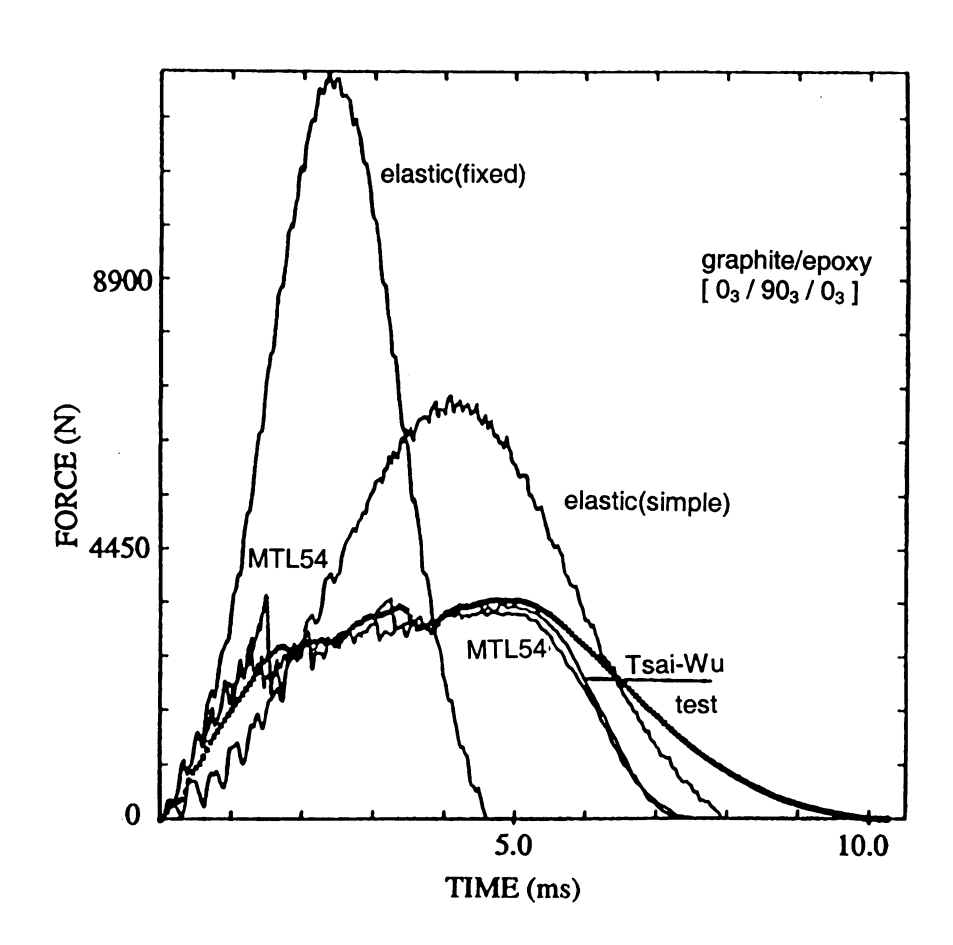


Figure 4.11 - Force histories of 9-layer laminate subjected to 2.8m/s impact and simulated by various failure criteria

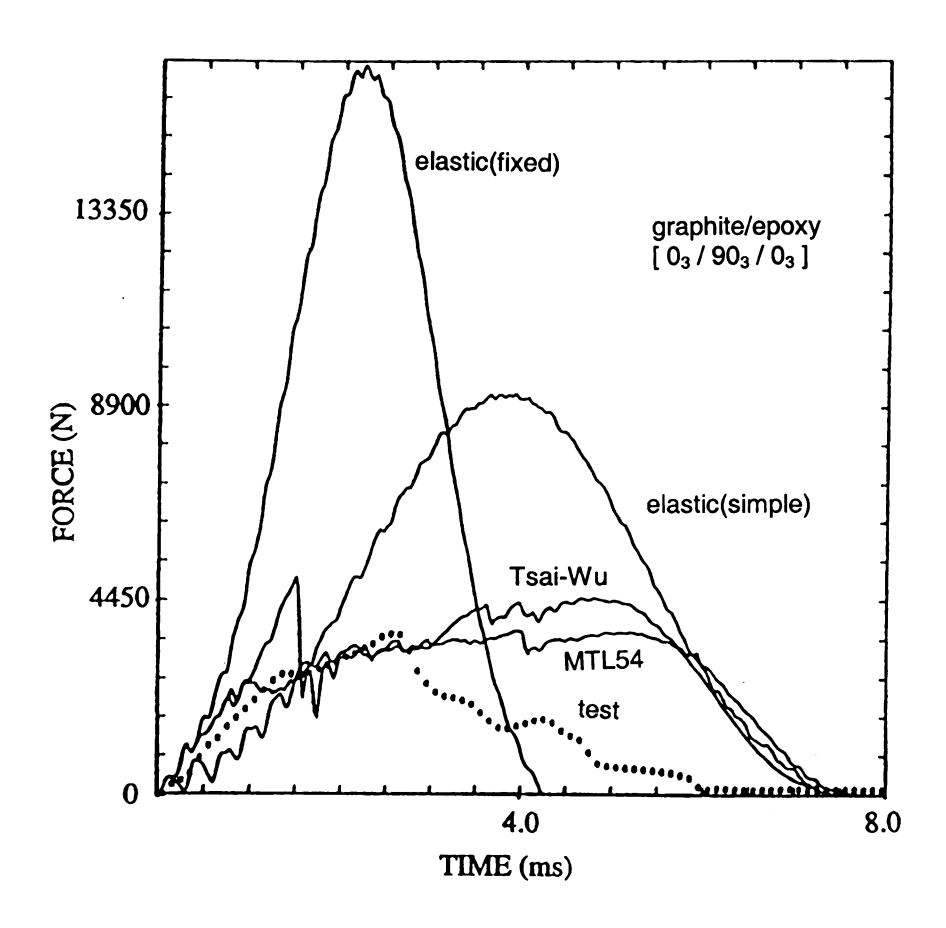


Figure 4.12 - Force histories of 9-layer laminate subjected to 3.5m/s impact and simulated by various failure criteria

ACKNOWLEDGMENT

The authors wish to express their sincere thanks to Ford Motors Company for financial support through the University Research Initiation Program. Partial support from the U.S. Army TARDEC (Warren, Michigan) is also greatly appreciated.

4.7 References

- 4.1. Abrate, S., "Impact on Laminated Composite Materials," Applied Mechanics Review, 44(4), 155-190, 1991.
- 4.2. Abrate, S., "Impact on Laminated Composites: Recent Advances," Applied Mechanics Review, 47(11), 517-544, 1994.
- 4.3. Liu, D. and Malvern, L.E., "Matrix Cracking in Impacted Glass/Epoxy Plates," Journal of Composite Materials, 21(7), 594-609, 1987.
- 4.4. Liu, Dahsin, "Impact-induced Delamination A View of Material Property Mismatching," J. Composite Materials, 22 (7), 674-691, 1988.
- 4.5. Tan, T.M. and Sun, C.T., "Use of Statical Indentation Laws in the Impact Analysis of Laminated Composite Plates," J. Applied Mechanics, 52, 6-12, 1985.
- 4.6. Chen, J.K. and Sun, C.T., "Dynamic Large Deflection Response of Composite Laminates Subjected to Impact," Composite Structures, 4, 59-73, 1985.
- 4.7. Sun, C.T. and Chen, J.K., "On the Impact of Initially Stressed Composite Laminates," J. Composite Materials, 19(6), 490-504, 1985.
- 4.8. Wu, E. and Yen, C., "The Contact Behavior Plates and Rigid Spheres," J. Applied Mechanics, 61, 60-66, 1994.

- 4.9. Tsai, S.W. and Wu, E.M., A General Theory of Strength for Anisotropic Materials," Journal of Composite Materials, 5(1), 58-80, 1971.
- 4.10. Chang, F.-K. and Chang, K.-Y., "Post-Failure Analysis of Bolted Composite Joints in Tension or Shear-Out Mode Failure," Journal of Composite Materials, 21(5), 809-833, 1987.
- 4.11. LS-DYNA3D User's Manual.

Chapter 5

SIMULATION OF COMPOSITE LAMINATES UNDER LOW-VELOCITY IMPACT WITH CONTINUUM-BASED FINITE ELEMENT METHOD

ABSTRACT

Delamination played the primary role of damage process in composite laminates under low-velocity impact. In order to simulate impact process, a computational scheme capable of identifying interlaminar stresses and presenting delamination failure was imperative. Because of the complexity of the impact analysis and delamination simulation, both numerical accuracy and computational efficiency should be considered in the development of a computational scheme. Considering interlaminar shear stress continuity and having degrees of freedom independent of layer number, a laminate theory named the Generalized Zigzag Theory was formulated into a finite element subroutine and integrated into a commercial package called ABAQUS. Due to the uses of the Truesdell rate of Cauchy stress and the rate of deformation tensors for large deformation analysis, the computational scheme was able to present reasonable interlaminar shear stresses via an updated Lagragian algorithm. Combining the calculated interlaminar shear stresses and a delamination failure criterion, the computational scheme adequately simulated the response of composite laminates under impact loading when the impact velocity is low.

5.1 Introduction

Owing to their high stiffness-to-weight and high strength-to-weight ratios, fiberreinforced polymer-matrix composite laminates are excellent materials for highperformance structures. Their properties in the thickness direction, however, are poor as they are assembled by weak polymeric matrices through laminate interfaces. Accordingly, when a composite laminate is subjected to impact loading, high interlaminar stresses, due to concentrated impact loading and sudden material change across laminate interfaces, combined with low interlaminar strengths could easily cause interlaminar damage such as delamination in the composite laminate. Although the impact-induced damage could be very complex, experimental investigations [5.1] had shown that delamination was the primary damage mode if the impact velocity was relatively low.

As a first step to simulate impact response of composite laminates, LSDYNA3D was used in a previous study [5.2]. However, due to its inability to calculate interlaminar stresses, no delamination simulation could be achieved in the study. The objective of this study was to improve the impact simulation, at least for low-velocity impact. Hence, a computational scheme capable of identifying interlaminar stresses and presenting delamination damage was imperative. Because of the complexity process of impact analysis delamination simulation, both numerical accuracy and computational efficiency should be considered in the development of a computational scheme. Considering interlaminar shear stress continuity and having degrees of freedom independent of layer number, a laminate theory named the Generalized Zigzag Theory [5.13] was chosen and formulated into a finite element subroutine. It was then integrated into a commercial package called ABAQUS for impact simulation. The development of the computational scheme was closely parallel to that of Lee [5.4], Experimental investigations was also performed to verify the computational results.

5.2 Experimental Investigation

In order to characterize the response of composite laminated subjected to impact loading, a DYNATUP GRC 8250 machine was used for impact testing. A schematic diagram of the impact testing machine was given in Figure 1. According to the diagram, the impactor consisted of three components: a dropping crosshead, an impactor rod, and an impactor nose. The steel impactor rod had a diameter of 12.5 mm and was attached to the dropping crosshead. A force transducer having a capacity of 22.24 kN was mounted on the front end of the impactor rod and encapsulated by a hemispherical nose. The total mass of the impactor was 11.9 kg. The impactor was set at a dropping height up to 0.8m to give an impact velocity at 4 m/s.

In impact tests for glass/epoxy laminates, specimens with dimensions of 150mm x 150mm was placed between two steel plate holders, namely the top holder and the bottom holder as shown in Figure 5.1. Each holder had an opening of 125mm x 125mm in the center. In imapet tests for graphite/epoxy laminates, the specimen dimensions were of 150mm x 100mm and the holder opening was 100mm x 75mm. The top holder was removable while the bottom one was attached to the frame of the impact testing machine which was fixed on a solid foundation. The specimen and the top steel holder were then C-clamped at four corners to the bottom steel holder. The composite specimen thus had a fixed boundary condition.

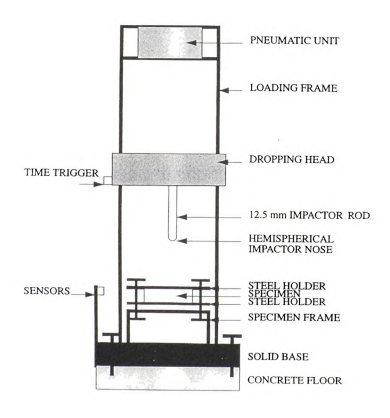


Figure 5.1 - Schematic diagram of impact testing setup

In each impact test, the crosshead was released from a preset height, and dropped freely according to the gravitational force. The impactor contacted the center of the composite specimen, resulting in so-called central impact.

As the impactor dropped and approached the composite specimen, its time trigger passed through a time sensor right before contact-impact occurred. The initial impact velocity was then calculated from the distance between the two edges of the time trigger and the time interval they passes through the sensor. Once impact began, the contact forces at many consecutive instants were detected by the force transducer attached to the impactor. The force history was recorded in a computer. The corresponding velocity history of the impactor could then be calculated from integrating the force history (after being divided by the mass of the impactor) and using the initial impact velocity. Subsequently, the corresponding displacement history of the impactor could be calculated from integrating the velocity history.

Based on the force and displacement histories, the force-displacement relation could be established. Assuming the impactor was perfectly rigid and the energy loss on the contact-impact interface between the impactor and the specimen was negligible, the force-displacement curve of the impactor could be considered as the force-deflection curve of the composite specimen.

In order to gain an overall view of the feasibility of a computational scheme in impact simulation, several composites was investigated. They included draphite.epoxy as well as glass/epoxy. A composite laminate with a stacking sequence of $[0_5/90_5/0_5]$ was taken as the basic case. Other stacking sequences concerning different laminations such as $[0_3/90_3/0_3/90_3/0_3]$ and $[0/90/0/...]_{15}$, different fiber orientations such as $[0]_{15}$, $[0_5/15_5/0_5]$,

 $[0_5/30_5/0_5]$ and $[0_5/45_5/0_5]$, and different thicknesses such as $[0_7/90_7/0_7]$ and $[0_9/90_9/0_9]$ were also tested. In addition, various impact velocities were applied to the basic laminate to identify the feasible range of impact simulation.

5.3 Computational Scheme

To begin with, a variational approach is performed to convert the differential governing equations, i.e. the equations of motion, into variational equations. Because this computional scheme was implemented through a user subroutine in ABAOUS, the Hilber-Hughes-Taylor scheme combined with the Newmark formulae was provided for numerical time integration, and the Newton iteration for nonlinear analysis was used in every time increment. In order to construct the Jacobian matrix and the residual vector for the Newton iteration, a consistent linearization technique based on Taylor's expansion was used to transform the nonlinear variational equations into linear approximate equations. Subsequently, the Truesdell rate of Cauchy stress and the rate of deformation tensor were introduced into the linearized equations. With the uses of the Generalized Zigzag Theory [5.13] and bilinear shape functions, a 4-node shell element was established in the finite element formulation. Hence, from above mentioned time integration scheme and Newton iteration method, nonlinear solutions could be obtained systematically from many small increments. With the Zigzag Jacobian for the geometric description of deformed element, the computational scheme was of the updated Lagrangian type.

A similar procedure had been used by Lee [5.4] in the development of a computational scheme for composite laminates subjected to static loading. The

development given below was aimed at dynamic analysis and was closely parallel to Lee's procedure. In fact, many details could be found in Reference [5.4].

1. Equations of Motion

Consider that a displacement vector u_i satisfies the equations of motion

$$\sigma_{ii.i} + b_i = \rho u_{i.ii} \tag{1}$$

throughout a body which has a volume V over a time interval and is subjected to the following conditions:

A. displacement (essential) boundary condition

$$u_i = g_i(x_i, t) \text{ on } \Gamma_g$$
 (2)

B. traction (natural) boundary condition

$$h_i(x_i, t) = \sigma_{ii} n_i \text{ on } \Gamma_h$$
 (3)

C. initial conditions

$$u_i(x_i, 0) = u_i^o(X_i)$$
 (4a)

$$u_{i,i}(x_i,0) = v_i^o(X_i)$$
 (4b)

where $\Gamma_g \cup \Gamma_h = S$, $\Gamma_g \cap \Gamma_h = 0$, and S is the surface of the body.

In addition, the variables appear in the above equations are defined as follows:

 X_i is the vector of initial (or material) coordinate,

 x_i is the vector of current (or spatial) coordinate and $x_i = X_i + u_i$

 $\sigma_{ii}(x_i,t)$ is Cauchy (true) stress,

 $b_i(x_i,t)$ is the body force vector of unit volume,

 $\rho(x_i,t)$ is the mass density,

 n_i is the unit normal vector of the surface with specified traction.

The indicies i and j denote Cartesian coordinates relative to a fixed reference frame and they range from 1 to 3.

2. Variational Formulation

The variational form of the equations of motion, i.e. Eq. (1), can be written as follows

$$\int_{V} \delta u_{i} (\sigma_{ij,j} + b_{i} - \rho u_{i,i}) dV = 0$$
(5)

where δu_i is an arbitrary weight function and must satisfy the homogeneous form of the displacement boundary condition, i.e.

$$\delta u_i = 0$$
 on Γ_g (6)

Performing integration by parts for Eq. (5), it leads to

$$\int_{V} \delta u_{i} b_{i} dV + \int_{\Gamma_{h}} \delta u_{i} h_{i} d\Gamma - \int_{V} \frac{\partial \delta u_{i}}{\partial x_{i}} \sigma_{ij} dV + F_{del} = \int_{V} \delta u_{i} \rho u_{i,n} dV$$
 (7)

It should be noted that the fourth term on the right-handed side of Eq. (7) is the virtual work done by tractions on all delaminated interfaces. It does not exist until delamination takes place. Since the tractions on the two surfaces created by each delamination have same magnitude but opposite direction and the weight function is discontinuous across each delaminated interface, F_{del} can be written as

$$F_{del} = \sum_{k=1}^{n-1} \int_{\Gamma^k} t_i^k \left(\delta u_i^k - \delta u_i^{k+1} \right) d\Gamma$$
 (8)

where n is the total number of layers and t_i is the traction vector on the kth interface between the kth layer and the k+1th layer and is defined as $t_i = \sigma_{ij} n_j$ on Γ_k (k is omitted). The domain of area integration Γ^k stands for the kth interface. Eq. (8) vanishes when there is no delamination because the weight function should be continuous across interfaces.

3. Laminate Theory

Since delamination plays a very important role in damage process, a computational scheme capable of identifying interlaminar stresses and accounting for both numerical accuracy and computational efficiency is imperative for impact simulation. Considering interlaminar shear stress continuity and having degrees of freedom independent of layer number, a laminate theory named the Generalized Zigzag Theory [5.3] is chosen for the description of displacement increments [5.4].

According to the Generalized Zigzag Theory, the components of displacement increments of a particle P at time t to time $t + \Delta t$ have the following forms:

$$\Delta u^{k}(x, y, z) = \Delta u_{0}(x, y) + (S_{1}^{k} + R_{1}^{k}z + A_{1}z^{2} + B_{1}z^{3})\Delta u_{1}(x, y) +$$

$$(S_{2}^{k} + R_{2}^{k}z + A_{2}z^{2} + B_{2}z^{3})\frac{\partial}{\partial y}\Delta w_{0}(x, y)$$

$$\Delta v^{k}(x, y, z) = \Delta v_{0}(x, y) + (P_{1}^{k} + O_{1}^{k}z + C_{1}z^{2} + D_{1}z^{3})\Delta v_{1}(x, y) +$$

$$(P_{2}^{k} + O_{2}^{k}z + C_{2}z^{2} + D_{2}z^{3})\frac{\partial}{\partial y}\Delta w_{0}(x, y)$$

$$\Delta w^{k}(x, y, z) = \Delta w_{0}(x, y)$$
(9)

where x, y and z are Cartesian coordinates of a particle P at time t, k is layer order, counting from the bottom to the top.

The independent variables are $\Delta u_0(x,y)$, $\Delta v_0(x,y)$, $\Delta w_0(x,y)$, $\Delta u_1(x,y)$ and $\Delta v_1(x,y)$. The coefficients are associated with material properties, fiber orientations and thicknesses. They are established from imposing displacement continuity conditions and interlaminar shear stress continuity conditions on laminate interfaces, and zero shear stress conditions on laminate surfaces.

In order to follow engineering conventions for finite element formulation, the independent variables are transformed into engineering variables (see Appendix C). Hence, $\Delta u_0(x,y)$, $\Delta v_0(x,y)$ and $\Delta w_0(x,y)$ are translational increments at a point on the mid-surface of composite laminates while $\Delta u_1(x,y)$ and $\Delta v_1(x,y)$ are rotational increments of a mid-surface point about x- and y-axis, respectively.

4. Large Deformation

In the development of a computational scheme, the rate of deformation tensor is used in kinematic relations for large deformation analysis, not only because of its linearity and simplicity to be incorporated into the Generalized Zigzag Theory but also because of its frame indifference. The rate of deformation tensor is defined as the symmetric part of velocity gradient, i.e.

$$D_{ij} = \frac{1}{2} (v_{i,j} + v_{j,i}) \equiv v_{(i,j)}$$
 (10)

It vanishes when a continuum undergoes a rigid body motion.

In describing kinetic relations, both frame indifference (also called objectivity) condition and energy conjugate condition between stress and strains components must be satisfied. Thus, the Truesdell rate of Cauchy stress [5.4] given below is used in conjunction with the aforementioned rate of deformation tensor in the analysis:

$$\nabla \sigma'_{ij} = \sigma_{ij} \Delta u_{k,k} - \sigma_{kj} \Delta u_{i,k} + \Delta \sigma_{ij} - \sigma_{il} \Delta u_{j,l}$$
(11)

where $\Delta \sigma_{ij}$ is the Cauchy stress rate. In addition, the Truesdell kinetic relation has a form of

$$\nabla \sigma_{ij}^t = C_{ijkl}^t \Delta u_{(k,l)} \tag{12}$$

in which

$$C_{ijkl}^{t} = C_{ijkl} + \sigma_{ij}\delta_{kl} - \frac{1}{2}(\sigma_{ik}\delta_{jl} + \sigma_{jl}\delta_{il} + \sigma_{il}\delta_{jk} + \sigma_{jl}\delta_{ik})$$

$$(13)$$

and C_{ijkl} is the stiffness matrix of the generalized Hooke's law. By combining Eqs. (11) and (12), the Cauchy stress rate becomes

$$\Delta \sigma_{ii} = C_{iikl}^t \Delta u_{(k,l)} - \sigma_{ii} \Delta u_{k,k} + \sigma_{ki} \Delta u_{i,k} + \sigma_{il} \Delta u_{i,l}$$
 (14)

This equation can be used for updating Cauchy stress.

5. Finite Element Formulation

Among the commercial finite element packages, ABAQUS has been commonly used in engineering analysis. It is especially useful to researches due to its capability of integrating with user's subroutines. The present study is aimed at presenting a subroutine for composite laminates subjected to impact loading. The computational scheme is to be imposed into the ABAQUS for impact simulation.

In ABAQUS/Standard, the implicit dynamic analysis is realized through the Hilber-Hughnes-Taylor scheme. According to this scheme, the solution at time $t + \Delta t$ is not only dependent on the condition at time t, but also is dependent on that at time $t + \Delta t$. Hence, the Newton iteration method is used to solve the nonlinear equations.

In the Newton method, the formulation of Jacobian matrix is essential though sophisticated. It is an expensive numerical process and not always reliable. Hence, a closed form is preferred in the formulation of the Jacobian matrix. In order to do so, a consistent linearization technique is introduced into the variational equations given earlier. Details of the consistent linearization technique and its application to the variational equations can be found in Appendix A.

Performing the consistent linearization for the variational equations and using the Newton iteration method for establishing the Hilbert-Hughnes-Taylor scheme, the following linear system is obtained:

$$-M(\Delta \ddot{u}) - (1+\alpha) \left[K_s(\Delta u) - K_{del}(\Delta u) \right] = M_{inert}(\ddot{u}) \Big|_{t+\Delta t} - (1+\alpha)G \Big|_{t+\Delta t} + \alpha G \Big|_{t}$$
 (15)

where

$$M(\Delta \ddot{u}_{i}) = \int_{\nu_{0}} \delta u_{i} \rho_{0} \Delta u_{i,tt} dV_{0}$$

$$K_{s}(\Delta u) = K^{matl} + K^{geom}$$

$$K^{matl} = \int_{\nu} \delta u_{i,j} C^{t}_{ijkl} \Delta u_{(k,l)} d\nu$$

$$K^{geom} = \int_{\nu} \delta u_{i,j} \sigma^{\nu}_{kj} \Delta u_{i,k} d\nu$$

$$K_{del}(\Delta u) = \sum_{k=1}^{n-1} \int_{\tau_{k}} \left(C^{t}_{ijkl} \Delta u_{(k,l)} + \sigma^{\nu}_{kj} \Delta u_{i,k} \right) n_{s} \left(\delta u^{m}_{i} - \delta u^{(m+1)}_{i} \right) da$$

$$G = F_{ext} - F_{int} + F_{del}$$

$$F_{ext} = \int_{\nu} \delta u_{i} b_{i} d\nu + \int_{\Gamma_{h}} \delta u_{i} h_{i} da$$

$$F_{int} = \int_{\nu} \delta u_{ij,j} \sigma_{ij} d\nu$$

$$F_{del} = \sum_{k=1}^{n-1} \int_{\tau_{k}} t^{k}_{i} \left(\delta u^{k}_{i} - \delta u^{(k+1)}_{i} \right) da$$

$$M_{inert} = \int_{\nu} \delta u_{i} \rho u_{i,tt} d\nu$$

They can also be found in Appendix A and B. It should be mentioned that the left side of Eq.(15) is referred as Jacobian matrix and the right side of the Eq.(15) is termed as

residual vector (or residual). In the residual part, the first term is the inertial force and the rest part is named as "static" residual.

5.1. Finite Element Discretization

As mentioned earlier, the incremental displacements at any material point of a composite laminate can be represented by five independent variables (three translational increments and two rotational increments with respect to the mid-plane of the composite laminate). Hence, a two-dimensional quadrilateral element is chosen and associated bilinear shape functions are used for interpolation of incremental displacements within each element, i.e.,

$$\Delta u_0 = \sum_{a=a}^4 N_a(\xi, \eta)(\Delta u_0)_a$$

$$\Delta u_1 = \sum_{a=a}^4 N_a(\xi, \eta)(\Delta u_1)_a$$

$$\Delta v_0 = \sum_{a=a}^4 N_a(\xi, \eta)(\Delta v_0)_a$$

$$\Delta v_1 = \sum_{a=a}^4 N_a(\xi, \eta)(\Delta v_1)_a$$
(16)

In the above equations, N_a is the bilinear shape function at the a^{th} node of the element whereas ξ and η are natural coordinates. And, $(\Delta u_0)_a$, $(\Delta u_1)_a$, $(\Delta v_0)_a$ and $(\Delta v_1)_a$ are increments of nodal displacement variables for the a^{th} node. Because the out-of-plane displacement increment Δw_0 is also dependent on $\frac{\partial}{\partial x} \Delta w_0(x,y)$ and $\frac{\partial}{\partial y} \Delta w_0(x,y)$, the Hermite cubic shape function should be used for interpolation of the transverse displacement increment to ensure C^1 continuity, i.e.,

$$\Delta w_0 = \sum_{a=a}^{4} [H_{a1}(\xi, \eta)(\Delta w_0)_a + H_{a2}(\xi, \eta)(\frac{\partial}{\partial x} \Delta w_0)_a + H_{a3}(\xi, \eta)(\frac{\partial}{\partial y} \Delta w_0)_a]$$
 (17)

With the above interpolation descriptions based on the nodal displacement variables, the displacement increments and strain increments can be exercised [5.4].

The description of geometry is implemented with the Zigzag Jacobian [5.4]. In the deformed element at a current time increment, the segments of the zigzag line through the laminate thickness are assumed linear within each layer. Based on this assumption, the Jacobian matrix for geometry description is formulated and referred as the Zigzag Jacobian [5.4].

5.2. Hilber-Hughess-Taylor Scheme

In order to understand the Hilber-Hughes-Taylor scheme, the individual terms in Eq. (15) should be carefully addressed.

A. contribution of inertial force to Jacobian Matrix

According to Eq. (B.3.5) of Appendix B,

$$M(\Delta \ddot{u}) = \frac{1}{\beta \Delta t^2} \int_{V_0} \delta u_i \rho_0 \Delta u_i dV_0.$$

By using Eq. (5.29)-(5.31) in Ref. [5.4], it yields

$$M(\Delta \ddot{u}) = \frac{1}{\beta \Delta t^2} \int_{V_0} \rho_0 (\delta u_k \Delta u^k + \delta v^k \Delta v^k + \delta w^k \Delta w^k) dV_0$$
$$= \frac{1}{\beta \Delta t^2} \delta \{u\}^T M \Delta \{u\}$$
(18)

where M is the mass matrix and is defined as

$$\mathbf{M} = \int_{V_0} \rho_0 \left[\left(\left\{ X U_0 \right\} + \left\{ X U_1 \right\} z + \left\{ X U_2 \right\} z^2 + \left\{ X U_3 \right\} z^3 \right)^T \left(\left\{ X U_0 \right\} + \left\{ X U_1 \right\} z + \left\{ X U_2 \right\} z^2 + \left\{ X U_3 \right\} z^3 \right) + \left(\left\{ X V_0 \right\} + \left\{ X V_1 \right\} z + \left\{ X V_2 \right\} z^2 + \left\{ X V_3 \right\} z^3 \right)^T \right]$$

$$(\{XV_0\} + \{XV_1\}z + \{XV_2\}z^2 + \{XV_3\}z^3) + \{XW_0\}^T \{XW_0\}] dV_0$$
(19)

details of the matrices appeared in above equations can found in Eqs.(5.29)-(5.31) of Ref. [5.4].

B. stiffness matrix

A similar procedure used by Lee [5.4] has been followed for formulation of stiffness matrix, (Eq.(5.63) for material stiffness matrix and Eq.(5.64) for geometric stiffness matrix in Ref.[5.4]). It is expressed below:

$$[K_s] = [K^{mall}] + [K^{geom}]$$
(20)

where

$$K^{mail} = \int_{V} \delta u_{i,j} C'_{ijkl} \Delta u_{(k,l)} dv$$

$$K^{geom} = \int_{V} \delta u_{i,j} \, \sigma^{v}_{kj} \Delta u_{i,k} \, dv$$

C. Contribution of delamination to Jacobian matrix

This term does not exist before delamination takes place. Once delamination occurs, this term becomes imperative as delamination affects the impact response of composite laminates. A more rigorous derivation of this term requires an additional interfacial theory for modeling laminate interfaces and could result in a very complicated incremental displacement field. In order to avoid the potential complexity, an interfacial layer technique and a stress re-calculation technique are introduced to delamination simulation process to replace the delamination related terms in the formulation procedure. With these two techniques, the incremental displacement description, i.e. Eq.(9), still holds.

Therefore, in this formulation procedure, the delamination related terms are neglected, i.e.

$$K_{del}(\Delta u) = 0 \tag{21}$$

D. contribution of inertial force to residual

This term can be easily determined from its definition and Eq. (19), i.e.

$$M_{inert}(\ddot{u}) = \int_{V_0} \delta u_i \rho_0 \ddot{u}_i dV_0 = \delta \{u\}^T M \{\ddot{u}\}$$
 (22)

E. static residual at the end of current time increment

As mentioned earlier, if delamination has no contribution to residual vector, it yields

$$\left\{G\right|_{t+\Delta t}\right\} = \left\{F_{ext}\right\} - \left\{F_{\text{int}}\right\} \tag{23}$$

where

$$F_{ext} = \int_{V} \delta u_{i} b_{i} dv + \int_{\Gamma_{h}} \delta u_{i} h_{i} da$$

$$F_{int} = \int_{V} \delta u_{ij,j} \sigma_{ij} dv$$

F. static residual at the end of previous time increment

Similarly to above, but for the end of previous time increment, it gives

$$\{G|_{t}\} = \{F^{ext}|_{t}\} - \{F^{int}|_{t}\}$$

$$(24)$$

6. Delamination Analysis

6.1. Quadratic Stress Criterion

Since the interlaminar shear stress is predicted from the Generalized Zigzag Theory is accurate [5.4], the prediction of delamination initiation based on U102 is implemented with a mechanics of materials approach. A quadratic stress criterion [5.5] is used to judge the initiation of in delamination in laminate interfaces. The interlaminar normal stress is neglected in the Generalized Zigzag Theory for simplicity of formulation as well as the

fact that it does not contribute the delamination initiation. Hence, the quadratic stress criterion implemented in U102 is

$$\left(\frac{\overline{\sigma}_{13}}{S_1}\right)^2 + \left(\frac{\overline{\sigma}_{23}}{S_2}\right)^2 = 1$$

where $\overline{\sigma}_{13}$ and $\overline{\sigma}_{23}$ are the averaged shear stresses on the concerned interface of an element whereas S_1 and S_2 are the interlaminar shear strengths for 1-3 and 2-3 planes, respectively. Once the above quadratic stress criterion is satisfied, the delamination is assumed to occur interface of the element.

6.2. Interfacial Layer Technique

The calculation of the interlaminar shear stresses on a concerned interface of an element is performed via the assumption of an interfacial layer on the interface. The interfacial layer is artificially inserted into the laminate interface with thickness about one-tenth of the adjacent laminae. The integration points for numerical analysis are imposed in the interfacial layer. The interlaminar shear stresses on all integration points within the interfacial layer are calculated at every time increment. The calculation of the averaged interlaminar shear stresses can be carried out the condition of the laminate interface can be investigated with use of the quadratic stress criterion.

6.3. Stress Re-calculation.

At any time increment, if every interface of an element is delaminated after checking the averaged stresses against the quadratic stress criterion, the element is then considered as organized by many sub-elements with the total sub-element number equal to the number. Each sub-element has the same thickness as the original composite layer though it has free surfaces on both top and bottom surfaces. However, all the sub-elements

separated from the original element share the same four nodal displacements. A process for stress re-calculation then should be carried out at this time increment. The re-calculation process is divided into two steps. In the first step, the stress tensor at every integration point in the original element is set to zero. In the second step, the stress tensor is then re-calculated from the total displacements at the current time for all integration points in every sub-element.

5.4 Results and Discussions

1. Comparisons with LS-DYNA3D

In order to verify the finite element scheme presented in the study, i.e. code U102, computer simulations based on the scheme and two commercial packages, i.e. LS-DYNA3D and ABAQUS, were performed for comparison. The commercial packages had been used by some researchers for laminate analysis although they were based on solid elements and did not account for the continuity of interlaminar stresses on laminate interfaces. Figure 5.2(a) showed the force histories of a [0₃/90₃/0₃/90₃/0₃] graphite/epoxy laminate under 1 m/s impact [5.2]. The mass of the hemispherical impactor was 24g and the diameter was 12.5mm. Apparently, the results from both U102 and LS-DYNA3D agreed very well with those from the experiment. The material response shown in Figure 5.2(b), i.e. the displacement histories, also agreed well among the three groups.

When a thinner composite laminate such as $[0_3/90_3/0_3]$ was investigated, U102 gave a better comparison with the experiment than LS-DYNA3D, as shown in Figure 5.3(a). It was believed that delamination was an important damage mode under the impact condition and the ability of U102 to calculate interlaminar shear stresses and to model

delamination was responsible for the result. However, if the impact velocity was increased from 1 m/s to 2.8m/s, the discrepancy became greater, as shown in Figure 5.3(b). Apparently, delamination failure criterion alone was not enough to account for the damage of the composite laminate under the impact condition. Failure criteria accounting for other damage modes such as matrix crack and fiber breakage should be included in the simulation.

2. Effect of Velocity and Thickness

The comparison between U102 and ABAQUS (based on S4R shell element) was presented in Figure 5.4 for a glass/epoxy laminate with a stacking sequence of $[0_5/90_5/0_5]$. The impactor had identical geometry and mass as that used in the LS-DYNA3D investigations while the impact velocity was set as 1.12m/s. As mentioned earlier, in low-velocity impact, delamination was the primary damage mode. Since U102 accounted for interlaminar shear stresses, it was able to present simulate delamination up to some extent, resulting in a closer comparison with the experiment than ABAQUS. However, as the impact velocity increased, the force-displacement relation deviated further from the corresponding experimental result. Four different impact velocities were presented in Figure 5.5.

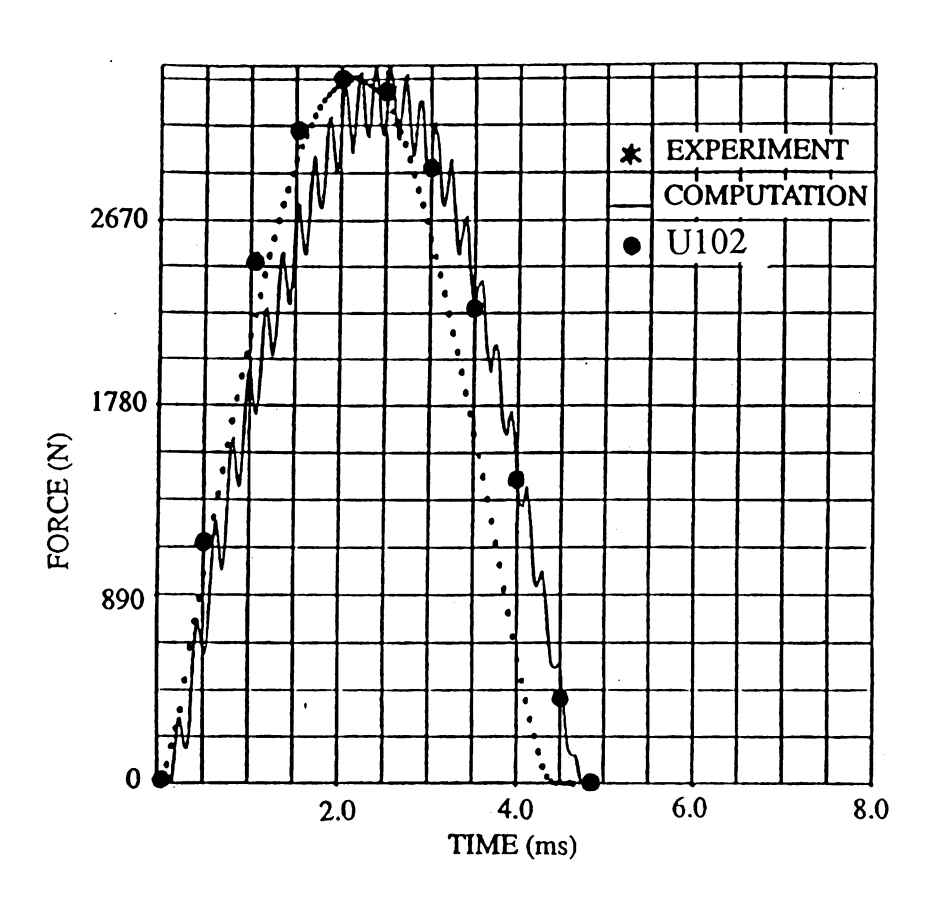


Figure 5.2(a) - Force history of 15-layer laminate with fixed boundary condition and subjected to 1m/s impact

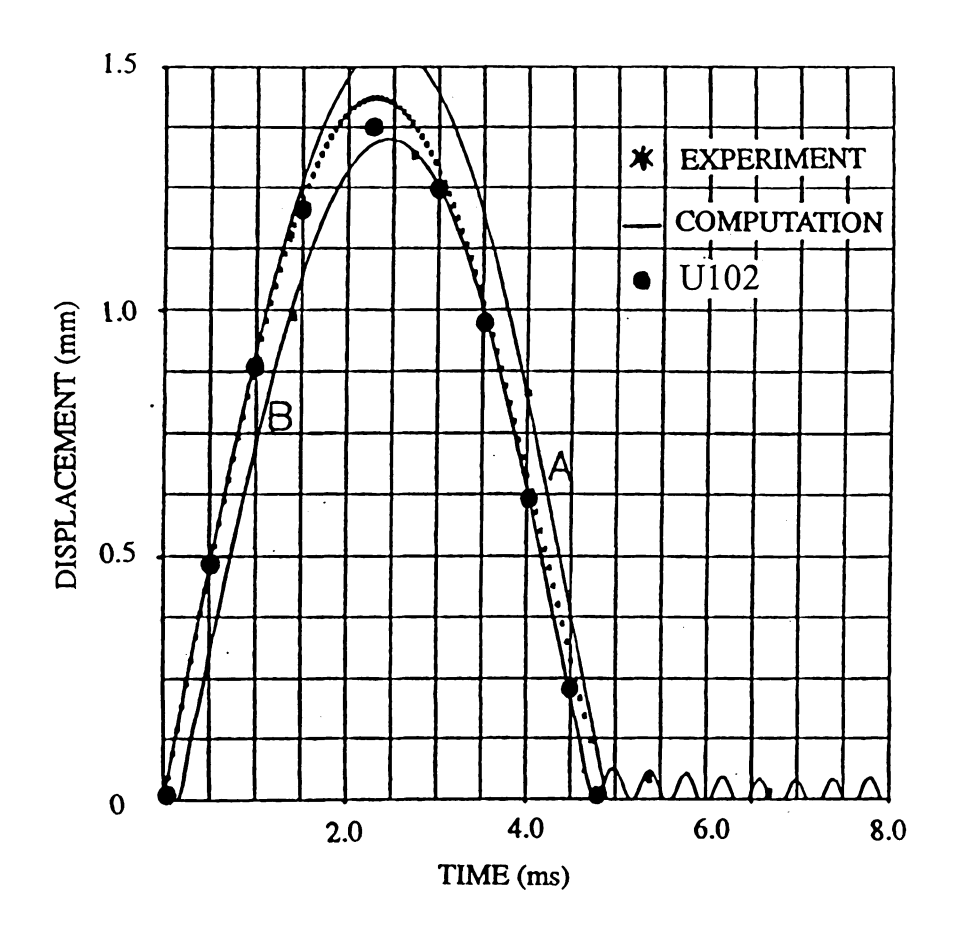


Figure 5.2(b) - Displacement history of 15-layer laminate with fixed boundary condition and subjected to 1m/s impact

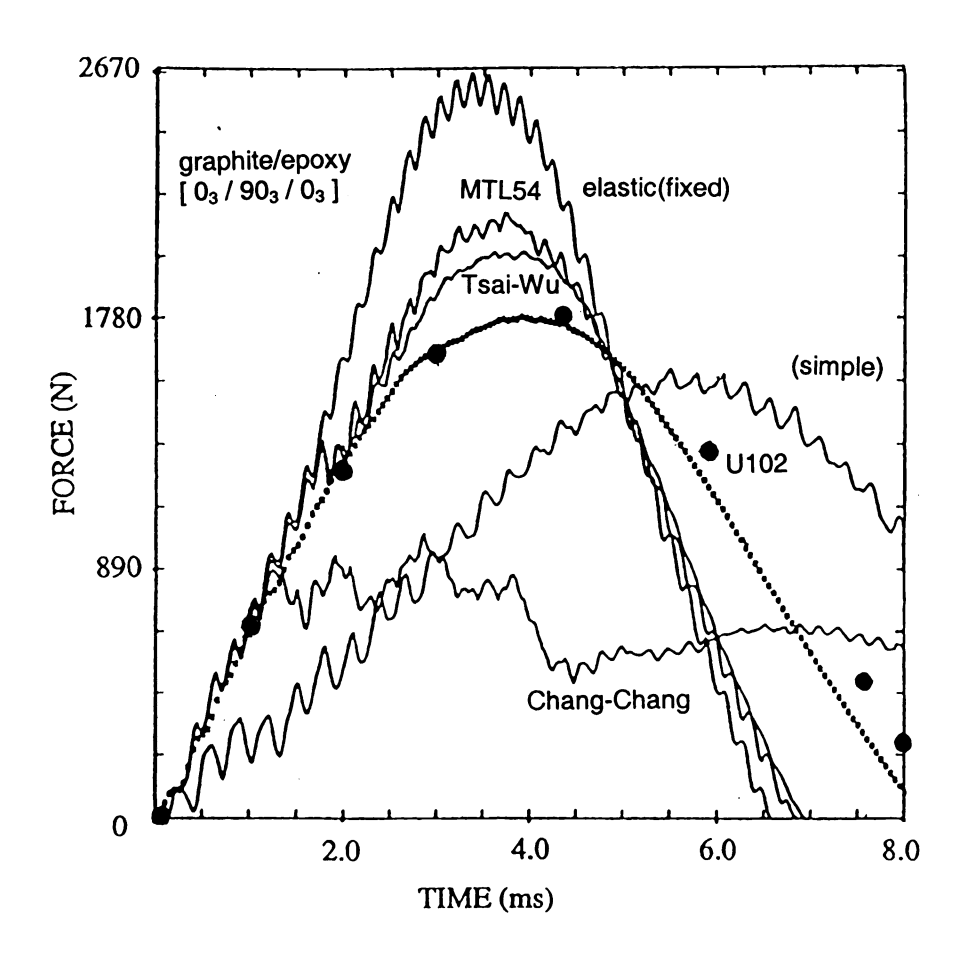


Figure 5.3(a) - Force histories of 9-layer laminate subjected to 1m/s impact and simulated by various failure criteria

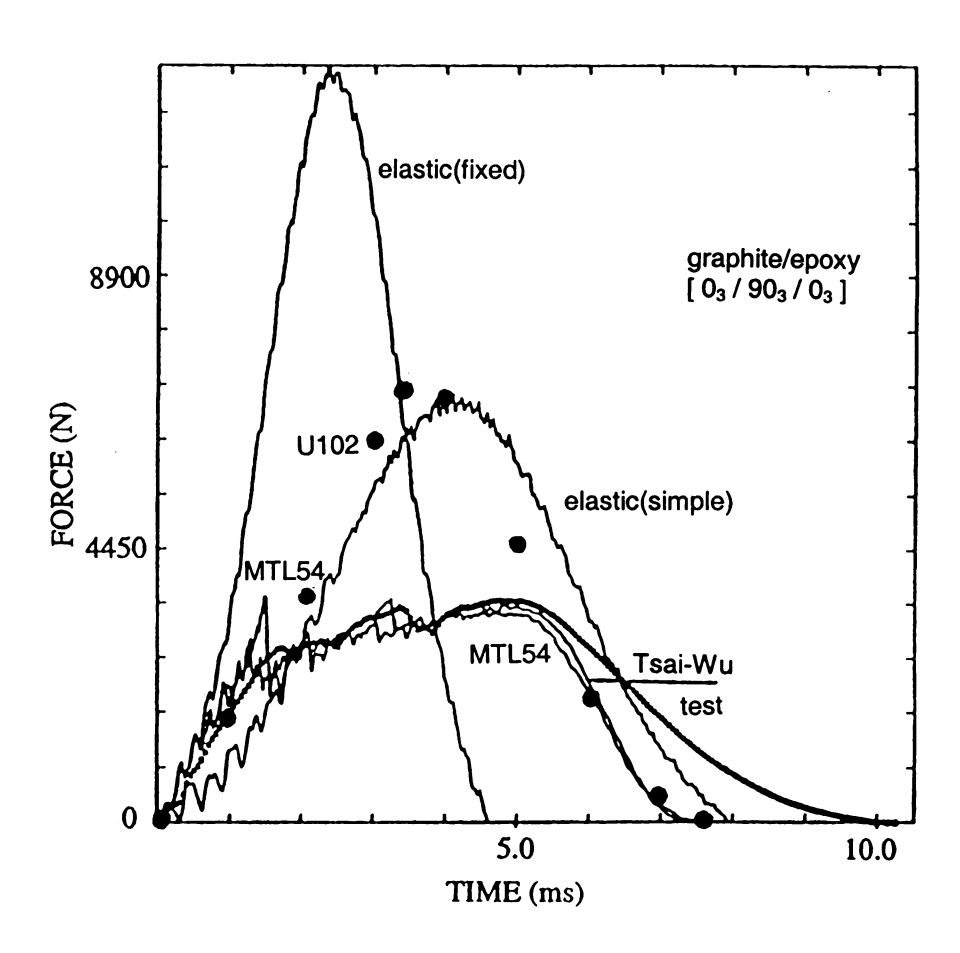


Figure 5.3(b) - Force histories of 9-layer laminate subjected to 2.8m/s impact and simulated by various failure criteria

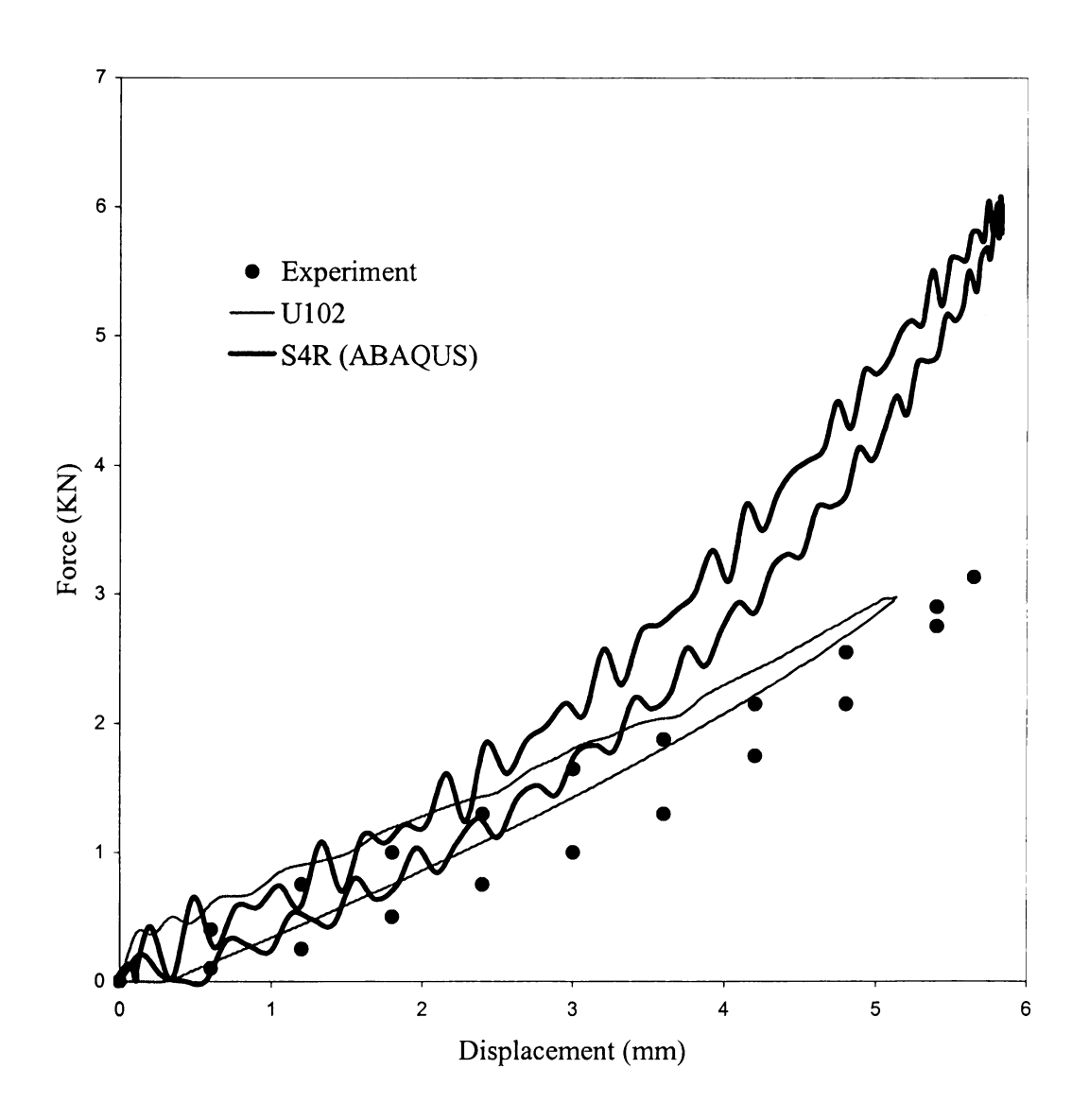


Figure 5.4 - Force Vs. Displacement for [05/905/05] at $V_0=1.12$ m/s

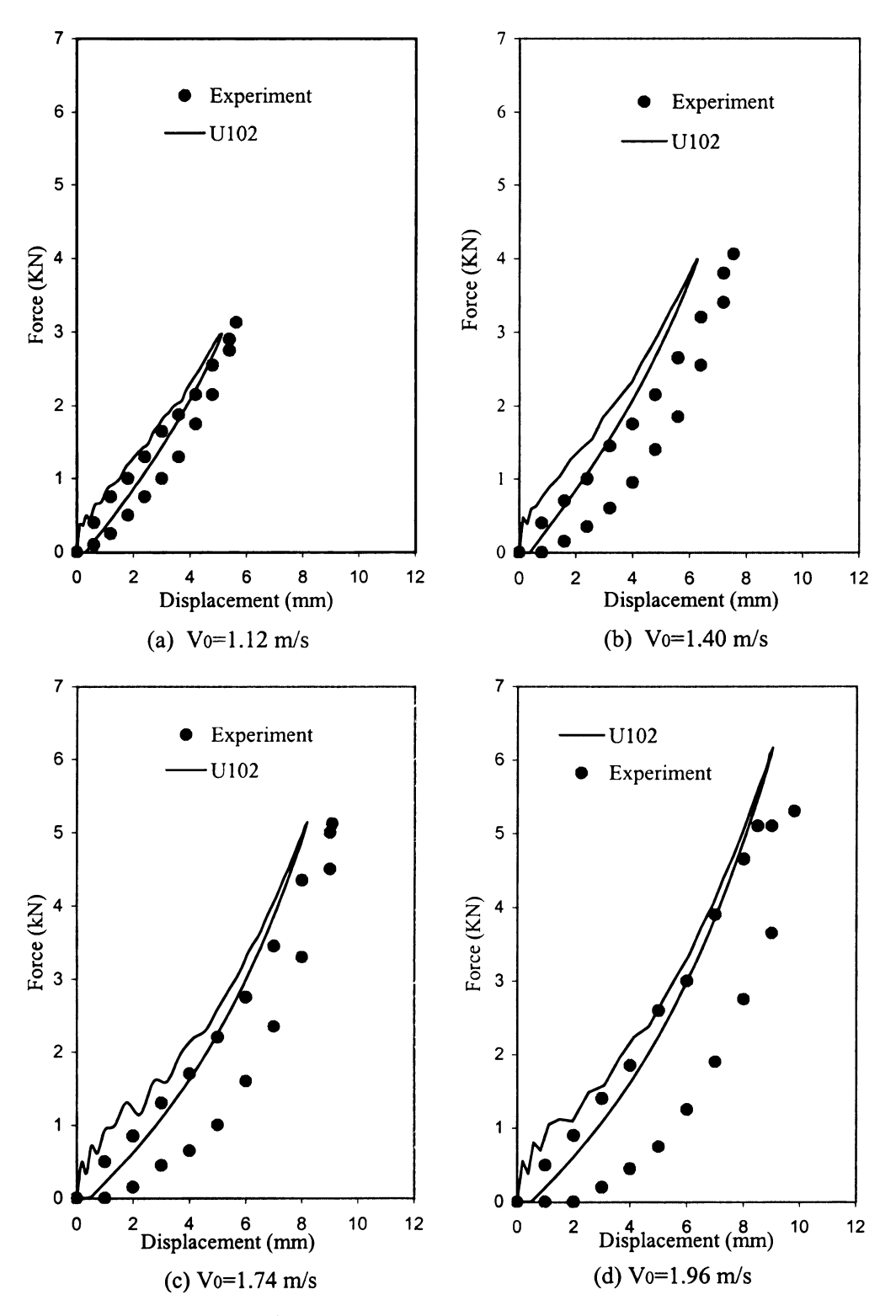


Figure 5.5 - Force vs. displacement for differenr impact velocities on [0s/90s/0s

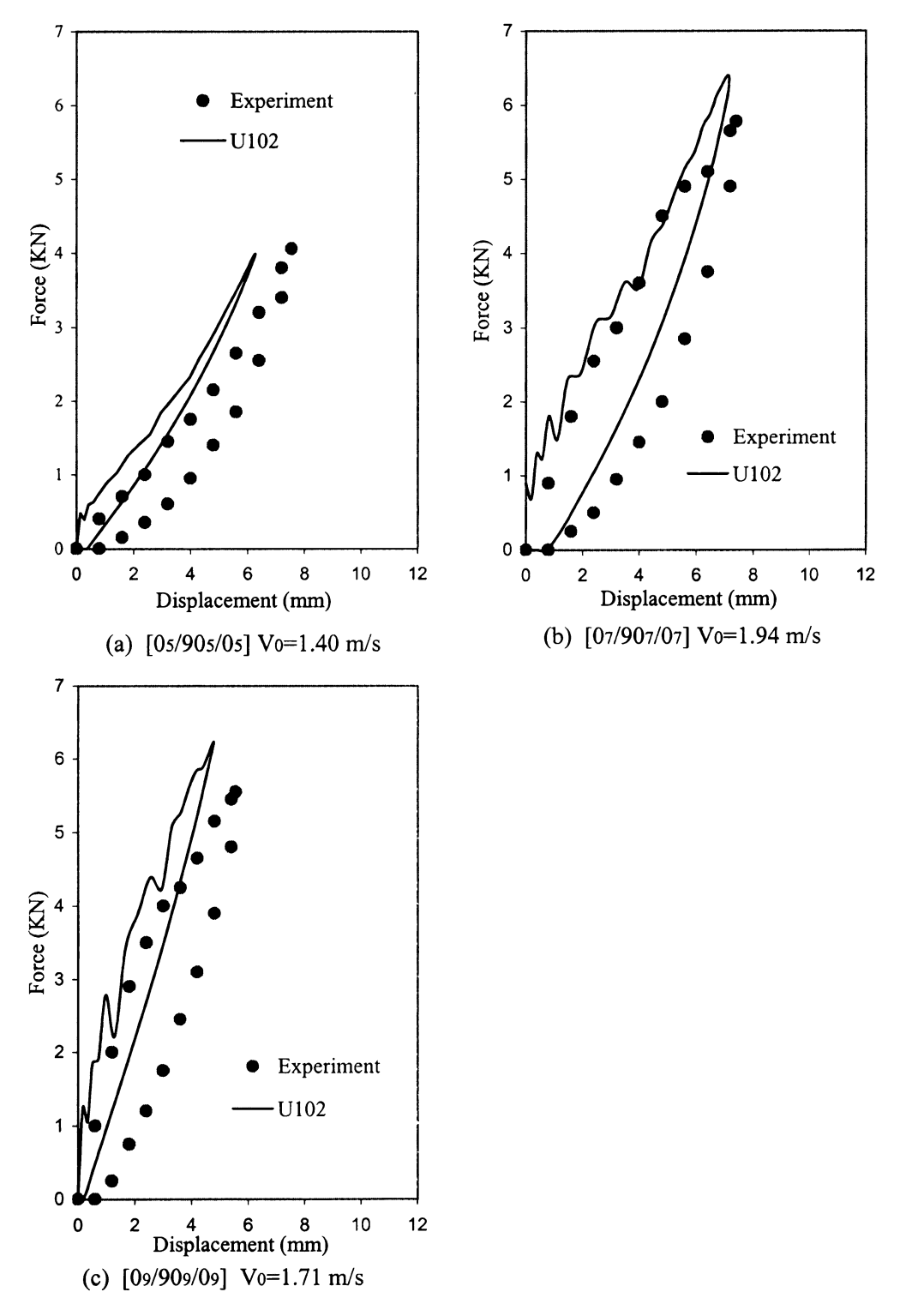


Figure 5.6 - Force vs. displacement for different laminate thicknesses

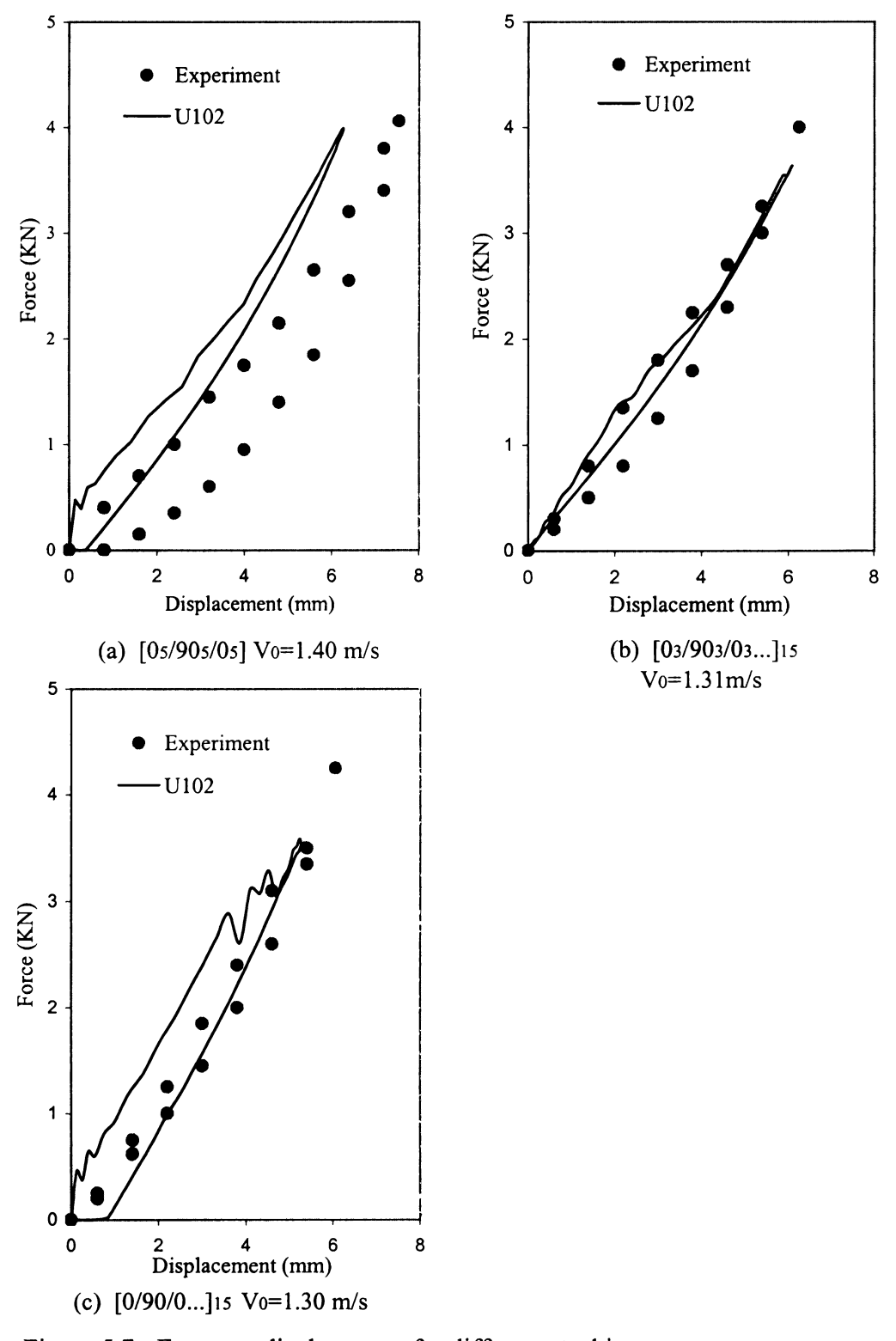


Figure 5.7 - Force vs. displacement for different stacking sequences

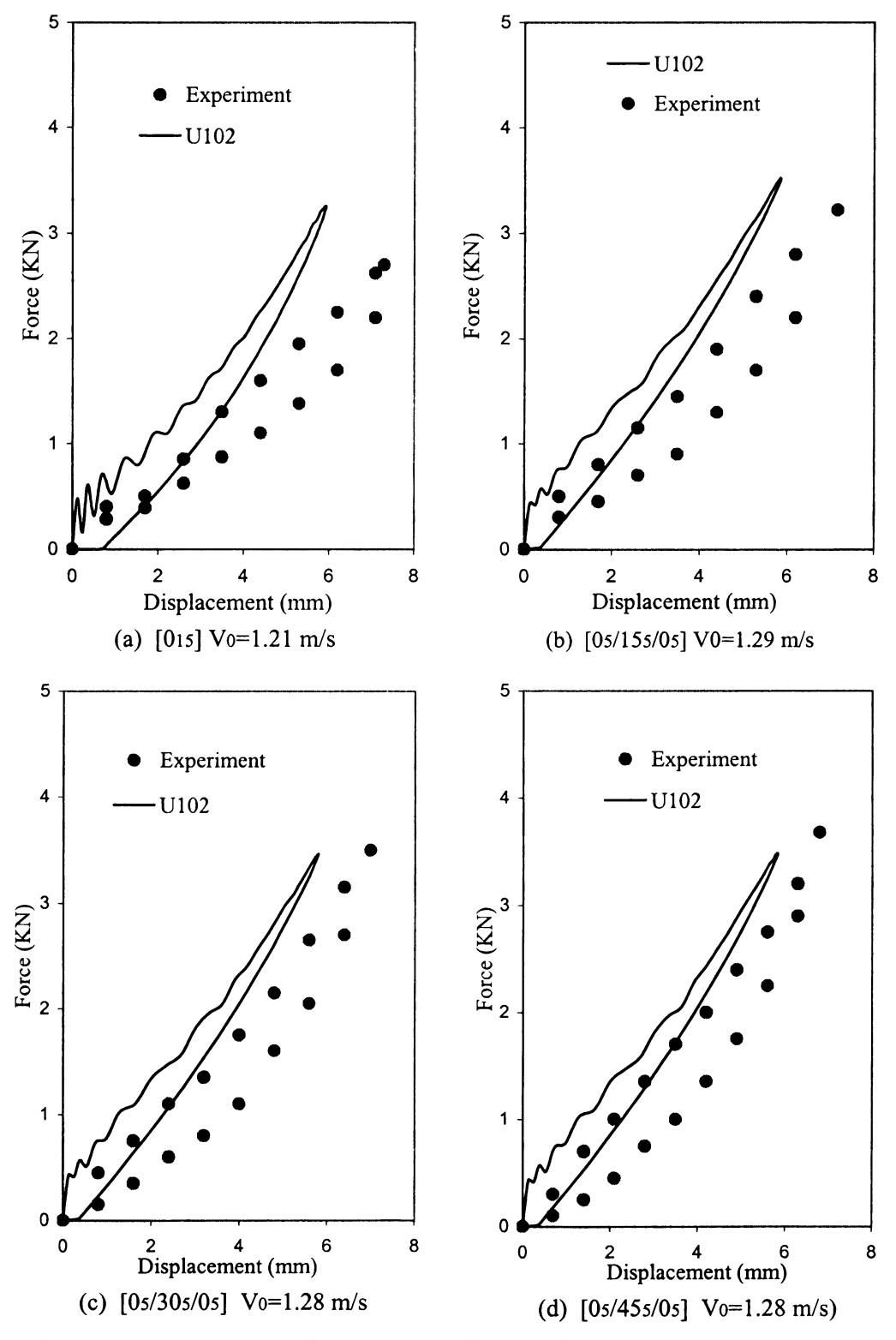


Figure 5.8 - Force vs. displacement for different fiber angles

An equivalent investigation to the velocity effect was the thickness effect. In addition to the 15-layer laminate, i.e. $[0_5/90_5/0_5]$, 21-layer and 27-layer laminates with stacking sequences of $[0_7/90_7/0_7]$ and $[0_9/90_9/0_9]$, respectively, were also investigated. Although the impact velocities were not scaled proportional to the laminate thickness, the results (see Figure 5.6) showed that the simulation result of the 15-layer case was higher than the corresponding experimental result. That of the 21-layer case seemed to agree very well with the experimental results while that of the 27-layer case were lower.

3. Effect of Lamination

Simulation results based on U102 for cross-ply laminates with same number of layers but different stacking sequences were investigated. They were $[0_5/90_5/0_5]$, $[0_3/90_3/0_3/90_3/0_3]$ and $[0/90/0/...]_{15}$, namely 3-lamina, 5-lamina and 15-lamina. Figure 5.7 depicted the results. Although the impact velocities were not quite identical, the simulation result compared to the experimental result seemed to be higher for the 3-lamina case, well overlapped for the 5-lamina case whereas lower for the 15-lamina case.

Another comparison concerning effect of lamination was for composite laminates with similar type of lamination but different fiber orientations. The laminates involved in the study were $[0]_{15}$, $[0_5/15_5/0_5]$, $[0_5/30_5/0_5]$ and $[0_5/45_5/0_5]$. Apparently, they were all of 3-lamina cases. However, the middle lamina had fiber orientation ranging from 0° , 15° , 30° to 45° . Based on the results given in Figures 5.8, the simulation seemed to become worse as the fiber orientation of the middle lamina became smaller. It is believed that bending-twisting coupling became more significant as the fiber orientation of the middle lamina became smaller, resulting in damage modes other than delamination.

5.5 Conclusions

- 1. The Generalized Zigzag Theory was formulated into a finite element subroutine (named U102) and integrated into ABAQUS code. Due to the uses of the Truesdell rate of Cauchy stress and the rate of deformation tensors, the computational scheme was able to predict reasonable interlaminar shear stresses via an updated Lagragian algorithm for composite laminates under large deformation due to impact loading.
- 2. A interfacial layer technique was presented for the calculation of the shear stresses on the laminate interfaces. With the interfacial layer, the integration points on the laminate interfaces could be specified and the stress tensor at these points could be calculated.
- 3. A delamination failure criterion, namely Quadratic Stress Criterion was integrated into the presented element U102 for the judging of delamination on the laminate interfaces of an element.
- 4. A stress re-distribution technique was presented to simulate the delamination of an element. Because of the stress re-distribution, the energy dissipation caused by delamination is simulated and a degradated transverse stiffness was estimated
- 5. Combining the calculated interlaminar stresses with a delamination failure criterion, and a stress re-distribution technique, the presented shell element U102 was able to simulate the response of composite laminates under impact loading. Experimental results seemed to agree with computational studies when the impact velocity was relatively low.

5.6 References

- 5.1 D. Liu, B. B. Raju, and X. Dang, "Size effects on impact response of composite laminates," *International Journal of Impact Engineering*, Vol. 21, No. 10, 1998
- 5.2 Liu,D. and Dang, X.,"Testing and simulation of laminated composites subjected to impact loading," Composite materials: fatigue and Fracture, 7th Vol., ASTM STP 1330, pp.273-284, 1998
- 5.3 Dahsin liu and Xiaoyu Li, "An overall view of laminate theories based on displacement hypothesis", Journal of Composite Materials, 30(14), 1996
- 5.4 Chienhom Lee, "A continuum-based shell element for laminated composites under large deformation", Ph. D dissertation, Michigan State University, 1998
- 5.5 John C. Brewer and Paul A. Lagace, "Quadratic stress criterion for initiation of delamination", Journal of Composite Materials, Vol. 22-December, 1988
- 5.6 ABAQUS/Standard Example Problems Manual, Vol. I and II, Version 5.5, Hibbitt, Karlsson & Sorensen, Inc., Pawtucket, RI., 1996
- 5.7 ABAQUS/Standard User's Manual, Vol. I, II and III, Version 5.8, Hibbitt, Karlsson& Sorensen, Inc., Pawtucket, RI., 2000
- 5.8 ABAQUS/Standard Theory Manual, Version 5.8, Hibbitt, Karlsson & Sorensen, Inc., Pawtucket, RI., 2000
- 5.9 ABAQUS/Standard Verification Manual, Version 5.8, Hibbitt, Karlsson & Sorensen, Inc., Pawtucket, RI., 2000
- 5.10 Bathe, K. J., "finite element procedure", Pretice-Hall, Englewod Cliffs, New Jersey

- 5.11 Dahsin Liu, Lan Xu, and Xianqiang Lu, "Stress analysis of imperfect composite laminates with an interlaminar bonding theory," International Journal for Numerical Methods in Engineering, 37, 2819-2839, 1994
- 5.12 Xianqiang Lu and Dahsin liu, "Assessment of interlayer shear slip theory for delamination modeling," Composite Materials: Fatigue and Fracture, 4th Vol, ASTM STP 1156, 218-235, 1993
- 5.13 X. Li and D. Liu, "A Zigzag Theory for composite laminates", AIAA Journal, 33(6), 1163-1165, 1995

Chapter 6

CONCLUSIONS AND RECOMMENDATIONS

6.1 Conclusions

Owing to their high stiffness-to-weight and high strength-to-weight ratios, fiber-reinforced polymer-matrix composite laminates are excellent materials for high-performance structures. However, their properties in the thickness direction are very poor as they are weakly bonded by polymeric matrices through laminate interfaces. Accordingly, when a composite laminate is subjected to impact loading, high interlaminar stresses along with the low interlaminar strengths could easily result in interlaminar damage such as delamination. This thesis investigated the response of composite laminates under low-velocity impact and presented numerical techniques for impact simulation.

To begin with, instrumented drop-weight impacts ranging from subperforation to perforation levels were introduced to composite laminates having various dimensions and thicknesses. Damaged composite laminates were then subjected to compression-after-impact tests for evaluations of residual properties. In order to understand more about the relationship between laminate thickness and perforation resistance, and to present an economical method to improve perforation resistance, thick laminated composite plates and their assembled counterparts were investigated and compared. An energy profile was established correlating the impact energy and absorbed energy at all energy levels for each type of composite plate investigated. This profile addressed the relationship between energy and damage. As a first step to simulate composite response to impact loading, LS-

DYNA3D was used for numerical analysis. However, due to this software's inability to describe interlaminar stresses, no delamination simulation could be achieved. As delamination played a very important role in damage process, a computational scheme capable of identifying interlaminar stresses and considering both numerical accuracy and computational efficiency was required for impact simulation. A laminate theory named Generalized Zigzag Theory was formulated into a finite element subroutine and integrated into ABAQUS code accounting for interlaminar shear stress continuity and having degrees of freedom independent of layer number. Due to the uses of the Truesdell rate of Cauchy stress and the rate of deformation tensors, the computational scheme was able to predict reasonable interlaminar shear stresses via an updated Lagragian algorithm. Combining the calculated interlaminar stresses with a delamination failure criterion, the computer program was able to predict the response of composite laminates up to the onset of delamination

The following conclusions can be drawn from the four investigations:

A. For size effects

1. Once perforation takes place, both impact characteristics(such as peak force of impact, impact-contact duration and absorbed energy during impact) and mechanical properties degradation(such as residual compressive maximum force and residual compressive absorbed energy) reach turning points. Accordingly, these five parameters can be used to identify the perforation thresholds of composite laminates. Since these parameters are important elements of material response, perforation is the most important damage stage, as far as material response is concerned, in composite laminates subjected to impact loading,

- 2. The study of size effects on impact response of composite laminates should be divided into two categories: in-plane dimensional effect and thickness effect. Among the ratios based on specimen in-plane dimensions, specimen thickness and impactor diameter, the ratio of specimen thickness to impactor diameter seems to best agree with the experimental results. Since the impactor diameter is kept constant in this study, the thickness of composite laminates becomes the most important parameter in impact response. Hence, the thickness effect is much more significant than the in-plane dimensional effect.
- 3. To rationalize the superiority of thickness effect to in-plane dimensional effect on impact response, bending rigidity should be considered as an important element for perforation analysis since it is proportional to the third power of thickness while only to the first power of in-plane dimension. Its capability of discriminating between thickness and in-plane dimension seems to be consistent with the experimental results that the thickness effect is more significant than the in-plane dimensional effect.
- 4. Although perforation is the most important damage stage, as far as material response is concerned, in composite laminates subjected to impact loading, perforation alone causes a small portion of mechanical properties degradation. It is delamination which also plays an important role in impact energy absorption and mechanical properties degradation since delamination has been identified as the other primary damage mode in impacted composite laminates.
- 5. The utilization of bending rigidity for perforation analysis can also be extended to delamination analysis. In fact bending rigidity has been successfully used in a previous study for predicting the potential for delamination of composite laminates subjected to

impact loading. The use of bending rigidity in interpreting the mechanical properties' degradation is well supported by the experimental results that both compressive maximum force and compressive absorbed energy degrade rapidly when delamination exists while compressive stiffness does not.

B. For assembly effects

- 6. Various joining techniques such as mechanical riveting, adhesive bonding, stiching joining and their combinations were used in assembling two-laminate and four-laminate composite plates. Pure epoxy bonding proved to be the most efficient joining technique in assembling the composite laminates together since it gave the highest bending stiffness and perforation threshold.
- 7. Among the assembled two-laminate composite plates, the perforation threshold increased as the bending stiffness increased. However, the increase in perforation threshold based on the improvement of bending (joining) stiffness was limited. A more efficient way to significantly increase the perforation threshold was to increase the thickness of composite laminates or to use assembled multi-laminate composite plates.
- 8. A technique named whole energy profile was presented for characterizing impact-perforation resistance. When penetration took place, the absorbed energy was approximately equal to the impact energy. When perforation occurred, the absorbed energy was again smaller than the impact energy. Experimental results revealed that the equal-energy interval, which was the difference between the penetration threshold and perforation threshold, increased as the thickness of composite plates increased.
- 9. Assembled composite plates were very comparable to laminated composite plates in both bending stiffenss and perforation threshold. This result verified the

advantage of using assembled composite plates over thick laminated composite plates since the cost of making thick laminated composite plates with high quality increased significantly as the thickness increased.

C. For evaluation of LS-DYNA3D

10. The LS-DYNA3D gives accurate predictions for the response of impacted composites before delamination takes place. In order to closely simulate the progress of impact-induced damage, a new type of finite element and a new failure criterion, which account for interlaminar stresses, are required.

D. For improvement of impact simulation

- 11. The Generalized Zigzag Theory was formulated into a finite element subroutine (named U102) and integrated into ABAQUS code. Due to the uses of the Truesdell rate of Cauchy stress and the rate of deformation tensors, the computational scheme was able to predict reasonable interlaminar shear stresses via an updated Lagragian algorithm for composite laminates under large deformation due to impact loading.
- 12. A interfacial layer technique was presented for the calculation of the shear stresses on the laminate interfaces. With the interfacial layer, the integration points on the laminate interfaces could be specified and the stress tensor at these points could be calculated.
- 13. A delamination failure criterion, namely Quadratic Stress Criterion was integrated into the presented element U102 for the judging of delamination on the laminate interfaces of an element.

- 14. A stress re-distribution technique was presented to simulate the delamination of an element. Because of the stress re-distribution, the energy dissipation caused by delamination is simulated and a degradated transverse stiffness was estimated
- 15. Combining the calculated interlaminar stresses with a delamination failure criterion, and a stress re-distribution technique, the presented shell element U102 was able to simulate the response of composite laminates under impact loading. Experimental results seemed to agree with computational studies when the impact velocity was relatively low.

6.2 Recommendations

- 1. To identify the residual properties of laminated composites after impact, the tension and bending test can be introduced into experimental studies to specify the fiber breakage and matrix crack effects on the degradation of laminated composite material properties.
- 2. A bilinear element can be developed based on C^0 continuous for transverse deformation. This can significantly reduce number of nodal variables. So the degree of freedom of every element can be reduced significantly.
- 3. The stress update based on the Truesdell rate of Cauchy stress is good for small incremental strain. This implies that the time increment still must be small to ensure the convergence in the nonlinear analysis. Since every strain increment can be treated as finite strain for large deformation analysis, the integration of the deformation rate through a time increment may improve the accuracy of strain calculation and accelerate the convergence speed.

- 4. Since the transverse normal stress is not well predicted from the Generalized Zigzag Theory, the recover technique may be used to recover the transverse normal stress. And this stress can be integrated into the delamination failure criteria and considered as normal pressure to determine the friction between delaminated plies.
- 5. Further studies should include all failure models when laminated composite are subjected to impact loading. The matrix crack and fiber breakage determine the perforation threshold. Therefore it is imperative to incorporate the all failure modes into impact simulation.
- An independent program may be developed to stay alone with ABAQUS.
 This program can even use explicit time integration methods to improve convergence characteristics.
 - 7. Delamination can be easily integrated into static analysis.
- 8. A contact algorithm may be introduced into this element for impact simulation. This will help to develop an independent program for laminated composite structural analysis.

APPENDICES

APPENDIX A

CONSISTENT LINEARIZATION AND APPLICATION TO VARATIONAL EQUATIONS

A.1 Consistent Linearization

Let's suppose

$$x^{\nu} = X + u(x,t)^{\nu} \tag{A.1}$$

where ν denotes the ν -th iteration. X is the vector of initial (or material) coordinate. x is the vector of current (or spatial) coordinate and x = X + u, u is the displacement vector. For the $(\nu+1)$ -th iteration, we has

$$x^{(\nu+1)} = x^{\nu} + \Delta u \tag{A.2}$$

Now, consider a nonlinear function defined by equation

$$f(x^{(\nu+1)}) = 0 (A.3)$$

The left side of equation (A.3) can be expanded in Taylor series at the ν -th iteration point x^{ν} ,

$$f(x^{(\nu+1)}) = f(x^{\nu}) + \left(\frac{\partial}{\partial \varepsilon} f(x^{\nu} + \varepsilon \Delta u)\right)_{\varepsilon=0} + R(x^{\nu})$$
(A.4)

The verification of the 2nd term in the right side of equation (A.4) is given below.

Using Taylor expansion to function $f(x + \Delta x)$, it gives

$$f(x + \Delta x) = f(x) + \left(\frac{\partial}{\partial x}f(x)\right)\Delta x + R \tag{A.5}$$

The 2nd term in the right side of equation (16) can be transformed into,

$$\left(\frac{\partial}{\partial \varepsilon} f(x + \varepsilon \Delta x)\right)_{\varepsilon=0} = \left(\frac{\partial}{\partial y} f(y)\right)_{\varepsilon=0} \Delta x \tag{A.6}$$

Then, we can finish our verification by replacing the dummy variable y with x.

$$\left(\frac{\partial}{\partial y}f(y)\right)_{\varepsilon=0}\Delta x = \left(\frac{\partial}{\partial x}f(x)\right)_{\varepsilon=0}\Delta x \tag{A.7}$$

Now, we can go back to (A.4). By neglecting the R term in (A.4), we write (A.3) as

$$f(x^{\nu}) = -\left(\frac{\partial}{\partial \varepsilon} f(x^{\nu} + \varepsilon \Delta u)\right)_{\varepsilon=0} \tag{A.8}$$

or

$$f(x^{\nu}) = -L(f) \tag{A.9}$$

where L is a operator, and defined by the following operation,

$$L(f) = \left(\frac{\partial}{\partial \varepsilon} f(x^{\nu} + \varepsilon \Delta u)\right)_{\varepsilon=0} \tag{A.10}$$

and this operation is referred as Consistent Linearization.

The following examples with the use of the operator L will benefit us in later derivations:

(1) Deformation Gradient and its transpose

By definition, we have

$$L(F_{ij}) = \left(\frac{\partial^2}{\partial \varepsilon \partial X_j} (x_i^{\nu} + \varepsilon \Delta u_i)\right)_{\varepsilon = 0}$$
(A.11)

Then, directly we get

$$L(F_{ij}) = \frac{\partial}{\partial X_i} \Delta u_i \tag{A.12}$$

Similarly, we can get

$$L(F_{nm}^{T}) = \frac{\partial}{\partial X_{n}} \Delta u_{m} \tag{A.13}$$

where the superscript T denotes the transpose of the matrix.

(2) The determent of Jacobian matrix

From definition,

$$L(J) = \left(\frac{\partial}{\partial \varepsilon} \det \left(\frac{\partial}{\partial X_j} (x_i^{\nu} + \varepsilon \Delta u_i)\right)\right)_{\varepsilon = 0}$$
(A.14)

by expanding $\det \left(\frac{\partial}{\partial X_j} (x_i^{\nu} + \varepsilon \Delta u_i) \right)$ according its definition, then doing the

differentiation, we can obtain

$$L(J) = J^{\nu} \Delta u_{i,j} \tag{A.15}$$

(3). Inverse of F and its transpose

Let's consider

$$FF^{(-1)} = 1$$
 (A.16)

then, applying the operator, we have

$$L(F)F^{(-1)} + FL(F^{(-1)}) = 0 (A.17)$$

Now using equation (A.12), we get

$$L(F_{ij}^{(-I)}) = -F_{ik}^{(-I)} \left(\frac{\partial}{\partial X_I} \Delta u_k\right) F_{ij}^{(-I)}$$
(A.18)

Please note, where superscript (-I) represents the inverse of a matrix.

Similarly, by using equation (A.13), we have

$$L(F_{ij}^{(-T)}) = -F_{ik}^{(-T)} \left(\frac{\partial}{\partial X_k} \Delta u_l\right) F_{ij}^{(-T)}$$
(A.19)

where (-T) denotes the inverse of a transposed matrix.

A.2 Linearization of the Variational Equations

We can rewrite equation (7) as

$$F_{ext} - F_{int} + F_{del} - M_{inert} = 0 (A.20)$$

or

$$F_{ext}(x^{(v+1)}) - F_{int}(x^{(v+1)}) + F_{del}(x^{(v+1)}) - M_{inert}(x_{i,tt}^{(v+1)}) = 0$$
(A.21)

where

$$F_{ext} = \int_{V} \delta u_i b_i dv + \int_{\Gamma_h} \delta u_i h_i da$$
 (A.22)

$$F_{\rm int} = \int_{V} \delta u_{(i,j)} \sigma_{ij} dv \tag{A.23}$$

$$u_{(i,j)} = \frac{1}{2}(u_{i,j} + u_{j,i})$$

$$M_{inert} = \int_{V} \delta u_{i} \rho u_{i,tt} dv$$

$$F_{del} = \sum_{k=1}^{n-1} \int_{-\frac{1}{k}} t_i^k \left(\delta u_i^k - \delta u_i^{(k+1)} \right) da$$

Applying Consistent Linearization on equation (23) will lead to

$$-L(F_{ext}) + L(F_{int}) - L(F_{del}) + L(M_{inert}) = F_{ext}(x^{\nu}) - F_{int}(x^{\nu}) + F_{del}(x^{\nu}) - M_{inert}(x_{i,tt}^{\nu})$$
(A.24)

A detailed discussion of every term in equation (A.24) is given below.



(1) The derivation of the 2^{nd} term in left side of equation (A.24)

Recall that

$$F_{\rm int} = \int_{V} \delta u_{i,j} \sigma_{ij} dv$$

or

$$F_{\text{int}} = \int_{V_0} \left(\frac{\partial}{\partial X_k} \delta u_i \right) X_{k,j} \sigma_{ij} J dV_0$$

Hence, we have

$$L(F_{\text{int}}) = \int_{V_0} \left(\frac{\partial}{\partial X_k} \delta u_i \right) [L(F_{ij}^{(-I)}) \sigma_{ij}^{\nu} J^{\nu} + F_{kj}^{(-I)} L(\sigma_{ij}) J^{\nu} + F_{kj}^{(-I)} \sigma_{ij}^{\nu} L(J)] dV_0$$
 (A.25)

By defining

$$L(\sigma_{ij}) = \Delta \sigma_{ij}$$

and using equation (A.14), (A.18) and

$$J^{\nu}dV_{0} = d\nu$$

we can reach

$$L(F_{\text{int}}) = \int_{\nu} \left(\frac{\partial}{\partial X_{k}} \delta u_{i} \right) \left(-F_{km}^{(-1)} \left(\frac{\partial}{\partial X_{l}} \delta u_{m} \right) F_{ij}^{(-1)} \sigma_{ij} + F_{kj}^{(-1)} \Delta \sigma_{ij}^{\nu} + F_{kj}^{(-1)} \Delta \sigma_{ij}^{\nu} \Delta u_{l,l} \right) dv$$
(A.26)

Because of the following relations,

$$\left(\frac{\partial}{\partial X_k} \delta u_i\right) F_{km}^{(-1)} = \delta u_{i,m}$$

$$\left(\frac{\partial}{\partial X_{k}} \delta u_{i}\right) F_{kj}^{(-I)} = \delta u_{i,j}$$

$$\left(\frac{\partial}{\partial X_{l}} \delta u_{m}\right) F_{ij}^{(-1)} = \delta u_{m,j}$$

equation (A.26) becomes

$$L(F_{\text{int}}) = \int_{V} \delta u_{i,j} \left(\Delta \sigma_{ij} + \sigma_{ij}^{V} \Delta u_{k,k} - \sigma_{ik}^{V} \Delta u_{j,k} \right) dV$$
(A.27)

But please note that the increments of Cauchy stress tensor still need to be further specified. Otherwise, equation (A.27) is useless.

As we well known, the relationship between the symmetric Second Piola-Kirchhoff (2^{nd} PK) Stress Tensor S_{ij} (which is defined with respect to initial reference configuration X) and the Cauchy Stress Tensor σ_{kl} is

$$S_{ij} = JF_{ik}^{(-1)}\sigma_{kl}F_{il}^{(-1)} \tag{A.28}$$

By using Linearization operator to equation (A.28), we have

$$L(S_{ij}) = L(J) (F_{ik}^{(-I)})^{\nu} \sigma_{kl}^{\nu} (F_{jl}^{(-I)})^{\nu} + J^{\nu} L (F_{ik}^{(-I)}) \sigma_{kl}^{\nu} (F_{jl}^{(-I)})^{\nu} + J^{\nu} (F_{ik}^{(-I)})^{\nu} L (\sigma_{kl}^{\nu}) (F_{jl}^{(-I)})^{\nu} + J^{\nu} (F_{ik}^{(-I)})^{\nu} \sigma_{kl}^{\nu} (F_{jl}^{(-I)})$$
(A.29)

When we chose the instantaneous motion configuration x at the end of ν -th iteration (instantaneous motion state) as the reference configuration X, we have,

$$J^{\nu} = 1$$

$$\left(F_{ij}^{(-I)}\right)^{\nu} = \delta_{ij} \tag{A.30}$$

$$L(J) = \Delta u_{k,k}$$

$$L(F_{ij}^{(-I)}) = -\Delta u_{i,j} \tag{A.31}$$

So, if we define

$$L(S_{ij}) = \Delta \sigma'_{ij}$$

namely the Truesdell rate of Cauchy stress, and substitute above equations into equation (A.29), it gives

$$\Delta \sigma_{ij}^{t} = \sigma_{ij}^{v} \Delta u_{k,k} - \sigma_{kj}^{v} \Delta u_{i,k} + \Delta \sigma_{ij} - \sigma_{il}^{v} \Delta u_{j,l}$$
 (A.32)

Hence, form ν -th to (ν +1)-th iteration, the increments of Cauchy stress tensor are

$$\Delta \sigma_{ij} = \Delta \sigma_{ij}^{\prime} - \sigma_{ij}^{\nu} \Delta u_{k,k} + \sigma_{kj}^{\nu} \Delta u_{i,k} + \sigma_{il}^{\nu} \Delta u_{i,l}$$
 (A.33)

This equation can be used to update the Cauchy stress tensor. The Truesdell rate of Cauchy stress is the increment of 2^{nd} P.K. stress tensor with respect to the reference configuration at time t. It can be determined experimentally with Total Lagrange formula, in which the engineering stress increments are determined by constitutive equations, and then transformed into 2^{nd} P.K stress tensor with respect to present configuration. Therefore the Truesdell rate of Cauchy stress can be further specified as

$$\Delta \sigma_{ij}^{\prime} = C_{ijkl}^{\prime} \Delta u_{(k,l)} \tag{A.34}$$

Inserting (A.34) into (A.33), we obtain

$$\Delta \sigma_{ij} = C^{t}_{ijkl} \Delta u_{(k,l)} - \sigma^{v}_{ij} \Delta u_{k,k} + \sigma^{v}_{kj} \Delta u_{i,k} + \sigma^{v}_{il} \Delta u_{j,l}$$
(A.35)

Let's consider equation (A.27) again and define

$$\Delta \sigma_{ij}^{syb} = \Delta \sigma_{ij} + \sigma_{ij}^{\nu} \Delta u_{k,k} - \sigma_{ik}^{\nu} \Delta u_{j,k}$$
(A.36)

Hence, equation (A.27) becomes to

$$L(F_{\text{int}}) = \int_{V} \delta u_{i,j} \Delta \sigma_{ij}^{syb} dv \tag{A.37}$$

On the other hand, by substituting (A.35) into (A.36), it gives

$$\Delta \sigma_{ij}^{syb} = C_{ijkl}^t \Delta u_{(k,l)} + \sigma_{kj}^v \Delta u_{i,k} + \sigma_{il}^v \Delta u_{j,l} - \sigma_{ik}^v \Delta u_{j,k}$$

or

$$\Delta \sigma_{ij}^{syb} = C_{ijkl}^t \Delta u_{(k,l)} + \sigma_{kj}^v \Delta u_{i,k}$$
(A.38)

Therefore, the following formula are obtained:

$$L(F_{\text{int}}) = \int_{V} \delta u_{i,j} C_{ijkl}^{t} \Delta u_{(k,l)} dv + \int_{V} \delta u_{i,j} \sigma_{kj}^{v} \Delta u_{i,k} dv$$

or

$$L(F_{int}) = K^{mall} + K^{geom} \tag{A.39}$$

where

$$K^{matl} = \int_{V} \delta u_{i,j} C'_{ijkl} \Delta u_{(k,l)} dv$$
 (A.40)

$$K^{geom} = \int_{V} \delta u_{i,j} \, \sigma_{kj}^{\nu} \Delta u_{i,k} \, dv \tag{A.41}$$

(2) The derivation of the 4th term of the left side of equation (A.24)

In equation (A.23), the integration can be expressed as with respect to the initial configuration X.

$$M_{inert} = \int_{V_0} \delta u_i \rho_0 u_{i,tt} dV_0 \tag{A.42}$$

Hence, we have

$$L(M_{inert}) = \int_{V_0} \delta u_i \rho_0 L(u_{i,tt}) dV_0$$
 (A.43)

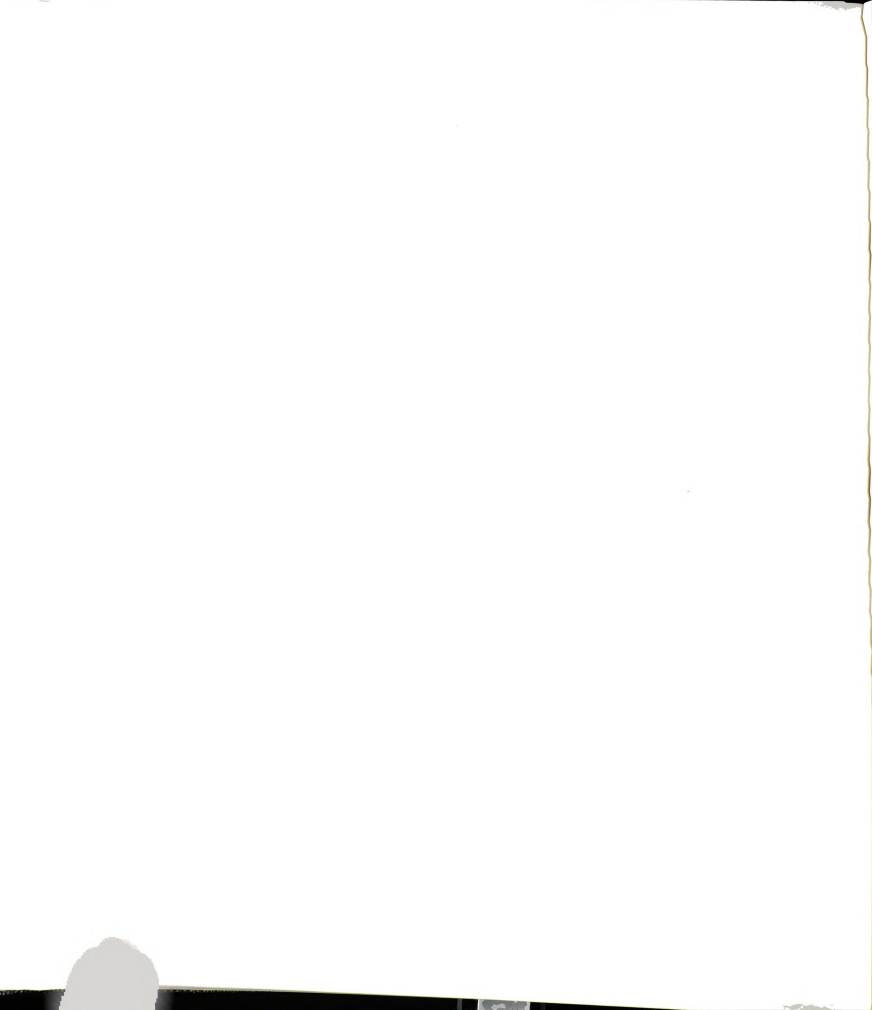
or

$$L(M_{inert}) = \int_{V_0} \delta u_i \rho_0 \Delta u_{i,n} dV_0$$
 (A.44)

(3) The derivation of the first term of the left side of equation (A.24)

From equation (A.20), and

$$b_i dv = \rho_0 b_i^p dV_0$$



(where the superscript p represents the prescribed body force vector acted on an unit mass), we have

$$F_{ext} = \int_{V_0} \delta u_i \rho_0 b_i^p dV_0 + \int_{\Gamma_h} \delta u_i h_i da$$
 (A.45)

When the Consistent Linearization operation is performed on F_{ext} ,

$$L(F_{ext}) = L\left(\int_{V_0} \delta u_i \rho_0 b_i^p dV_0 + \int_{\Gamma_h} \delta u_i h da\right)$$

the first term of the right side will vanish. Then, we obtain

$$L(F_{ext}) = L(\int_{\Gamma_h} \delta u_i h \ da) \tag{A.46}$$

Apparently, this term is important to contact problem, but, for non-contact problem, such as prescribed constant boundary, this term can be neglected. Since contact problem is not our concern in this dissertation, this term is neglected in following derivation.

(4) The derivation of the 3-rd term of the left side of the equation (A.24)

In equation, $t_i = \sigma_{ij} n_j$ on Γ_h , n is the unit normal vector of k-th layer surface glued together with, or delaminated from, (k+1)-th layer. Therefore, the infinitesimal surface element on a surface of the deformed configuration is

$$a_i = n_i da$$

Now, we introduce Nanson's Formula, which is

$$n_i da = JF_{is}^{(-T)} n_s^o dA$$

where the superscript o represents at time t = 0. (-T) represents the inverse of a transposed matrix.

With Nanson's Formula, equation (8) can be rewritten as

$$F_{del} = \sum_{k=1}^{n-1} \int_{r_k} \sigma_{ij} J F_{js}^{(-T)} n_s^o \left(\delta u_i^k - \delta u_i^{(k+1)} \right) dA$$

where again, subscript o denotes at time t = 0, corresponding to the undeformed configuration.

Based on above preparation, we can perform Consistent Linearization on $F_{\it del}$,

$$L(F_{del}) = \sum_{k=1}^{n-1} \int_{i}^{k} L(\sigma_{ij} J F_{js}^{(-T)}) n_s^o \left(\delta u_i^k - \delta u_i^{(k+1)} \right) dA$$

or, in detail

$$L(F_{del}) = \sum_{k=1}^{n-1} \int_{i}^{k} \left(L(\sigma_{ij}) J F_{js}^{(-T)} + \sigma_{ij} L(J) F_{js}^{(-T)} + \sigma_{ij} J L(F_{js}^{(-T)}) \right) n_{s}^{o} \left(\delta u_{i}^{k} - \delta u_{i}^{(k+1)} \right) dA$$

By using equation (A.15), (A.19), and definition

$$L(\sigma_{ij}) = \Delta \sigma_{ij}$$

we obtained

$$L(F_{del}) =$$

$$\sum_{k=1}^{n-1} \int_{t_{i}} \left(\Delta \sigma_{ij} J F_{js}^{(-T)} + \sigma_{ij} J^{\nu} \Delta u_{m,m} F_{js}^{(-T)} - \sigma_{ij} J F_{jr}^{(-T)} \left(\frac{\partial}{\partial X_{r}} \Delta u_{t} \right) F_{ls}^{(-T)} \right) n_{s}^{o} \left(\delta u_{i}^{k} - \delta u_{i}^{(k+1)} \right) dA$$

Substituting

$$F_{jr}^{(-T)} \left(\frac{\partial}{\partial X_r} \Delta u_I \right) = \Delta u_{i,j}$$

into previous equation, it leads to

$$L(F_{del}) = \sum_{k=1}^{n-1} \int_{r_i} \left(\Delta \sigma_{ij} F_{js}^{(-T)} + \sigma_{ij} \Delta u_{m,m} F_{js}^{(-T)} - \sigma_{ij} \Delta u_{i,j} F_{ls}^{(-T)} \right) J n_s^o \left(\partial u_i^k - \partial u_i^{(k+1)} \right) dA$$

By exchanging the position of dummy 1 and j in the 3-rd term of the right side in above equation, and using Nanson's Formula again, we have

$$L(F_{del}) = \sum_{k=1}^{n-1} \int_{I_{i}} \left(\Delta \sigma_{ij} + \sigma_{ij} \Delta u_{m,m} - \sigma_{ij} \Delta u_{i,j} \right) n_{s} \left(\delta u_{i}^{k} - \delta u_{i}^{(k+1)} \right) da$$

Comparing this equation with equation (A.27), and doing the same derivation procedure as done from (A.27) to (A.38), we finally get

$$L(F_{del}) = \sum_{k=1}^{n-1} \int_{r_i} \left(C_{ijkl}^t \Delta u_{(k,l)} + \sigma_{kj}^v \Delta u_{i,k} \right) n_s \left(\delta u_i^m - \delta u_i^{(m+1)} \right) da$$
(A.46*)

But, we'd like to mention that the computational implement of (A.46*) is somehow difficult, since the difference of the virtual displacement across the delaminated interfaces of laminates is impossible for an element. That is the delaminated element has the same 4-node as pre-delamination, therefore no any degrees of freedom can be introduced into the element to simulate the delamination. For this reason, the implementation of delamination simulation was based on a thin film technique and stress re-distribution technique. They both were discussed in Chapter 5.

(5) The final form of Consistent Linearization of Variational Equation

Based on above derivation and discussion, the Linearized Variational Equation is

$$M(\Delta \ddot{u}_{i}) + K(\Delta u) - K_{del}(\Delta u) = F_{ext}(x^{v}) - F_{int}(x^{v}) + F_{del}(x^{v}) - M(\ddot{x}_{i}^{v})$$
(A.47)

where the following definitions are used

$$M(\Delta \ddot{u}_i) = \int_{V_0} \delta u_i \rho_0 \Delta u_{i,u} dV_0 \tag{A.48}$$

$$K(\Delta u) = K^{mall} + K^{geom} \tag{A.49}$$

$$K^{matl} = \int_{V} \delta u_{i,j} C_{ijkl}^{t} \Delta u_{(k,l)} dv$$
 (A.50)

$$K^{geom} = \int_{V} \delta u_{i,j} \, \sigma_{kj}^{\nu} \Delta u_{i,k} \, d\nu \tag{A.51}$$

$$K_{del}(\Delta u) = \sum_{k=1}^{n-1} \int_{\Gamma_i} \left(C'_{ijkl} \Delta u_{(k,l)} + \sigma^{\nu}_{kj} \Delta u_{i,k} \right) n_s \left(\delta u_i^m - \delta u_i^{(m+1)} \right) da$$
(A.50*)

$$F_{ext} = \int_{V} \delta u_{i} b_{i} dv + \int_{\Gamma_{h}} \delta u_{i} h_{i} da$$
 (A.52)

$$F_{\text{int}} = \int_{V} \delta u_{ij,j} \sigma_{ij} dv \tag{A.53}$$

$$F_{del} = \sum_{k=1}^{n-1} \int_{t_i} t_i^k \left(\delta u_i^k - \delta u_i^{(k+1)} \right) da$$
 (A.53*)

$$M_{inert} = \int_{V} \delta u_{i} \rho u_{i,tt} dv \tag{A.54}$$



APPENDIX B

NONLINEAR SOLUTION PROCEDURE

Within this APPENDIX, the numerical methods used by ABAQUS/Standard to solve nonlinear equations and nonlinear ordinary differential equations are briefly introduced.

2.1 Nonlinear Solution Methods

For a static problem, a set of nonlinear algebra equations (equilibrium equations) needs to be solved with numerical methods. The equilibrium equations, symbolically, have a form of

$$F^{N}(u^{M}) = 0$$
 (B.1.1)

where, N indicates the Nth equations that conjugate to the Nth variable in the problem and M is the M-th variable. So, solving Eq. (B.1.1) is our basic problem

A numerical technique, named as Newton's method, for solving the nonlinear equilibrium equations is generally used in ABAQUS/Standard, which is stated as follows. Assume that, in an increment of a step, after iteration i, an approximation u_i^M , to the solution has been obtained. If C_{i+1}^M , termed as (i+1)th correction, is the difference from this solution to the exact solution of Eq. (B.1.1), then,

$$F^{N}(u_{i}^{M} + C_{i+1}^{M}) = 0 (B.1.2)$$

Taking expansion with Taylor series, neglecting all terms but linear terms, and denoting

$$K_i^{NP} = \frac{\partial F^N}{\partial u^P} (u_i^M)$$
 (B.1.3)

Then gives

$$K_i^{Np}C_{i+1}^p = -F_i^N (B.1.4)$$

where K_i^{NP} is the Jacobian matrix and F_i^N is the residual. Residual is the value of left side of Eq. (B.1.1) for approximation u_i^M .

After solving Eq. (B.1.4), the next approximation to the solution is then

$$u_{i+1}^{M} = u_{i}^{M} + C_{i+1}^{M}$$

And the iteration continues.

The measurement of the convergence of Newton's method is based on ensuring that all entries of current residual and correction are sufficiently small. If the convergence is reached, then the first iteration of the next increment begins after updating the loading or/and boundaries to the next increment.

In Newton's method, usually, it is important but difficult to formulate the Jacobian matrix in close form or to calculate it numerically – an expensive (and not always reliable) process.

To formulate the Jacobian matrix in close form, the consistent linearization is done in APPENDIX A, although the linearization is completed before finite element discretization. The similarity between Eq. (A.47) in APPENDIX A and above Eq. (B.1.4) is easy to see by comparing two sides of them since the left side of both equations is linear change induced by current correction, and the other side of them is the residual of the last approximation. Therefore, after discrezation, Eq. (A.47) will result in an exact form of Eq. (B.1.4), directly in the corresponding side.

Hence, in our finite element formulation procedure, the Jacobian matrix will be constructed directly from left side of Eq. (A.47) in APPENDIX A, and the residual from the other side, by finite element discretization.

2.2 Implicit Dynamic Analysis

For a time-dependent problem, particularly, for severely nonlinear dynamic analysis, a direct-time integration method, using central differencial operator with implicit schemes, is provides by ABAQUS/Standard. While explicit schemes obtain dynamic the solution at time $t + \Delta t$ based entirely on available the solution at time t, implicit schemes obtain dynamic solution at the time $t + \Delta t$ based not only on the solution at time t, but also on the same solution at time $t + \Delta t$. Hence, nonlinear equations must be solved by using Newton's method for every time increment. Recall Eq. (B.1.1), since we are dealing with dynamic problem now, we can rewrite Eq. (B.1.1) as

$$F^{N}(u^{M}) = -M^{NM}\ddot{u}^{M} + G^{N}(u^{M}) = 0$$
 (B.2.1)

Where we separate the dynamic equilibrium into two parts, d'Alembert force part, $-M^{NM}\ddot{u}^{M}$, which is directly depends on the double time derivatives, and the rest part, $G^{N}(u^{M})$, which is the total force at degree of freedom N, excluding d'Alembert force, and often referred to as the "static residual."

By comparing Eq. (A.20) with Eq. (B.2.1), it is easy to see that, $-M_{inert}$ is the d'Alembert force, and $F_{ext} - F_{inet} + F_{del}$ is the "static residual."

In ABAQUS/Satndard, the Hilber-Hughness-Taylor scheme is used for time integration of the dynamic problem. According to this scheme, at time $t + \Delta t$, the overall dynamic equilibrium equation, Eq. (B.2.1), is replaced by

$$F^{N}|_{t+\Delta t} = -M^{NM} u^{M}|_{t+\Delta t} + (1+\alpha)G^{N}|_{t+\Delta t} - \alpha G^{N}|_{t} = 0$$
 (B.2.2)

This scheme is completed by the Newmark formulae for displacement and velocity integration:

$$u|_{t+At} = u|_{t} + \Delta t \dot{u}|_{t} + \Delta t^{2} \left(\left(\frac{1}{2} - \beta \right) \dot{u}|_{t} + \beta \dot{u}|_{t+\Delta t} \right)$$
(B.2.3)

and

$$\dot{u}\big|_{t+\Delta t} = \dot{u}\big|_{t} + \Delta t \Big((1-\gamma) \dot{u}\big|_{t} + \gamma \dot{u}\big|_{t+\Delta t} \Big) \tag{B.2.4}$$

with

$$\beta = \frac{1}{4}(1-\alpha)^2,$$

$$\gamma = \frac{1}{2} - \alpha$$

and

$$-\frac{1}{3} \le \alpha \le 0.$$

Where α , β , and γ are the (Newmark) parameters of the integration scheme.

Therefore, Eq. (B.2.2) – (B.2.4) are the equations must be solved for time $t + \Delta t$ if we assume that the approximate solutions at time t are already achieved. Apparently, they are nonlinear equations, since the solution at time $t + \Delta t$ is not only based on solution at time t, but also on the same solution at time $t + \Delta t$. The Newton's method again is used to solve the nonlinear equations, with including the Jacobian contributions from effects that depend on time derivatives.

Now, assume that, at time $t + \Delta t$, after i - th iteration, approximations, $u_i^M \big|_{t+\Delta t}$, \dot{u}_i^M and $\ddot{u}_i^M \big|_{t+\Delta t}$, to the solution have been obtained. Let $C_{i=1}^M \big|_{t+\Delta t}$ be the

difference between $u_i^M|_{t+\Delta t}$ and the exact solution to Eq. (B.2.2). After the same procedure from Eq. (B.1.2) to Eq. (B.1.4), we reach the same form of linear system of equation:

$$K_i^{NP}\big|_{t+\Delta t} C_i^M\big|_{t+\Delta t} = -F_i^N\big|_{t+\Delta t}$$
(B.2.5)

Where, the residual vector is

$$F_i^N \Big|_{t+\Delta t} = -M^{NM} u_i^M \Big|_{t+\Delta t} + (1+\alpha) G_i^N \Big|_{t+\Delta t} - \alpha G_i^N \Big|_{t}$$
 (B.2.6)

and the Jacobian matrix is,

$$k_{i}^{NP}\big|_{t+\Delta t} = \frac{\partial F^{N}}{\partial u^{P}}\big|_{t+\Delta t} + \frac{\partial F^{N}}{\partial \dot{u}^{P}}\big(\frac{d\dot{u}^{P}}{du}\big)\big|_{t+\Delta t} + \frac{\partial F^{N}}{\partial \ddot{u}^{P}}\big(\frac{d\ddot{u}}{du}\big)\big|_{t+\Delta t}$$

Considering following relations derived from Eq. (B.2.3) – (B.2.4),

$$\left(\frac{d\dot{u}}{du}\right)\Big|_{t+\Delta t}=\frac{\gamma}{\beta\Delta t},$$

and

$$\left. \left(\frac{d\ddot{u}}{du} \right) \right|_{t+\Delta t} = \frac{1}{\beta \Delta t^2} \,,$$

and relations derived from Eq. (B.2.2),

$$\frac{\partial F^{N}}{\partial u^{P}}\Big|_{t+\Delta t} = (1+\alpha) \frac{\partial G^{N}}{\partial u^{P}}\Big|_{t+\Delta t}$$

$$\frac{\partial F^{N}}{\partial \dot{u}^{P}}\Big|_{t+\Delta t}=0$$

$$\frac{\partial F^{N}}{\partial \ddot{u}^{P}}\Big|_{t+\Delta t}=-M^{NP},$$

the Jacobian matrix becomes

$$K_{i}^{NP}\big|_{t+\Delta t} = (1+\alpha) \frac{\partial G^{N}}{\partial u^{P}}\big|_{t+\Delta t} - M^{NP} \frac{1}{\beta \Delta t^{2}}$$
 (B.2.7)

Once Eq. (B.2.5) is solved, the next approximations to the solution are then determined by

$$u_{i+1}^{M}\Big|_{t+\Delta t} = u_{i}^{M}\Big|_{t} + C_{i+1}^{M}\Big|_{t+\Delta t},$$

$$u_{i+1}^{M}\Big|_{t+\Delta t} = u^{M}\Big|_{t} + \Delta t \dot{u}^{M}\Big|_{t} + \Delta t^{2} \left((\frac{1}{2} - \beta) \ddot{u}^{M}\Big|_{t} + \beta \dot{u}_{i+1}^{M}\Big|_{t+\Delta t} \right)$$

$$\dot{u}_{i+1}^{M}\Big|_{t+\Delta t} = \dot{u}^{M}\Big|_{t} + \Delta t \left((1 - \gamma) \ddot{u}^{M}\Big|_{t} + \gamma \ddot{u}_{i+1}^{M}\Big|_{t+\Delta t} \right),$$

and the iteration continues.

2.3 Consistent Linearization Applied in Hilber-Hughess-Taylor Scheme

Follow the same procedure described as above for implicit dynamic analysis, but develop a detailed, direct implicit dynamic integration procedure according to APPENDIX A. First, rewrite Eq. (A.20) as

$$F(u) = -M_{inert}(\ddot{u}) + G(u) \tag{B.3.1}$$

where,

$$M_{inert}(\ddot{u}) = M_{inert}$$

and

$$G(u) = F_{ext} - F_{int} + F_{del}$$
 (B.3.2)

Then, for the Hilber-Hughess-Taylor scheme, at time $t + \Delta t$, replace Eq. (B.3.1) by

$$F\big|_{t+\Delta t} = -M_{inert}(\ddot{u})\big|_{t+\Delta t} + (1+\alpha)G\big|_{t+\Delta t} - \alpha G\big|_{t} = 0$$
 (B.3.3)

With Eq. (B.2.3) and Eq. (B.2.4), a complete form of Hilber-Hughess-Tayor scheme for implicit dynamic integration is obtained.

Accordingly, corresponding to Eq. (B.2.5) to Eq. (B.2.7), the following equations are given, with superscript ν to present the ν -th iteration, instead of subscript i, which is used in section 2.2 and 2.3:

$$K^{\nu}\Big|_{t+\Delta t}C^{\nu}\Big|_{t+\Delta t}=-F^{\nu}\Big|_{t+\Delta t}$$
,

or $L[F|_{t+\Delta t}] = -F^{\nu}|_{t+\Delta t}$, (consistent linearization form, since $K^{\nu}|_{t+\Delta t}C^{\nu}|_{t+\Delta t} = L[F|_{t+\Delta t}]$, see APPENDIX A),

$$\begin{split} F^{\nu}\big|_{t+\Delta t} &= -M_{inert}(\ddot{u}^{\nu})\big|_{t+\Delta t} + (1+\alpha)G^{\nu}\big|_{t+\Delta t} - \alpha G^{\nu}\big|_{t}, \\ L\big[F^{\nu}\big|_{t+\Delta t}\big] &= -L\big[M_{inert}(\ddot{u})\big|_{t+\Delta t}\big] + (1+\alpha)L\big[G\big|_{t+\Delta t}\big] = \\ &-L\big[M_{inert}\big|_{t+\Delta t}\big] + (1+\alpha)L\big[F_{ext} - F_{int} + F_{det}\big]\big|_{t+\Delta t} \end{split}$$

By using the results obtained in Eq. (A.47), the linear system can be further determined as

$$-M(\Delta \ddot{u}) - (1+\alpha) \left[K_s(\Delta u) - K_{del}(\Delta u) \right] = M_{inert}(\ddot{u}) \Big|_{t+\Delta t} - (1+\alpha)G \Big|_{t+\Delta t} + \alpha G \Big|_{t}$$
(B.3.4)

and the definition of above terms can be found in Eq. (A.48)-(A.54).

Here, a further discussion of the first term in the left-hand side of Eq. (B.3.4) is needed.

Recall that

$$\left.\left(\frac{d\ddot{u}}{du}\right)\right|_{t+\Delta t}=\frac{1}{\beta\Delta t^2}\,,$$

therefore

$$-M(\Delta \ddot{u}) = -L[M_{inert}(\ddot{u})] = -\int_{\nu} \frac{\partial}{\partial \ddot{u}} (\delta u_{i} \rho \ddot{u}_{i}) \frac{d\ddot{u}}{du} \Delta u d\nu = -\int_{\nu 0} \frac{\partial}{\partial \ddot{u}} (\delta u_{i} \rho_{0} \ddot{u}_{i}) \frac{d\ddot{u}}{du} \Delta u dV$$

$$= -\int_{V_0} \delta u_i \rho_0 \left(\frac{1}{\beta \Delta t^2}\right) \Delta u_i dV = -\frac{1}{\beta \Delta t^2} \int_{V_0} \delta u_i \rho_0 \Delta u_i dV = -\frac{1}{\beta \Delta t^2} \int_{V} \delta u_i \rho \Delta u_i dV$$
(B.3.5)

Apparently, Eq. (B.3.4) will result in the linear system of dynamic equilibrium equations when finite element discretization applied,

$$\left[-M\frac{1}{\beta\Delta t^{2}}-(1+\alpha)(K_{S}-K_{sel})\right]\Delta U=M\ddot{U}-(1+\alpha)G\big|_{t+\Delta t}+\alpha G\big|_{t}$$

where ΔU is the correction vector of the nodal unknowns of the whole model; U and \ddot{U} are the "displacement" vector, and "acceleration" vector of the nodal unknowns of whole model, respectively.

2.4 Newmark Algorithm

In the Hilber-Hughess-Taylor scheme, parameter, α , is used to provide numerical damping, when $-\frac{1}{3} \le \alpha < 0$. The numerical damping with this form is controllable, slowly growing at low frequencies, with more rapid growth in damping at high frequencies. But when $\alpha=0$, the Hilber-Hughess-Taylor operator is the Newmark operator (Trapezoidal rule, at $\beta=1/4$, $\gamma=1/2$), hence, there is no numerical damping. Put $\alpha=0$ into Eq. (B.3.6), the Newmark Algorithm can be readily introduced as following a time-approximate recursion algorithm:

Predictor:

$$U_{t+\Delta t}^{(0)} = U_{t} + (\Delta t \dot{U}_{t} + \frac{1}{4} \Delta t^{2} \ddot{U}_{t})$$
 (B.4.1)

$$\dot{U}_{t+\Delta t}^{(0)} = \dot{U}_t + \frac{1}{2} \Delta t \ddot{U}_t \tag{B.4.2}$$

$$\ddot{U}_{t+\Delta t}^{(0)} = 0 \tag{B.4.3}$$

Solver:

$$K^{(\nu)} \Delta U_{t+\Delta t}^{\nu+1} = R_{t+\Delta t}^{(\nu)} \tag{B.4.4}$$

Where

$$K^{(\nu)} = M^{(\nu)} \frac{1}{\beta \Delta t^2} + K_S^{(\nu)} \Big|_{t+\Delta t} - K_{del}^{(\nu)} \Big|_{t+\Delta t}$$
 (B.4.5)

$$R_{t+\Delta t}^{(\nu)} = -M^{(\nu)} \ddot{U}_{t+\Delta t}^{(\nu)} + G_{t+\Delta t}^{(\nu)}$$
(B.4.6)

Corrector:

$$U_{t+\Delta t}^{(\nu+1)} = U_{t+\Delta t}^{(\nu)} + \Delta U_{t+\Delta t}^{(\nu+1)}$$
(B.4.7)

$$\dot{U}_{t+\Delta t}^{(\nu+1)} = \dot{U}_{t+\Delta t}^{(\nu)} + \frac{2}{\Delta t} \Delta U_{t+\Delta t}^{(\nu+1)}$$
(B.4.8)

$$\ddot{U}_{t+\Delta t}^{(\nu+1)} = \ddot{U}_{t+\Delta t}^{(\nu)} + \frac{4}{\Delta t^2} \Delta U_{t+\Delta t}^{(\nu+1)}$$
(B.4.9)

The Newmark Algorithm gives a complete direct implicit integration procedure for implicit dynamic analysis. But, for a clear understanding of this procedure, the following points are discussed:

- (1) At time t=0, initial "acceleration" is generally unavailable. Therefore, ABAQUS/Standard provides an option to estimate initial "accelerations" with mass matrix and initial residual. The same way is used for the calculation of accelerations after impact. If this option is not activated, the zero initial "accelerations" will be assumed; this may cause extremely expensive iterations to reach convergence for the first increment when large loads are applied suddenly.
- (2) In the Newmark Algorithm, there is no numerical or artificial damping, so energy is conserved. Again, when sudden loading is applied, such as an impact, high

frequencies will be induced, resulting in convergence difficulty. Under such cases, very small time increments are needed, and the computation cost will be high. To avoid these disadvantages, an option is available in ABAQUS/Standard: that is to introduce material damping to depress the high frequency noise, which require a structural damping matrix to be introduced to the model, but the accuracy of the damping is not easy to obtain.

- (3) The accuracy of the solution is controlled by half-step residual tolerance in implicit dynamic integration. Convergence check at the end of each time increment, which ensure any component of the residual vector and correction vector sufficiently small, just ensures equilibrium at these time points but does not say anything about the quality of equilibrium at intermediate time points. Based on the assumption that the accelerations vary linearly over the time interval, the magnitude of the large entry of residual at half time increment provides a measure of the transient solution. But, the calculation of the half-step residual, the storage of more intermediate results, increase the cost. A relative cost-effective half-step residual tolerance will be important (see ABAQUS Theory Manual)
- (4) The correction and prediction of vectors are easily carried out with the Newmark Algorithm, but finite element rotation is not a vector although angular velocity and angular acceleration are vectors. Therefore, the correction and prediction of finite element rotation is not so simple as given in above algorithm. Since the correction and prediction of finite rotation is carried out by ABAQUS automatically, we do not pay too much attention to this problem. And in impact simulation, the time increment

needs to be small, so the rotation increment will be small too, an infinitesimal rotation can be approximated as a vector.

APPENDIX C

IDENTIFICATION OF NODAL VARIABLES

The degrees of freedom at a node in user element U101 described in [5.4], do not follow the ABAQUS conventions—they are neither nodal displacements along, nor nodal rotation angular about any axis of local coordinate system, or global coordinate system. For convenience of use in an ABAQUS model including native element and user element, the nodal variables of a user element had better follow the ABAQUS conventions. In order to do so, this APPENDIX is given.

Suppose the mid-plane (at z=0) of laminate is located in the mp-th layer, then the incremental displacement field at the mid-plane can be written as

$$\Delta u^{mp}(x, y, 0) = \Delta u_0(x, y) + S_1^{mp} \Delta u_1(x, y) + S_2^{mp} \frac{\partial}{\partial x} \Delta w_0(x, y)$$
 (C.1)

$$\Delta v^{mp}(x, y, 0) = \Delta v_0(x, y) + P_1^{mp} \Delta u_1(x, y) + P_2^{mp} \frac{\partial}{\partial y} \Delta w_0(x, y)$$
 (C.2)

$$\Delta w^{mp}(x, y, 0) = \Delta w_0(x, y) \tag{C.3}$$

after substituting z=0 into Eq. (4.30)-(4.32) in [5.4].

From the spin tensor W, we know that, at any point P(x,y,z), the incremental rotations about x- and y-axis, respectively, are

$$\Delta \Psi_x = \Delta W_{23} = \frac{1}{2} \left(\frac{\partial}{\partial z} \Delta \nu - \frac{\partial}{\partial y} \Delta w \right),$$

$$\Delta \Psi_{y} = \Delta W_{13} = \frac{1}{2} \left(\frac{\partial}{\partial z} \Delta u - \frac{\partial}{\partial x} \Delta w \right).$$

By using Eq. (5.11)-(5.24) of [5.4] and then substitute z=0, above two equilibrium equations give the mid-plane incremental rotations about x- and y-axis,

$$\Delta \Psi_x^{mp} = \frac{1}{2} \left(O_1^{mp} \Delta v_1 + O_2^{mp} \frac{\partial}{\partial y} \Delta w_0 - \frac{\partial}{\partial y} \Delta w_0 \right),$$

and

$$\Delta \Psi_y^{mp} = \frac{1}{2} \left(R_1^{mp} \Delta u_1 + R_2^{mp} \frac{\partial}{\partial x} \Delta w_0 - \frac{\partial}{\partial x} \Delta w_0 \right),$$

respectively. And further from these two equations, we obtain

$$\Delta v_1 = \frac{1}{o_1^{mp}} \left[2\Delta \Psi_x^{mp} + (1 - O_2^{mp}) \frac{\partial}{\partial y} \Delta w_0 \right]$$
 (C.4)

$$\Delta u_1 = \frac{1}{R_1^{mp}} \left[2\Delta \Psi_y^{mp} + (1 - R_2^{mp}) \frac{\partial}{\partial x} \Delta w_0 \right]$$
 (C.5)

In order to solve Δu_0 , Δv_0 from Eq. (C.1)-(C.2), substitute Eq. (C.4)-(C.5) into them,

$$\Delta u^{mp}(x, y, 0) = \Delta u_0(x, y) + S_1^{mp} \frac{1}{R_1^{mp}} \left[2\Delta \Psi_y^{mp} + (1 - R_2^{mp}) \frac{\partial}{\partial x} \Delta w_0 \right] + S_2^{mp} \frac{\partial}{\partial x} \Delta w_0(x, y)$$

$$\Delta v^{mp}(x, y, 0) = \Delta v_0(x, y) + P_1^{mp} \frac{1}{O_1^{mp}} \left[2\Delta \Psi_x^{mp} + (1 - O_2^{mp}) \frac{\partial}{\partial y} \Delta w_0 \right] + P_2^{mp} \frac{\partial}{\partial y} \Delta w_0(x, y)$$

Then further we have

$$\Delta u_0^{mp}(x, y, 0) = \Delta u(x, y, 0) - S_1^{mp} \frac{1}{R_1^{mp}} [2\Delta \Psi_y^{mp} + (1 - R_2^{mp}) \frac{\partial}{\partial x} \Delta w_0] - S_2^{mp} \frac{\partial}{\partial x} \Delta w_0 \quad (C.6)$$

$$\Delta v_0^{mp}(x, y, 0) = \Delta v(x, y, 0) - P_1^{mp} \frac{1}{O_1^{mp}} [2\Delta \Psi_x^{mp} + (1 - O_2^{mp}) \frac{\partial}{\partial y} \Delta w_0] - P_2^{mp} \frac{\partial}{\partial y} \Delta w_0 \quad (C.7)$$

Recall Eq. (4.30)-(4.32)[5.4],

$$\Delta u^{k}(x, y, z) = \Delta u_{0}(x, y) + (S_{1}^{k} + R_{1}^{k}z + A_{1}z^{2} + B_{1}z^{3})\Delta u_{1}(x, y) +$$

$$(S_{2}^{k} + R_{2}^{k}z + A_{2}z^{2} + B_{2}z^{3})\frac{\partial}{\partial y}\Delta w_{0}(x, y)$$

$$\Delta v^{k}(x, y, z) = \Delta v_{0}(x, y) + (P_{1}^{k} + O_{1}^{k}z + C_{1}z^{2} + D_{1}z^{3})\Delta v_{1}(x, y) +$$

$$(P_{2}^{k} + O_{2}^{k}z + C_{2}z^{2} + D_{2}z^{3})\frac{\partial}{\partial y}\Delta w_{0}(x, y)$$

$$\Delta w^{k}(x, y, z) = \Delta w_{0}(x, y)$$

By substituting Eq. (C.3) and Eq. (C.4)-(C.7) into Eq. (4.30)-(4.32) in [5.4], we complete our transformation with following final increment displacement field,

$$\Delta u^{k}(x,y,z) = \Delta u^{mp}(x,y,0) - S_{1}^{mp} \frac{1}{R_{1}^{mp}} [2\Delta \Psi_{y}^{mp} + (1-R_{2}^{mp}) \frac{\partial}{\partial x} \Delta w_{0}] - S_{2}^{mp} \frac{\partial}{\partial x} \Delta w_{0}]$$

$$+ (S_{1}^{k} + R_{1}^{k}z + A_{1}z^{2} + B_{1}z^{3}) \frac{1}{R_{1}^{mp}} [2\Delta \Psi_{y}^{mp} + (1-R_{2}^{mp}) \frac{\partial}{\partial x} \Delta w_{0}] +$$

$$(S_{2}^{k} + R_{2}^{k}z + A_{2}z^{2} + B_{2}z^{3}) \frac{\partial}{\partial x} \Delta w_{0}(x,y)$$

$$= \Delta u^{mp}(x,y,0) + (S_{1t}^{k} + R_{1t}^{k}z + A_{1t}z^{2} + B_{1t}z^{3}) \Delta \Psi_{y}^{mp} +$$

$$(S_{2t}^{k} + R_{2t}^{k}z + A_{2t}z^{2} + B_{2t}z^{3}) \frac{\partial}{\partial x} \Delta w_{0}(x,y)$$

$$(C.8)$$

$$\Delta v^{k}(x,y,z) = \Delta v^{mp}(x,y,0) - P_{1}^{mp} \frac{1}{O_{1}^{mp}} [2\Delta \Psi_{x}^{mp} + (1-O_{2}^{mp}) \frac{\partial}{\partial y} \Delta w_{0}] - P_{2}^{mp} \frac{\partial}{\partial y} \Delta w_{0}$$

$$+ (P_{1}^{k} + O_{1}^{k}z + C_{1}z^{2} + D_{1}z^{3}) \frac{1}{O_{1}^{mp}} [2\Delta \Psi_{x}^{mp} + (1-O_{2}^{mp}) \frac{\partial}{\partial y} \Delta w_{0}] +$$

$$(P_{2}^{k} + O_{2}^{k}z + C_{2}z^{2} + D_{2}z^{3}) \frac{\partial}{\partial y} \Delta w_{0}(x,y)$$

$$= \Delta v^{mp}(x,y,0) + (P_{1t}^{k} + O_{1t}^{k}z + C_{1t}z^{2} + D_{1t}z^{3}) \Delta \Psi_{x}^{mp} +$$

$$(P_{2\iota}^{k} + O_{2\iota}^{k}z + C_{2\iota}z^{2} + D_{2\iota}z^{3})\frac{\partial}{\partial y}\Delta w_{0}(x, y)$$
 (C.9)

$$\Delta w^{k}(x, y) = \Delta w^{mp}(x, y, 0) \tag{C.10}$$

where, following notations are used (subscript t represent the transformed coefficients):

$$\begin{split} S_{1t}^k &= \frac{2}{R_1^{mp}} (S_1^k - S_1^{mp}), \qquad R_{1t}^k &= \frac{2}{R_1^{mp}} R_1^k, \qquad A_{1t}^k &= \frac{2}{R_1^{mp}} A_1^k, \qquad B_{1t}^k &= \frac{2}{R_1^{mp}} B_1^k \\ S_{2t}^k &= S_2^k + (S_1^k - S_1^{mp}) \frac{1}{R_1^{mp}} (1 - R_2^{mp}) - S_2^{mp}, \\ R_{2t}^k &= R_2^k + R_1^k \frac{1}{R_1^{mp}} (1 - R_2^{mp}) \\ A_{2t} &= A_2 + A_1 \frac{1}{R_1^{mp}} (1 - R_2^{mp}) \\ B_{1t}^k &= \frac{2}{O_1^{mp}} (P_1^k - P_1^{mp}), \qquad O_{1t}^k &= \frac{2}{O_1^{mp}} O_1^k, \qquad C_{1t}^k &= \frac{2}{O_1^{mp}} C_1^k, \\ D_{1t}^k &= \frac{2}{O_1^{mp}} D_1^k \\ P_{2t}^k &= P_2^k + (P_1^k - P_1^{mp}) \frac{1}{O_1^{mp}} (1 - O_2^{mp}) - P_2^{mp}, \\ O_{2t}^k &= O_2^k + O_1^k \frac{1}{O_1^{mp}} (1 - O_2^{mp}) \\ C_{2t} &= C_2 + C_1 \frac{1}{O_1^{mp}} (1 - C_2^{mp}) \qquad D_{2t} = D_2 + D_1 \frac{1}{O_1^{mp}} (1 - O_2^{mp}) \end{split}$$

Therefore, according to Eq.(C.7)-(C.10), the independent unknowns are three midplane displacements, two mid-plane rotations, and $\frac{\partial}{\partial x} \Delta w_0$, $\frac{\partial}{\partial y} \Delta w_0$. And the new incremental displacement field, after transformation, has same form of original ones. But please note that the new coefficients, defined in above equations, are calculated from original coefficients. Hence in finite element formulation, nodal variables are mid-plane engineering variables.



